Design and analysis of non-threaded drill pipe connector.

THAKUR, J.O.

2022

DESIGN AND ANAYSIS OF NON-THREADED DRILL PIPE CONNECTOR

Joshua Omar Thakur

Robert Gordon University

School of Engineering

Jan 2022

A thesis submitted in partial fulfilment of the requirements of Robert Gordon University for the degree of Master of Research (MRes)

Abstract

This thesis determines the feasibility and application opportunities of a Snap-Latch Ring design based on the Pin and Box non-threaded connectors designed. Modern drill pipes are connected by rotary threaded shouldered connections which have been prone to failure leading to fatal accidents on the drilling deck. The proposed connection mechanism is aimed to improve engagement and disengagement time of pipes by 50% as well as being a safer connection alternative. This research involved studying the existing design for Pin and Box connectors from previous study (Phase 1) and designing applicable solutions for the Snap-Latch Ring, which is a key component for the engagement and connection of the pipe connectors. The Snap-Latch Ring design needs to be able to withstand high tensile loads from operational use as well as possess magnetic properties to enable actuation of the rings.

Finite Element Analysis (FEA) was conducted using ANSYS Workbench software package to identify the maximum stress and deformation behaviors for the Snap-Latch Ring prototypes designed. The initially proposed Snap-Latch Ring parameters were optimized running several simulations to identify scope of further improvement. The Snap-Latch Ring Prototypes were shown to fail under the maximum tensile load target; however, all three components were simulated at a range of tensile loads to identify a safe working range of loads for the given components. Furthermore, a few scaled prototypes were manufactured using both 3D printing methods (plastic prototypes) as well as CNC machining (metal prototypes) to manufacture Pin, Box and Snap-Latch Ring prototypes.

The thesis concludes that within the current limitations with respect to all three components (Pin connector, Box connector and Snap-Latch Ring), the stress limit of the entire system is limited to that of the Snap-Latch ring. The Pin and Box connections due to their teeth like geometry features handle torsional stress. Hence the safe operational force that can be applied is 1,130kN (or 254,034 lbs) which is 13.2% of the original suggested maximum tensile force 8,565kN (or 1,925,541 lbs). Hence the application of the current design needs reconsideration. As the Snap-Latch ring is located (sandwiched) between the Pin and Box connectors, the only means of actuation is by non-contact forces. This is only

possible through magnetic actuation. However, the surface area of the ring is too small to be attracted with the required pull force.

The thesis further expands over the key considerations to be overcome for future work. It must be understood that there are certain technological restraints in the analyzed design such as the maximum tensile yield strength, magnetic permeability and having these two properties not become affected by the harsh corrosive conditions existing downhole. Pin and Box design could be altered to handle maximum shear contact between the components by changing the geometry as more shear contact area means more stress distribution and better stress and deformation performance.

Acknowledgements

I would sincerely and especially like to thank Dr. Nadimul Faisal and Professor James Njuguna for providing me with opportunity and support to pursue and complete the research undertaken. They provided a great level of mentoring and advice throughout the process to overcome different challenges which have overall helped with my growth on a research and personal level. I would also like to thank Mr Alan McPherson and Mr Alan McLean for their support and assistance in the lab, from technical advice to procurement of supplies to make this research progress as expected. I also greatly appreciate the funding support provided from Oil and Gas Innovation Centre (OGIC), the company (Stab-In-Pipe LTD) and RGU staff as whole who have provided the opportunity and funding to pursue such a novel idea and provide a wholesome learning experience.

Table of Contents

Chapter 1

INTRODUCTION

1.1 Background

The upstream sector of the oil and gas industry which is responsible for the physical extraction of crude oil and natural gases, makes use of long segments of hollow metal pipes with a drill bit at the end to drill through the formations of the earth to the required location and effectively procure the desired fuels. Since the depth of the oil reservoir can range from a few 100 meters to 10,000 meters, the hollow pipes must be segmented and connected, a process conducted on the drilling floor during the drilling operations. The bottom hole assembly tool string is hollow in design as this allows for multiple important processes: allowing drilling fluids to perform functions such as cleaning the drill bit and controlling pressure in the well and ensure controlled flow of oil and gas once the reservoir has been tapped [1-3].

The connection of these segments of drill pipe (usually 10 meters long) are threaded by design and this threaded connection had been improved and developed over the years. A standard drill pipe has a male connection (Pin connection) and a female connection (Box connection) at each end, where the Pin end of one pipe is connected to the Box end of the next pipe as seen in Figure 1.1. The implementation of a new connection configuration has not been seen to be applied in the industry and this could be attributed to many factors. The first being that the oil and gas sector do not generally look to change processes unless the existing ones are an obvious risk to the process and industry. The second could be because extensive research has already been conducted on a non-threaded connection and conclusions have provided reasonable justification for its lack of feasibility to this application. However, extensive literature review only shows a small collection of patents and limited articles regarding this area of study.

There are no published literature showing the justification for or against the design and application of a non-threaded connection for drill pipe joints. Hence the aim of this research is to provide quantitative and qualitative results to justify

the reasonability of a non-threaded drill pipe connection and if not so, what factors need to be pursued.

Failure in drill pipes occur primarily in the connection joints due to continuous and high variations of tensile and torsional loads, bending stresses and internal and external pressures. In threaded drill pipe joints, high stress concentration at the base of the tooth is unavoidable. These static and cyclical loads over time can result in cracks, which propagate and over time, in the harsh downhole environment result in tool joint failure. This is a massive issue in the drilling industry as a tool lost downhole means the well is practically useless until the string is fished out of the well, incurring substantial financial loses on the company [4-5].

There are 3 key outcomes expected from a newly proposed non-threaded drill pipe connection system. The first is to minimise the connection time on the drilling rig from 5-7 mins to a mere 30-60 seconds. This would reduce the drilling process time and in turn result in higher productivity in the same time frame with conventional threaded drill pipes. Furthermore, 10% of all accidents that occur on the drilling rig platform have been during engagement and disengagement of tool joints, mainly due to high torsion applied to connect the two segments together [6]. The concept on a non-threaded connection would replace the application of high torsion with a safer connection mechanism. This could be taken one step ahead by making the entire process automated, minimizing the possibility of injury to personnel. Due to the threaded design of tool joint connections, pipes can only be rotated in one orientation as any attempt to change the direction of rotation would possibly result in the tool joint being easily broken off if any segment were to be stuck. Hence a non-threaded connection would allow for the tool string to be rotated in both clockwise and anti-clockwise orientations allowing for new variations of drilling capabilities, without compromising the integrity of the system. Considering these outcomes, investigating the feasibility of a non-threaded connection is highly desirable. Furthermore, this investigation has

provided better insight for appropriate design considerations to be made for such an application.

Figure 1.1: Pin Connection (left), Box Connection (middle) and interface between pin and box (right) of a 3 1/2-inch drill pipe [1-3].

1.2 Scope and objectives of present research work

The aim of the thesis is to design a set of non-threaded pipe connections. The current model works on the concept of simply stabbing a pin connection into the box connection, however there will be a set of snap-latch rings that secure the pin and the box end connections which prevent the connections from separating axially and appropriate design features on both ends will prevent the joints from slipping due to torsion. The snap latch rings have been proposed to be actuated using an electromagnetic field. This project is inter-disciplinary and involves a combination of structural mechanics and electromagnetic principles.

The benefits of having such a design have already been discussed and hence the following objectives are as follows: -

1) To understand non-threaded drill pipe connections and the different mechanical, magnetic and electromagnetic principles to construct a new and improved design for the application.
2) To produce analytical and simulation data to understand the mechanical properties of such a design and to ascertain its safe working limits.
3) To produce physical prototypes to better visualise and understand the problems associated.
4) To exploit the results obtained from the modified design and identify further areas of study and application.

1.3 Methodology

This project as part of a commercially funded project demanded certain production aspects for better understanding of the problem. This involved 3D modelling and printing as well as CNC machining of scaled parts. The process for optimization of the snap-latch ring was done using Solidworks and ANSYS-Static Structural as tools to develop the CAD geometry and understand the stress and tensile load capacity of the components under investigation. The results obtained were analysed and used to determine quantitative parameters which are used to interpret the feasibility of the concept. Furthermore, the manufactured products offered qualitative insight to the ease and feasibility of the production process as well as allowing for the identification of limitations which would not normally be anticipated using purely theoretical analysis. This involved testing the actuation process with switch magnets and electromagnets to identify the potential of the application. Figure 1.2 illustrates a flow representation of the processes and methodology applied to attain the results for this thesis.

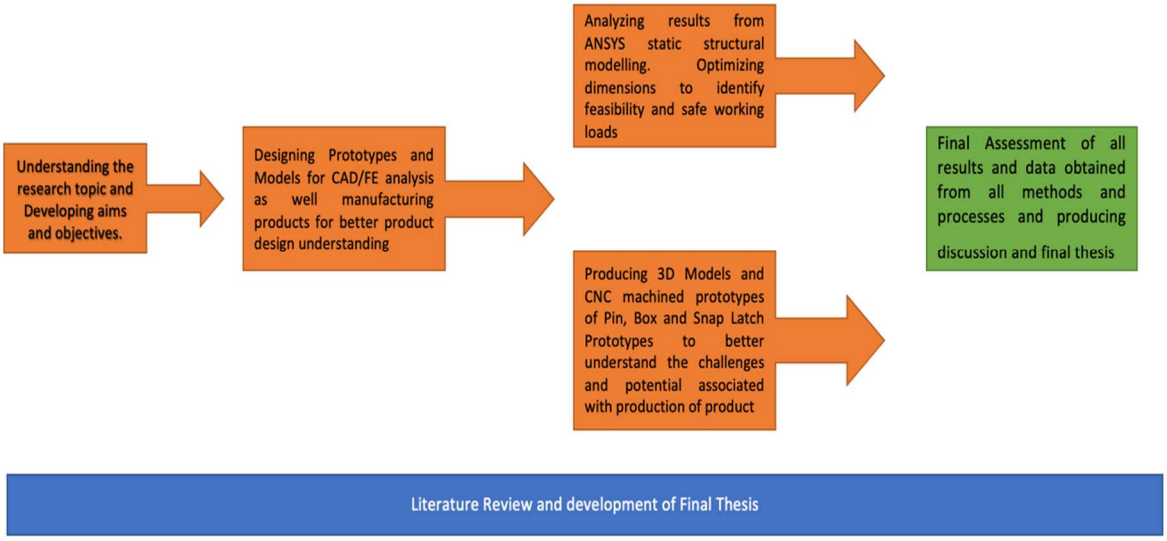

Figure 1.2: Design and process flow of research

1.4 Contribution to Knowledge

Over the decades several practical methods have been proposed regarding the conceptualisation of a non-threaded tool joint connection for the application specific to the oil and gas industry. However, there is no existing research available showing the feasibility of such a concept. This paper aims to look at the latest tool joint design, attempts to develop new non-threaded tool joint mechanical design and analyse the results using CAD software and other analytical tools. Furthermore, the paper shows attempts made at the physical construction of the prototype (non-threaded tool joint) to assess the practicability, the successes as well as the challenges associated with the production and application of such a product. This research has made a contribution to existing knowledge by identifying the core factors associated with this novel concept and supporting these claims with theoretical and practical methodologies and analysis.

1.5 Thesis Layout

Chapter 1: Introduction. This provides a layout of the research undertaken with a brief overview of drill pipe components, the challenges and potential aspects of improvement available as well as justification of these improvements. The methodology and expected outcomes as well the overall contribution to knowledge has been mentioned.

Chapter 2: Literature Review. This chapter provides literature review regarding current conventional drill pipe connections and studies on tool joint failures that occur. A progressive overview is provided on all the non-threaded tool joint patents and models conceptualised over time whilst also providing critical analysis on each model, critiquing the flaws in each design, and highlighting the positive outcomes that have been incorporated into the design investigated in this research. The chapter concludes with the contribution made from the literature review; the contribution to knowledge as well as methodology on the research undertaken.

Chapter 3: Methodology. This chapter begins with the overview of the existing design concept and the process involved to make it work practically work. Furthermore, a diverse range of proposed snap latch designs have been proposed

with justification and limitations associated with each design type. The chapter concludes with an overview of the methodology and the learnt outcome from the process.

Chapter 4: Finite Element Analysis (FEA). This chapter shows the CAD modelling methodology as well as a simple theoretical modelling for torsional springs to assist with understanding the parameters to be considered for out snap-latch design. Finite element modelling and analysis have been detailed showing the parameters applied and the results obtained. The chapter ends with a discussion on the results from this process. This chapter provides the results from the FE models where the height and width of the snap latch have been varied in 6 different setups to find the optimal size of a snap latch we can accommodate within the Pin and Box connections. This chapter will further explore the limitations and the safety factors or safe working loads under which our current model can work. The chapter will conclude with a critical discussion detailing the results and the justification of the optimal parameters.

Chapter 5: Prototype Manufacturing. This chapter provides the results from the FE simulation models where the height and width of the snap latch have been varied in 6 different setups to find the optimal size of a snap latch we can accommodate within the Pin and Box connections. This chapter will further explore the limitations and the safety factors or safe working loads under which our current model can work. The chapter will conclude with a critical discussion detailing the results and the justification of the parameters applied.

Chapter 6: Discussion. This chapter provides an elaborate discussion of the results based on the various methods and process applied to identify the key applications and limitations of the Snap-latch design and provide the gap in knowledge identified from the results of this research.

Chapter 7: Conclusion. This chapter will summarise the results and provide the learnt outcomes from the objects achieved

Chapter 8: Recommendations. This chapter provides recommendations that apply to this research that need critical consideration for further development.

Chapter 2

LITERATURE REVIEW

2.1 Introduction

This chapter is divided into two main sections. Sections 2.2-2.3 includes reviewed literature with respect to the latest tool joint design (patents), literature and models proposed for non-threaded tool joint connections. These designs have been listed and reviewed chronologically with their description and feasibility discussed. These sections will also review threaded tool joint connections to better understand the considerations required for the design of a completely new connection configuration. Section 2.4-2.7 lays out the current available mechanical, magnetic and electromagnetic principles which have been considered and can possibly be applied to the design of the up-to date non-threaded drill pipe connection.

2.2 Threaded Tool-Joint

According to the International Association of Drilling Contractors (IADC) manual, majority of tubular goods manufactured are as per the specifications approved by the America Petroleum Institution (API). These specifications cover the mechanical properties of the steel, physical and geometric dimensions of the pipe which includes the inner and outer diameter, wall thickness, length and weight to name a few. The Figure 2.1 shows some of the key parameters of a tool joint for both pin and box connection. The box connection is the receiving or female end, and the pin connection is the insertion or male end. A single pipe commonly has one pin end and one box end; however, this is subject to change based on the different types of connections made for the entire tool string. Furthermore, IADC records show that most fatigue failure occurs approximately about 1 inch from the pin shoulder. This is primarily caused due to insufficient make up torque applied to stabilise the pin and box shoulders and threads, allowing for stress that exceeds the strength limit of the material [11].

Apart from single shouldered tool joints, there are double shouldered tool joints which have a shoulder on the end of the pin that contacts a corresponding internal shoulder in the box. This feature further limits the axial deformation in the pin and

provides more torsional strength [12]. The design worked up in this project could be categorised as a double shoulder connection based on the definition. Other significant properties are the pipe length, which usually come in three ranges, however this is not of concern to our study.

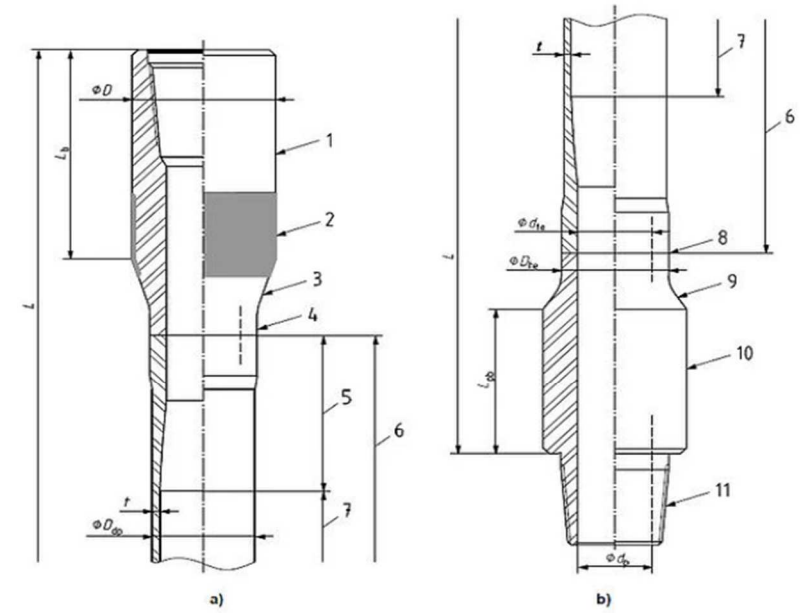

Key

1	tool-joint box	7	pipe body
2	hard banding (optional)	8	friction weld
3	tapered elevator shoulder	9	pin taper
4	drill-pipe weld neck	10	tool-joint pin
5	drill-pipe-body upset	11	rotary shouldered connection.
6	drill-pipe-body		

Figure 2.1: Schematic of a threaded tool joint showing both pin and box connection [10].

Tool joints are also categorised based on the type of upset. From Figure 2.2 the classification of upsets can be interpreted. Based on the types of upset, the non-threaded tool joint in our study the pin connection has an external upset, and the box connection has an internal-external upset. The grade of pipe is also a very important factor, and this has been set and standardised by the API. The four common grades are E-75, X-95, G-105 and S-135. Important to note here that in current investigation, S-135 stainless steel was used due to its high tensile strength compared to other materials used. There are other proprietary grades such as sour service grades which are used to resist Sulphide Stress Corrosion (SSC) and critical service grades which are used to resist high concentrations of carbon dioxide [11-12]. From a manufacturing perspective, the threaded section is manufactured separately and then welded to the rest of the pipe at a

manufacturing facility. The tool joints are responsible for providing high strength, high pressure resistance that are capable of surviving the harsh drilling conditions over numerous cycles of tightening and loosening of the threads and in turn the connections [13-15]

Figure 2.2: Different types of upsets [12]

2.3 Failure in Tool Joints

Failure in tool joint can be attributed to two significant factors: the mechanical wear due to tensile and torsional stresses and the material property degradation over time due to the harsh conditions such as high temperature and high corrosion. A study conducted on the failure analysis on the fracture of S135 drill pipe (Han et al., 2014) [16] stated that the primary failure of the S135 drill pipe under investigation was caused by sulphide stress corrosion cracking and this could have been avoided by using sour service grade drill pipes. However, it is important to note that materials with high anti-corrosivity properties lack high magnetic susceptibility that is required for the design of the non-threaded tool joint. Furthermore, it important to note that with the progression of technology, clients aim to use Logging While Drilling and Measurement While Drilling methods to save time and money. These methods desire the use of non-magnetic tool joints as the magnetic fields from the tool joints should not interfere with the information gathered by the logging and measurement components of the tool string.

A failure analysis study of drill pipe joint conducted by Zhang and Zhu (2019) [17] estimated that around 500 drill string failures occur in Chinese oil service fields which results in approximately 50 million dollar loses annually. This study attributed the failure of tool joints due to the complex alternating loads exerted on the tool joints. It is noted that in modern design methods, the failure

performance cannot be simply explained by using absolute values of stress and strain however, these stress and strain factors can be used to compare the advantages and disadvantages of different designs and to approximately provide a safety factor for the application. A Von-Mises stress yield criterion is typically used for the finite element analysis. Furthermore, fatigue life can be greatly improved by improving the surface geometry. This is an expected outcome as the stress on an object is directly proportional to the load being applied and inversely proportional to the area of contact. Since the conditions of the well and service are approximately a constant for any given situation, the only variable that can be changed to improve performance is the geometry and surface area of the tool joint. Other factors such as integrity of manufacturing and production also play a significant role in performance over time, but this is out of scope. Multiple studies make the use of the Von-Mises stress criterion for their finite element analysis and this is due to its common application in the drilling field where pipes are expected to be under high pressures and combined loading conditions. The Von-Mises criteria is used due to its theoretical identification of yield point of a component using the radial, axial and hoop components [18-21].

2.4 An Overview on Non-threaded Tool Joint Connections

The earliest non-threaded tool joint connection can be dated from 1938, by A.E. Nielsen [22]. Figures 2.3 and 2.4 show the pin and box connectors and an external cylindrical enclosure. The grooves in the box connection are used for packings to keep the joint sealed tight. The introduction of such a design challenges the use of the conventional threaded drill pipe connections but does not further expand on its installation configuration. Further investigation of the design shows that there are no geometrical features applied to any of the components to prevent torsional slipping during the drilling process. This is an important consideration, hence making this design invalid for further consideration.

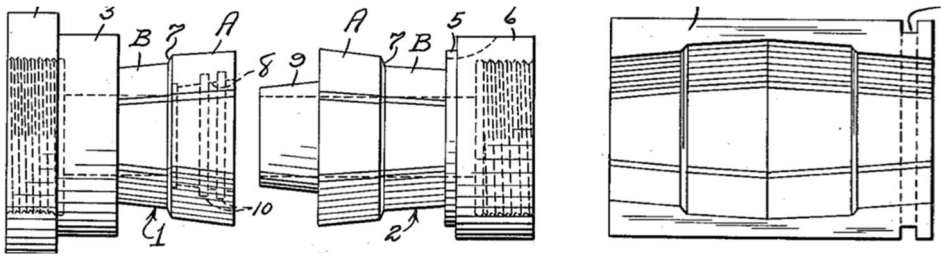

Figure 2.3: Non-Threaded Tool Joint Connection by Nielsen [22]

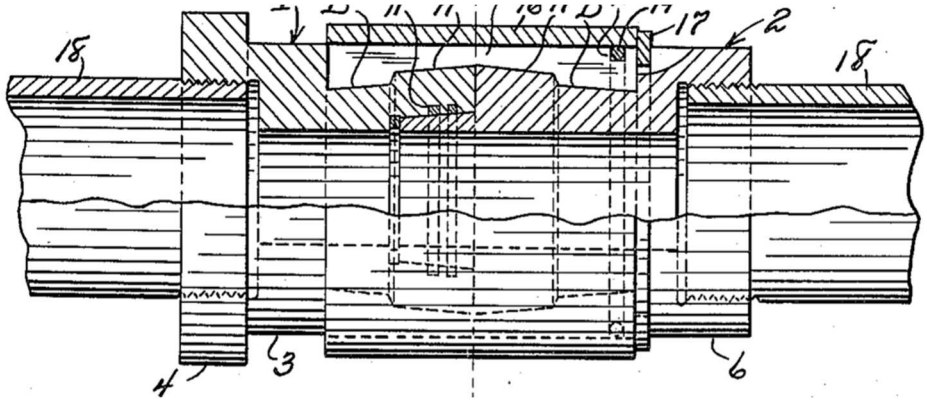

Figure 2.4: Pin and Box Connection (left) and external enclosure (right) by Nielsen [22].

The next design patented shortly after was in 1941, by Ohls [23]. This design concept proposed the introduction of 6 leaf springs, intricately manufactured into the pin connection as seen in Figure 2.5. This would allow for the pin to be easily connected to the box by simply applying a downward force, causing the pin to slide into the box. Once the pin is fully inserted into the box, the leaf springs would relax into their natural position, with the box "hanging" from the pin connection. The challenge here is during the disengagement process and this is resolved by having a series of small holes at the locations of the spring to apply a high pressure to cause the leaf springs to contract and hence remove the pin from the box. This design has not taken into consideration a few factors. The first being, under close inspection of the design, it would be noticed that the leaf springs would be bearing both the tensile load of the entire tool string as well as the torsional load exerted during the drilling process. The limited thickness of drill pipes and space for such a mechanism would not be able to handle such mechanical loads. Furthermore,

having an external hole for the sole purpose of actuation is not feasible as it leads to the risk of leakage. Furthermore, during the drilling process there are internal and external pressures exerted by the drilling fluids as well as the formations which can go as high as 15,000 psi. This means any drilling mud flowing to the annulus under high pressure could inadvertently actuate the leaf spring and cause it to disengage the connections, hence causing pipe to be lost in the well. From this model it should be understood that, if there are to be any extra components to the system apart from the pin and the box, it has to be sandwiched between the two components without any physical exposure to the internal and external environment. This requirement must be considered critically as it is also a particularly challenging parameter to overcome for this application.

The next design proposed in 1966 by Winberg and Mccurdy [24] consists of a rod like component used to lock the pin and box once connected. There are two problems with such a design, one is that the connecting rod ends are exposed to the harsh corrosive environments of the well, compromising their integrity over time in the well. Furthermore, upon investigation of Figure 2.6 it can be seen that connecting rod obstructs the flow of fluid through the pie and the internal diameter of the pipe is significantly reduced and this can result in concentrated flow of high pressure at the location of the joint which may cause the connecting rod to fail under high internal pressure and consequently result in the pipes from disengaging. The following design in 1969 by R.P. Vincent et al, as seen in Figure

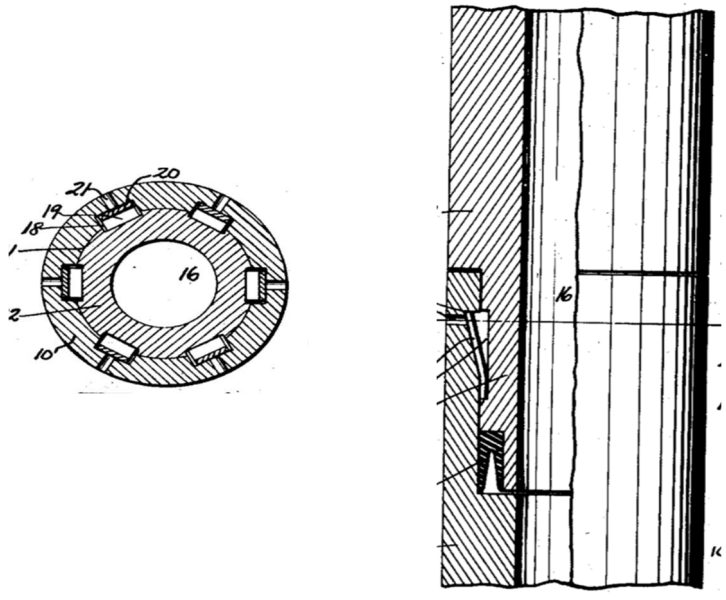

Figure 2.5: Pin and Box connection with leaf spring mechanism by Ohls [23].

2.7, uses a similar construct, however instead of a connecting rod, includes a geometric protrusion to handle the torsional stress and makes use of screws to simply connect the two pipes externally [25]. This is again an undesirable design feature as it exposes the screw to the harsh environments of the well and furthermore it is very reasonable to predict that two screws will not be able to handle thousands of newtons of tensile load exerted.

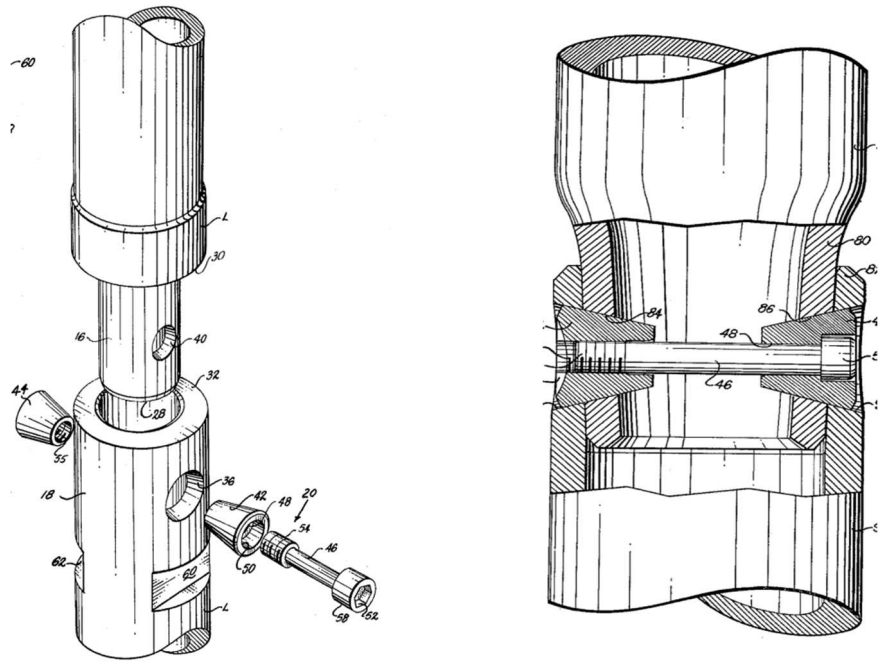

Figure 2.6: Non-threaded tool joint assembly by Winberg [24].

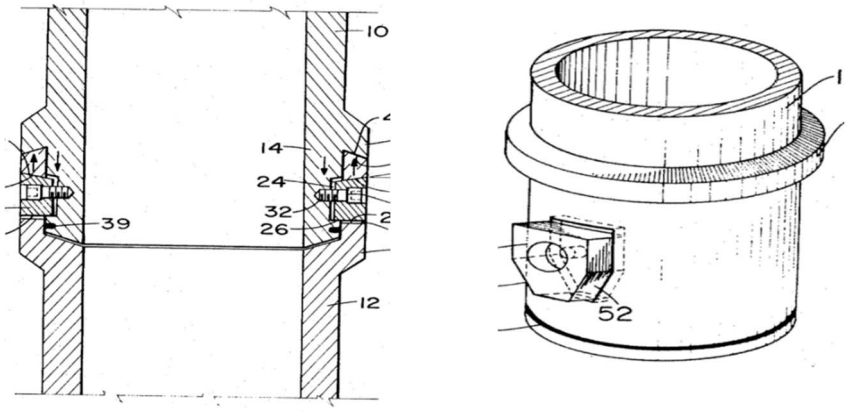

Figure 2.7: Non-threaded tool joint assembly by Vincent et al [25].

The next non-threaded tool joint connection proposal is seen in 1993, by Mefferd [26]. This design shares many similarities with the original design by Neilsen in 1938, however making improvements on the design. A tooth like design has been

integrated to both the pin and the box (Figure 2.8) and this feature would bear the torsional load exerted during the drilling process. The two connections are secured axially by an external enclosure which is locked with a simple lock mechanism. The issue with such a lock mechanism is that it is exposed to the external environment of the well and hence could be broken off to disengage the pipes downhole.

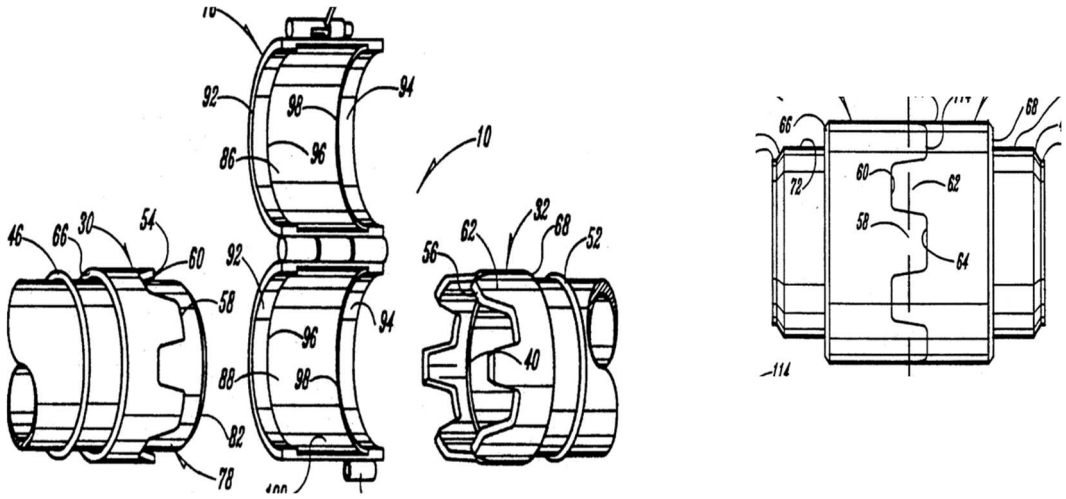

Figure 2.8: Non-threaded tool joint connection by Mefferd [26].

The next design proposal is rather an intricate design proposed by Lurie and Head [27]. The pin and box ends have complimentary step like geometry. A separate insertion tool has been proposed which would slide into the tool all the way till the end of the pin and then after a few processes this assembly would be stabbed into the box whilst "opening" up the box connector and once the two connections are aligned the, the internal insertion tool would be released, at which point the box connection would relax to its natural state and compress around the pin tightly as seen in Figure 2.9. This design does not consider the torsional slip that would take place and furthermore, the strength of the hold of the box on the pin is limited by the surface area and coefficient of friction which would be below the thousands of newton force exerted upon the tool string.

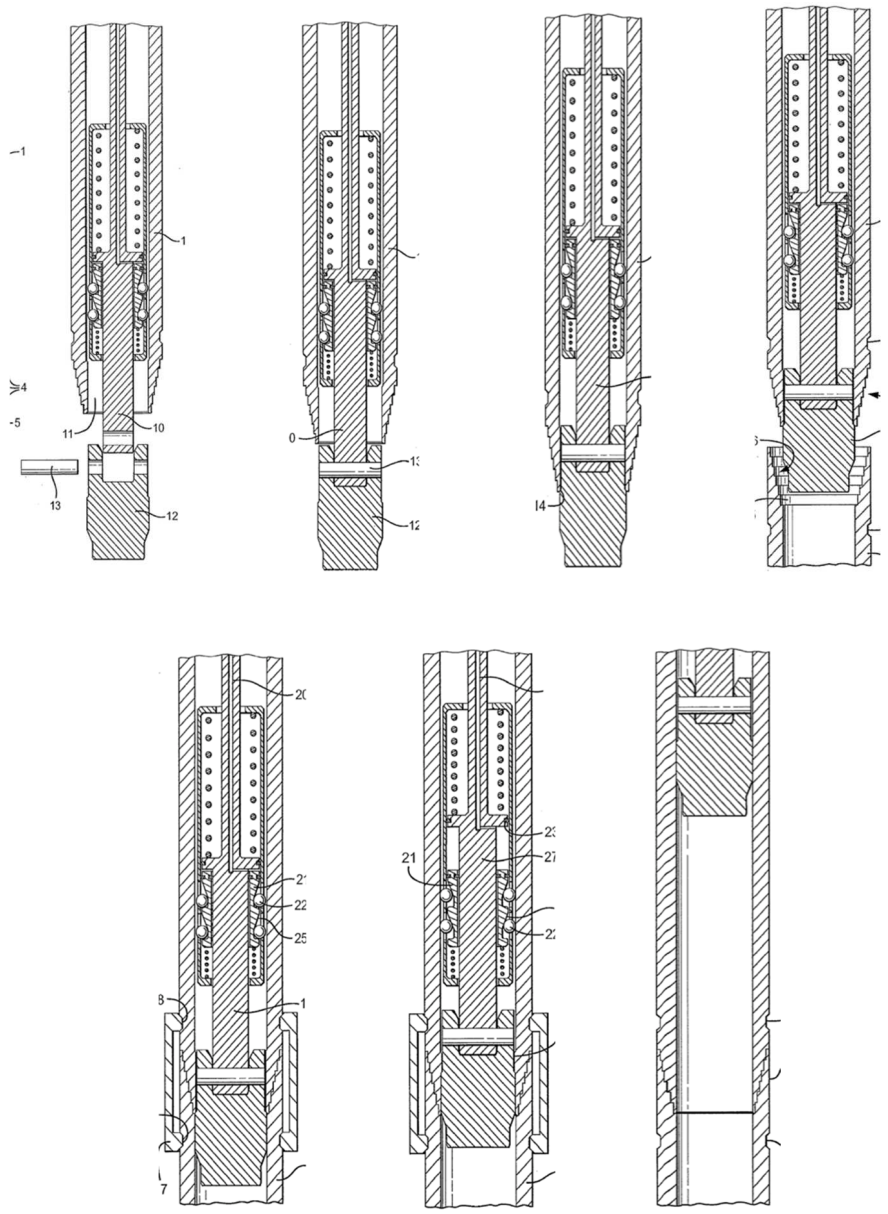

Figure 2.9: Non-threaded tool joint assembly process as proposed by Lurie and Head [27].

A model proposed by in 2010 by Buytaert [28], suggests the connection can be made by stabbing the pin into the box and then twist the pin whilst in the box to lock the connection axially. However, this mechanism prevents rotation in the backward orientation as this would cause the connection to slip apart. Furthermore, the design suggests having an external rod connection to further secure the connection (Figure 2.10).

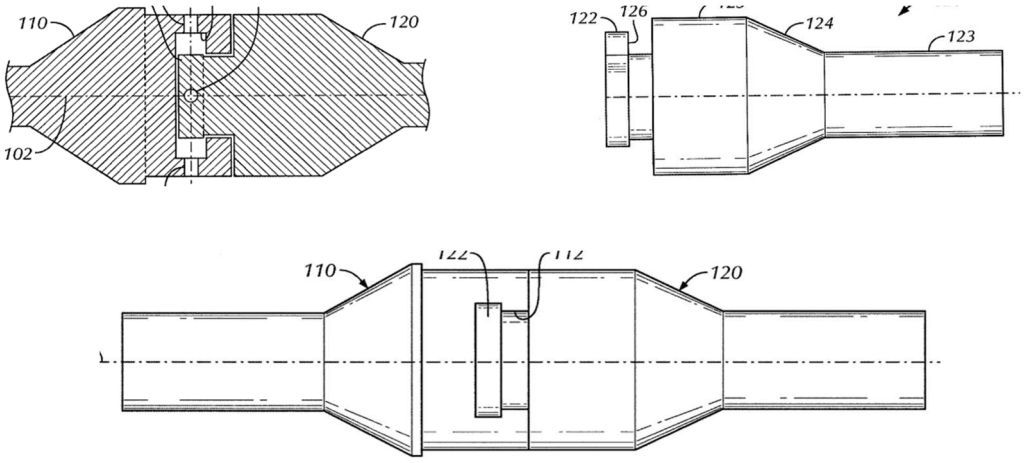

Figure 2.10: Non-threaded tool joint by Buytaert [28].

The latest design concept was proposed in 2013 by D. Hererra [29], which proposed the use of an electromagnetic snap-latch which would be sandwiched in between the pin and box connectors in grooved slots [29]. This concept overcomes the requirement of any physical actuation to lock the pipe connections axially, however this concept requires much investigation which will be further investigated in the later sections (Figure 2.11).

The series of patents and designs reviewed are only conceptual and there are no published sources available regarding the mechanical integrity of these designs. Hence the current investigation shall take the latest patent proposed and expand on its optimisation and further use CAD and simulation tools to understand the

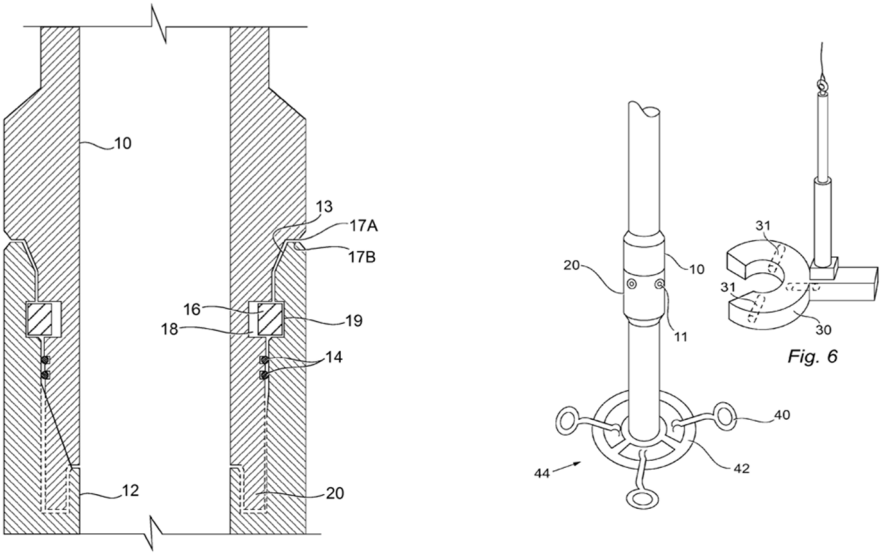

Figure 2.11: Non-threaded tool joint connection (left) and assembly process (right) by Hererra [29].

feasibility of the design for the required application. The following section will expand on the process of designing a new product and the engineering principles (primarily mechanical and magnetic) to take into consideration for this study.

2.5 Tool Joint design considerations and material selection

As per the IADC drilling manual, the tool joint is expected to successfully perform the following functions: Transmit and support axial and torsional loads as well as transmission of hydraulics. It is ideal for the box connection to be mechanically stronger than the pin connection as over time the box will be subjected to a larger range of wear. The connections strength is dependent on the strength of the steel used, the geometric parameters of the thread and coefficient of friction between the two connections.

However, for the design under investigation, only the type of material will be of a similar grade, i.e., S135 Carbon Steel which has a minimum tensile yield of 135 kpsi up to 145 kpsi. Mild steel will also be incorporate into design and will have a tensile yield range from 54 kpsi to 64 kpsi. The geometric design of the connections will be analysed using ANSYS-Static Structural in chapters 3 and 4. The feasibility of magnetic actuation has only been performed experimentally as a qualitative experiment to understand the potential of such an application.

Table 1: Chemical Composition (wt.%) of S-135 Grade Pipe [18]

C	Si	Mn	P	S	Ni	Cr	Mo	Ti	Cu	Fe
0.20	0.24	0.54	0.007	0.004	0.403	0.861	0.858	0.007	0.06	Balanced

2.6 Magnetostrictive Materials

Magneto-strictive materials consist of ferromagnetic particles such as iron, nickel or cobalt which have magnetic moments due to their electron configuration. On the application of a magnetic field the material will change its shape either enlarging or shrinking based on its electron configuration. This change in magnetic field that causes a change in the materials dimension is a consequence of *Magnetocrystalline Anisotropy* [30,31], a phenomenon which results is energy being absorbed more in one direction which produces an overall strain in the material once the material has achieved full saturation. If a mechanical force is applied to these materials, a magnetic field will be induced. Current applications include fuel injection systems, active noise and vibration cancellation systems and small-scale sensors and actuators. The volume change under magnetization for such materials is in the order of 10^{-6}.

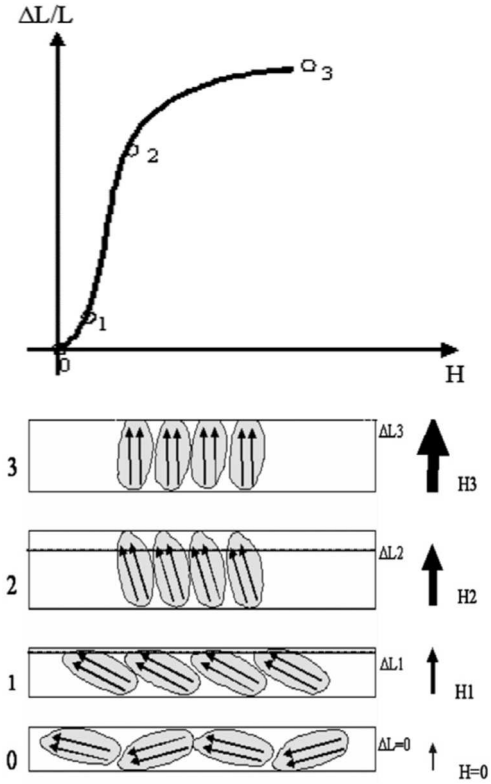

Figure 2.12: Strain vs Magnetic Field Trend of Magneto-strictive Materials and electron moment change with field [32].

Figure 2.12 shows the change in length with magnetic field, with the region from 0 and 1 showing low magnetic field. The region from 1-2 is a linear relationship and this is the region where most devices operate within, due to ease of predictability. Beyond point 2, the relationship is heading towards a saturation limit which is reached at point 3 where all the magnetic domains have become aligned with the magnetic field direction [32].

Some materials with high magnetostriction are Tb-Fe_2, Terfenol D, Sm-Fe_2 and Ni-Mn-Ga. Rare earth materials like Tb and Sm have large magnetostriction but only at low temperatures and hence their mixture with Fe as Tb-Fe_2 and Sm-Fe_2 allow for high magnetostriction at room temperature. Terfenol D has high magnetostriction but is limited due to its brittleness and expense due to the rare earth composition (Tb-Dy). Terfenol D has a high compressive strength but a

rather low tensile strength of 40MPa. Such materials are not applicable for high stress applications and hence there is a need for stronger magneto-strictive materials such as Ni-Ga, Fe-Ga and Fe-Al which have relatively low magnetostriction [33] and this is undesirable due to the large change in deflection expected in the snap latch design.

NiMnGa alloys are known due their effective magnetocaloric effect and potential applications in magnetic refrigeration devices. According to one set of experiments conducted by Zuberek. R et al (2018) showed, for low amplitudes of magnetic field and strain modulation, the magnetoelastic effects in thin films of polycrystalline NiMnGa alloys at room temperature (23 degrees Celsius) is relatively weak [34]. Another experiment by Zhao and Kang (2018) concluded that at roughly 5 to 17 degrees Celsius, NiMnGa strips can undergo a strain of 9.3% with complete retraction to original shape once the magnetic field is removed [35].

2.7 Magnetic Properties

This section will outline the relevant literature for Magnetic Properties and layout the fundamentals as well as equations that help understand the actuation basis. [36][37]. A magnetic field is the force between two magnetic poles is directly proportional to the product of their pole strengths, p, and inversely proportional to the square of the distance between them.

$$F \propto \frac{p_1 p_2}{r^2} \propto H p_2 \longrightarrow F = \frac{1}{4\pi\mu_0}\frac{p_1 p_2}{r^2}, newton. \qquad [1]$$

Where:

F is the Force

p_1 and p_2 are the Pole Strengths of two separate attracting objects but have equal strength

r is the distance between the poles

μ_0 is the permeability of Free Space

H is Magnetic Field Intensity

Meaning,

$$H \propto \frac{p_1}{r^2} \longrightarrow H = \frac{1}{4\pi\mu_0}\frac{p}{r^2}, \frac{ampere}{m} \qquad [2]$$

Magnetic Flux (Φ) is the amount of magnetic flux passing through an area A is equal to the product of the Magnetic Field Strength and the Area.

$$\Phi = \mu_0 \mathrm{HA}. \qquad [3]$$

When a magnetic field 'H' is applied to a material, the response of the material is called its magnetic induction 'B' and the magnetization vector is 'M'. This relationship between B and H is a property of the material.

$$\mathrm{B} = \mu_0(\mathrm{H} + \mathrm{M}), tesla \qquad [4]$$

The magnetic induction B is same as the density of flux Φ inside the medium. Flux density varies inside and outside the material. Materials are classified based on the difference between their internal and external magnetic flux.

- If $\Phi_{internal} < \Phi_{external}$, material is diamagnetic [bismuth and helium]
- If $\Phi_{internal} > \Phi_{external}$, material is either paramagnetic [Na and Al] or antiferromagnetic [MnO and FeO]
- If $\Phi_{internal} \gg \Phi_{external}$, material is ferromagnetic of ferrimagnetic

When a magnetic field is applied to a material, it will begin to magnetize depending on its properties and this measure of how much it can be magnetized is known as

Magnetic susceptibility. Magnetic susceptibility further describes a materials ability to be attracted or repelled from a magnetic field. Magnetic permeability is the measure of the ability of a material to retain the formation of a magnetic field within itself. A material which has a concentration of large amount of flux density in its interior has a high permeability [38]. The ratio of M to H is called susceptibility and the ratio of B to H is called permeability

$$\chi = \frac{M}{H}, dimensionless \qquad [5]$$

$$\mu = \frac{B}{H}, \frac{henry}{m} \qquad [6]$$

2.8 Magnetic Material Classifications

Diamagnetism

In a diamagnetic material the atoms have zero net magnetic moment or paired electrons in the presence of no magnetic field. Susceptibility is very small and negative, -10^{-6} to -10^{-8}, such that magnetization decreases as the magnetic field is increased. Diamagnetic materials possess repulsive nature in the presence of a magnetic field however due to its weak magnetization is insignificant at the physical scale and requires high values of Tesla force for any kind of deflection. Essentially all 'non-magnetic' materials are considered Diamagnetic in nature [39]. Diamagnetic materials have a relative magnetic permeability that is less than or equal to 1 and a magnetic susceptibility that is less than or equal to zero. Susceptibility is also temperature independent in such materials.

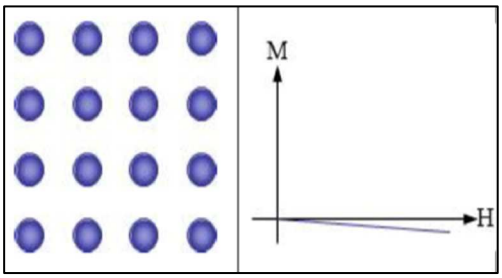

Figure 2.13: Atomic behaviour and magnetisation curve of diamagnetic material [40]

Paramagnetism

Paramagnetic materials have a net magnetic moment due to unpaired electrons in the partially filled orbits and are non-magnetic in the absence of a magnetic field. In such materials the magnetic moments are weakly coupled to each other and hence thermal energy causes random alignment of the magnetic moments [41]. In the presence of a magnetic field, the moments start to align, but only a small fraction is deflected along the magnetic field. Susceptibility is very small but positive, $+10^{-5}$ to $+10^{-3}$, and hence permeability is slightly greater than 1.

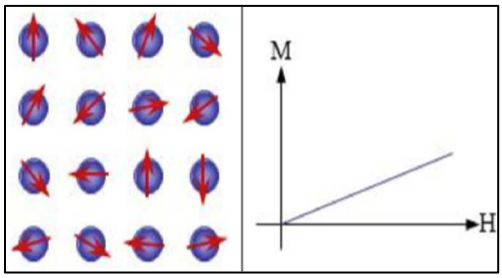

Figure 2.14: Atomic behaviour and magnetisation curve of paramagnetic material [40]

Ferromagnetism

These are materials that are visibly magnetic in nature as the atomic moments is such materials exhibit very strong intermolecular interactions which result in parallel alignment (all moments aligned in one direction) of atomic moments. The susceptibility is very large for such materials and results in the material creating a significant attractive force in the presence of a magnetic field.

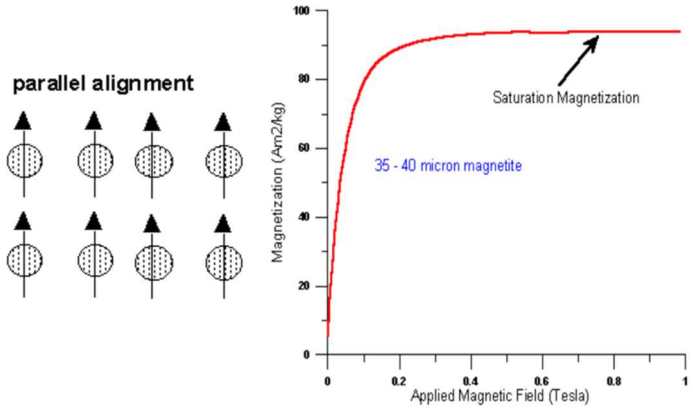

Figure 2.15: Atomic behaviour and magnetisation curve of ferromagnetic material [41]

The figure above shows the magnetization curve of a ferromagnetic material. The saturation magnetization is a threshold maximum induced moment that can be

attained in the presence of an applied magnetic field. The saturation magnetization is an intrinsic property of the ferromagnetic material that is independent of geometry but dependent on temperature. If placed in a high temperature environment that exceeds its Curie Temperature, the internal atomic structure of the ferromagnetic material will change, and its susceptibility and permeability will decrease to a behave non-magnetically. After the magnetic field is switched off, the ferromagnetic material may now behave like a magnet on its own based on its remanence characteristic which is the magnetization left behind after the magnetic field is removed. To remove this magnetic field a Coercive Force must be applied to reduce the remaining magnetic flux in the ferromagnet to zero.

Anti-ferromagnetism

Antiferromagnetic materials on an atomic level have an aligned atomic behavior like ferrimagnetic materials however, the magnetic moment in both directions are equal and effectively cancel each other out and behave paramagnetic in nature. In a magnetic field an Antiferromagnet will show ferrimagnetic properties which makes sense do their atomic alignment and this will vary with change in position in magnetic field [41]. Susceptibility is low for such materials, $+10^{-5}$ to $+10^{-3}$.

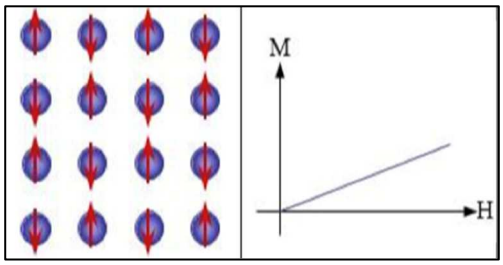

Figure 2.17: Atomic behaviour and magnetisation curve of antiferromagnetic material [40]

Curie Temperature

Curie Temperature is the temperature at which magnetic materials undergo an immediate change in their magnetic properties. Once the material is exposed to a temperature above its Curie Point, its magnetic properties will diminish, and this is of importance to our project due to high temperatures at downhole operations. The temperature above the Curie Point in ferromagnets results in the magnetic moments getting excited and no longer remain the parallel alignment that produces the overall attractive force [43].

2.9 Mag-Switch Magnets

The Application of Mag-Switch Magnets has been considered for this research due to its strong magnetic pull strength and capability of being switched OFF and ON without the need of an electrical supply. The Mag-Switch Magnets of high pull strength and field line can be capable of causing deflection in the SLR ring upon activation. The Mag-Switch Magnets are made of magnetically saturated ferromagnets with two poles. Two of such cylindrically manufactured magnets are placed one on top of the other as seen in Figure 2.18. When the two poles of both the magnets are aligned, the resultant magnetic field is in alignment to attract ferromagnetic objects with the strength rating of the Mag-Switch Magnet, which is a function of the Switch magnets geometry and material composition as well as saturation limit. To switch the Mag-Switch off, the top magnet is rotated 180 degrees mechanically and the resultant magnetic fields cancel each other out and hence the mag-switch device is non-magnetic or OFF [43,44]. This is mechanism is helpful in the snap latch design process as activating the magnet should actuate and open the snap latch rings and by deactivating the magnet the snap latch rings retract back to their natural position. This is preferred over the method of applying a voltage to induce a magnetic force as it would eliminate the need for an electrical source on the rig floor.

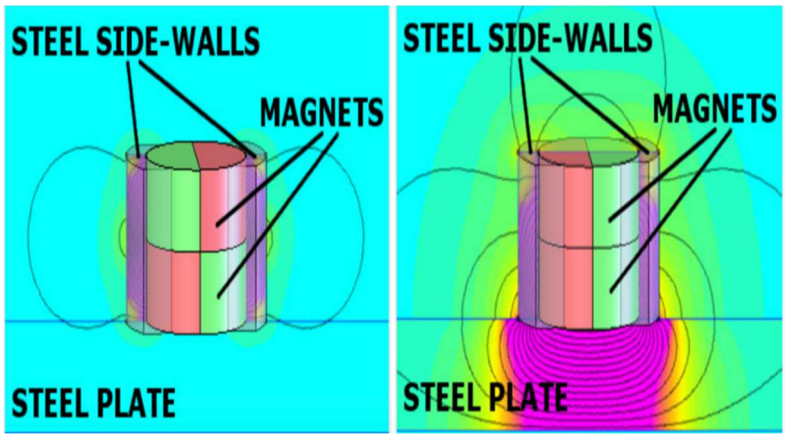

Figure 2.18: Mag-switch function diagram: Switch OFF (Left) and Switch ON (Right) [43].

2.10 Summary of the Literature Review

The literature review has provided an insight to anatomy of a tool joint, materials and the common types of failures and causes. Currently there exists no comparable literature or evidence with respect to the actuation of a snap-latch based non-threaded tool joint. Multiple practical methods and models have been reviewed in this chapter with their potential applications and limitations identified. This is critical in understanding what aspects from these designs can be adopted in producing a final working product. Identifying the limitations of each design assists to prevent making similar errors in the current design and also provides a different perspective for problem solving associated with this product and its desired application.

Material selection has been kept simple and realistic to what would be used in the industry and core principles of magnetism and magnetic properties have been touched upon to understand the feasibility and application potential of magnetic actuation of the snap latch ring. The use of a Mag-switch magnets has been adopted due its safe working principle and ease of use whilst also providing and experimental display of the feasibility of magnets on ferromagnetic metals.

Hence using the literature and finite element analysis approach, a set of parameters for operation have been identified using a safety factor for the desired application.

Chapter 3

CONCEPTUAL DESIGN OF THE SNAP LATCH

3.1 Introduction

This section will expand over the existing design concept along with the proposed application process. It will further display the alternative snap-latch concepts with proposed methods of production as well their current potential/limitations for the purpose of high tensile and radial load bearing.

3.2 Overview of the Existing Design Concept

The current design consists of three components, the pin connection, the box connection and a set of 6 snap-latch rings used to connect the two pipe segments together as seen in Figure 3.1. The figure shows the three components separately, the snap-latch ring as a part of the pin connection and finally the assembly as a complete connection. Figure 3.2 provides a radial view of the system where the snap-latch is in its relaxed state within the pin connection. An electromagnetic field is applied which results in the snap-latch to compress within the grooves of the pin connection and once the pin and box are completely connected, the

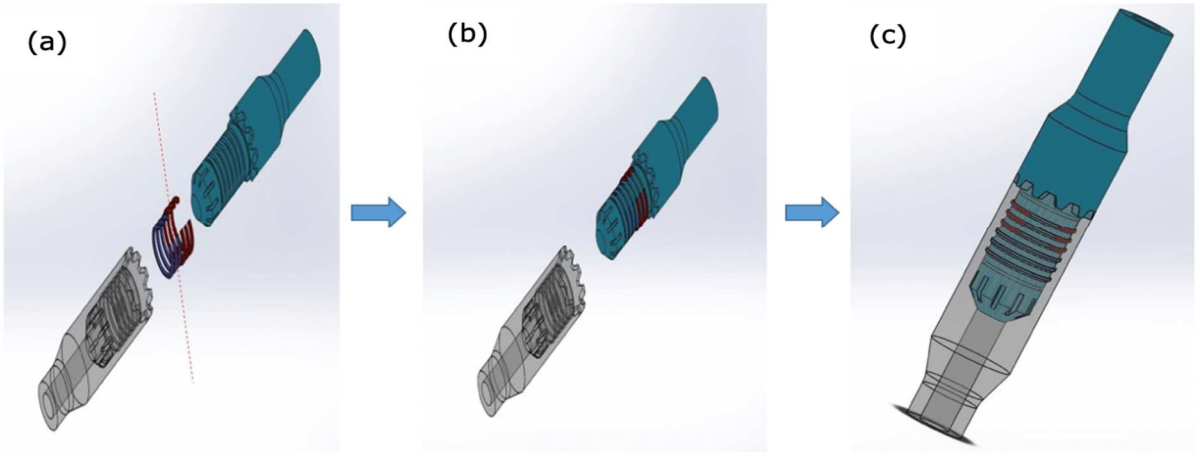

Figure 3.1: (a) Pin, Box and Snap Latch Ring Components separately (b) Snap Latch assembled onto Pin (c) Pin and Box connected with visible positions of the Snap Latch Rings

electromagnetic field will be removed causing the snap-latch ring to retract back into its natural shape, locking the pin and box together axially. Hence the bulk of

the stress would be exerted on the snap-latch ring and would be the key component to be optimised and analysed for this application. Furthermore, Figure 3.3 shows a chart with two possible actuation methods for the snap-latch system. The first corresponding to figure 1.2 and the other as an alternative where the snap-latch ring is inserted into the box connector.

3.3 Conceptual Design of new Snap Latch Rings

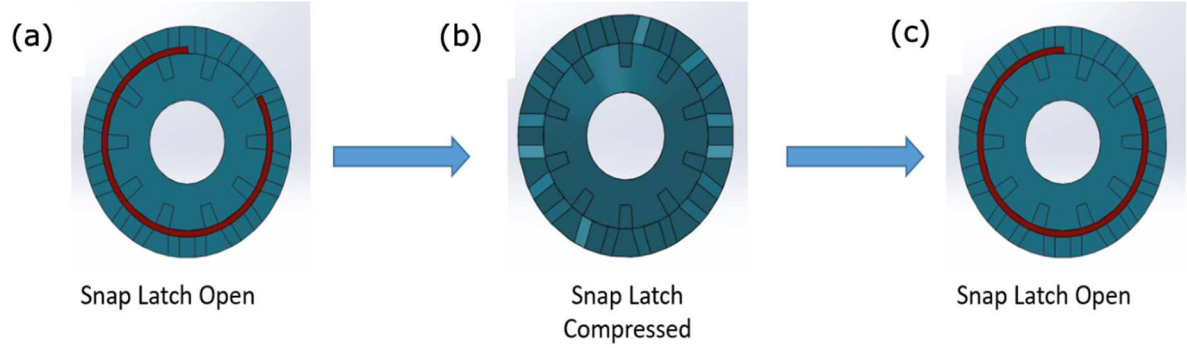

Figure 3.2: (a) Snap Latch Ring assembled onto Pin (b) Snap Latch Compressed into Pin while Pin is inserted into Box (c) Snap-Latch Ring relaxing back to original position locking Box and Pin together

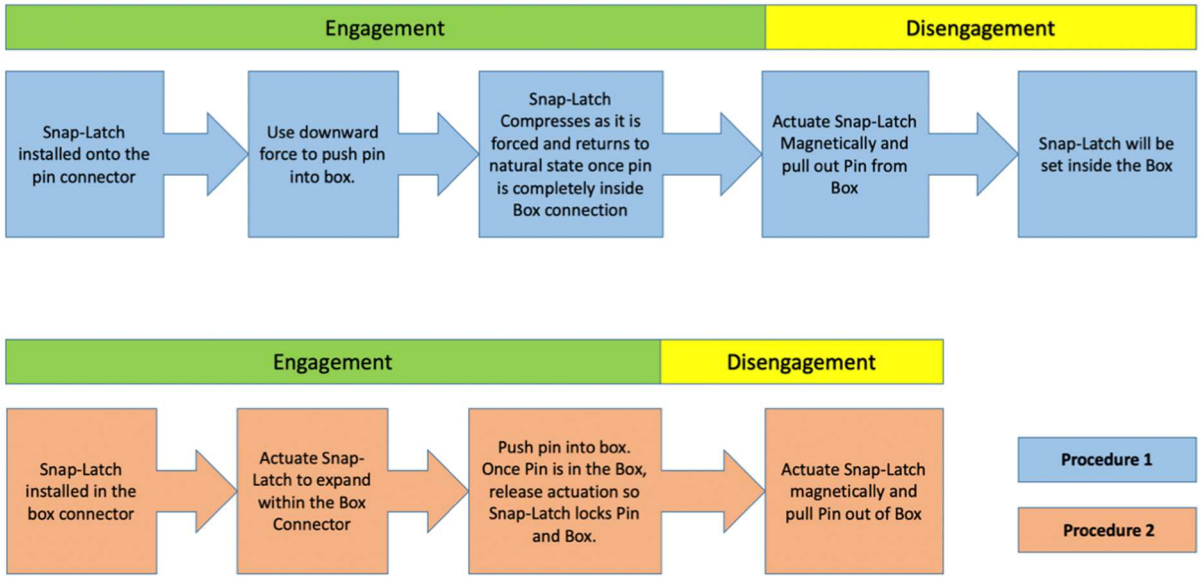

Figure 3.3: Flow Chart showing the two methods of operation based on whether the Snap Latch Ring is initially assembled on the Pin or Box connector

Several alternative models were considered during the duration of the project. Upon further critical analysis, the options were concluded not currently feasible due to technological capabilities such as available geometric space and the tensile

yield strength and magnetic permeability properties, but some key aspects should be considered for further work or application to other requirements.

3.3.1 Spiral Snap Latch Ring

An alternate to the single body Snap-Latch Ring and the 6 separate Snap-Latch Rings Prototype I, the Spiral Snap Latch Ring would be a single coil inserted into the Pin or Box connector and then upon magnetic actuation would open during engagement of pipes, as shown in Figure 3.4. Limitations of such a model include manufacturing of a singular piece to possess both high mechanical strength of operational drill pipes whilst possessing reasonably high magnetic permeability. Furthermore, due to lack of contact area the Spiral Snap-Latch Ring would not be able to handle high tensile loads.

Figure 3.4: 3D printing of spiral Snap-Latch Ring design (6 ring module), showing various views, at full made of Acrylonitrile-Butadiene-Styrene (manufactured using the INTAMSYS FUNMAT PRO HT 3D printer at School of Engineering in Robert Gordon University.

3.3.2 Torsion Spring Snap Latch

Based on Prototype II, torsion spring snap-latch ring (6 ring module) can also be an alternative design which can be produced by means of 3D printing, Figure 3.5. Upon further investigation it was found that there is a possibility of 3D production of singular component which may have high mechanical strength and high magnetic permeability. However, the technology is still behind, and 3D metal

manufacturing as a whole is still a new subject of study, a study which is being explored with Additive Manufacturing Research Group, University of Birmingham.

Figure 3.5: 3D printing of torsion spring snap-latch ring (6 ring module, Prototype II), showing various views, at full made of Acrylonitrile-Butadiene-Styrene (manufactured using the INTAMSYS FUNMAT PRO HT 3D printer at School of Engineering in Robert Gordon University (CAD model in Appendix I)

3.3.3 Segmented Snap Latch Design

A new model for the Snap-Latch Ring was proposed, which included multi-elements segmented design to actuate the ring. The idea was to include multiple magnetic parts inserted in the outer periphery of tool joint steel (S135), as shown in Figure 3.6. Figure 3.7 shows the link segments to secure primary segments. Figure 3.7 shows segmented snap-latch design in natural and actuate position. Figure 3.7 shows segment Snap-Latch Ring in natural and actuated position. Figure 3.8 shows operational diagram on Segmented Snap Latch Ring.

This segmented snap latch ring is made of multiple components: the frame which will withstand the tensile strength exerted on the entire assembly, the magnetic components which will pull/attract the segments outward changing the nominal diameter and the magnetic components which will attract the segments to each other returning the segmented snap latch ring to its natural position which will have a different nominal diameter.

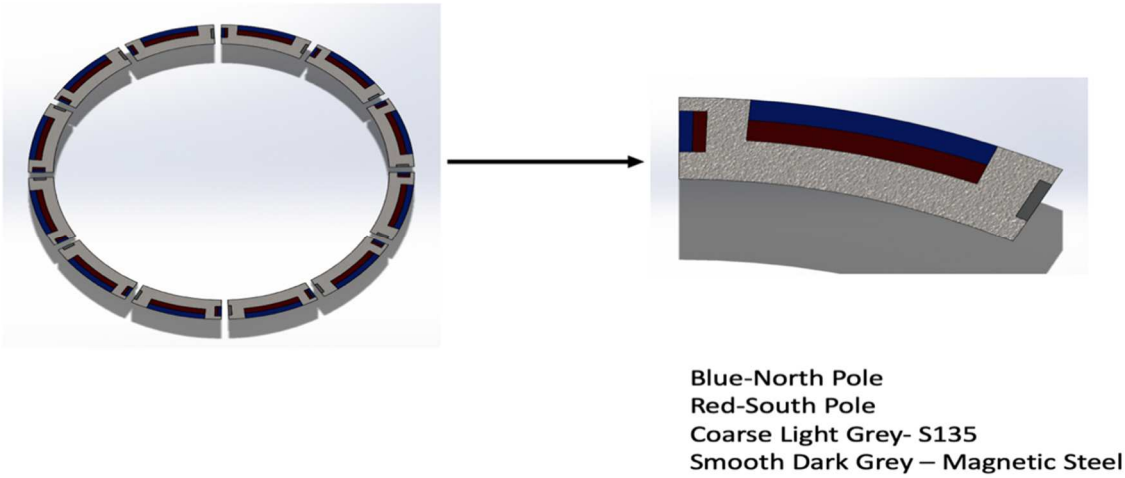

Figure 3.6: Segmented snap-latch design: Full-scale conceptual model.

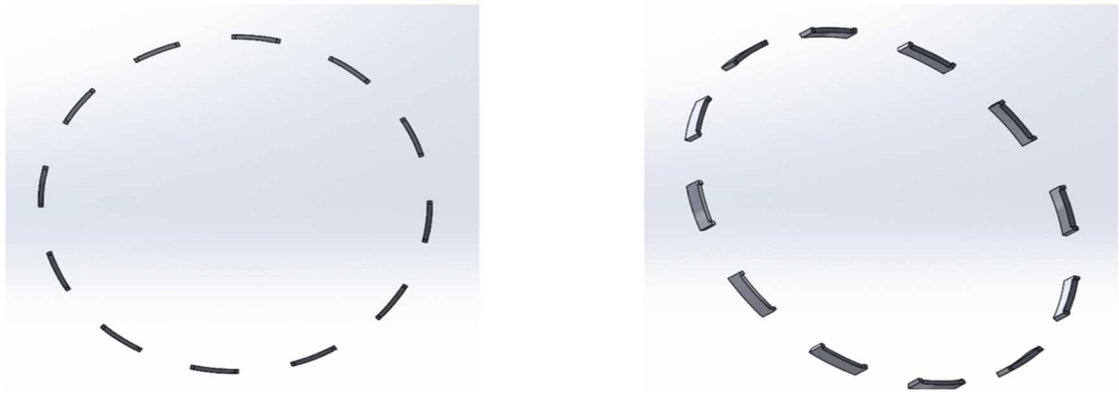

Figure 3.7: Segmented snap-latch design: Link segments to secure the primary segments.

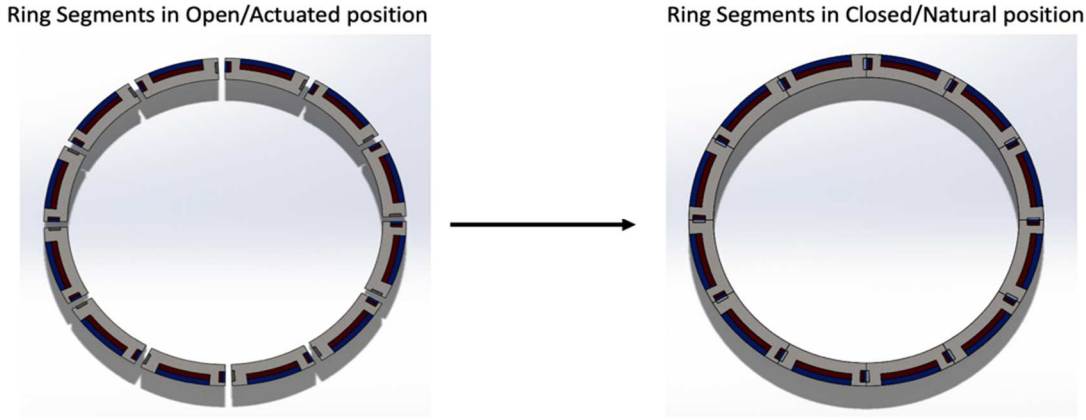

Figure 3.8: Segmented snap-latch design in open and closed position.

3.3.4 Actuation of Snap-Latch Ring as Assembly

Several options are to be considered for actuation of the Snap-Latch Ring as part of the assembly. The first option was that a hydraulic force could be applied to the Snap-Latch mechanism for the actuation process. It was acknowledged that this option may not be applicable to the current requirement but may be applicable for other pipe joint applications. It is important to note that Snap-Latch Ring is a component that is placed between the Pin and Box connectors in the assembly and hence to actuate it requires a physical connection from an external source. This implies that Pin or Box would have to have an opening (visible externally) to allow for the Snap-Latch Ring to be actuated. Hence due to the constraints of the assembly, the actuation must be non-contact. This is where magnetism and magnetic principles can be potentially applied.

The second option was to use magneto-strictive materials (materials that change shape/geometric dimensions when a magnetic field is applied) as part of the Snap-Latch Ring design. It was acknowledged that even the most advanced Magneto-strictive material made of Nickle-Manganese-Gallium (Ni-Mn-Ga) only has a maximum change in shape by 9.5%. The current thickness of the Snap-Latch Ring is 12 mm. To successfully actuate into the Pin/Box mechanism it must expand 6 mm to lock the system into place. This means the material used would have to be able to expand by 50% in order secure the system. A 9.5% change in geometry has no significant application to this system other than acting as a sealant. Furthermore magneto-strictive materials have low tensile load strength, not making them suitable for the application. Furthermore, when considering magneto-strictive materials, temperature and corrosivity are important considerations.

Further consideration was given to the use of magnetic steel Snap-Latch Rings for successful actuation. This can be done by applying a magnetic field that causes the ring to bend outward or inward (expand or contract) depending on the location of the Snap-Latch Ring within the assembly. The ring would be circular but with a gap to allow for assembly onto the Pin/Box connector as well as allow for room to expand within the confines of the Ring and Box Connector. A Snap-Latch Ring completely of magnetic steel would not be an ideal choice due to its low mechanical strength and low corrosion and temperature resistance. Furthermore, the Snap-

Latch Ring must possess radial flexibility in order to open/close within the confines of the Pin and Box Connections. Hence the proposed model for the Snap-Latch Ring would have to be a part made on many parts (minimum 3) to possess all the properties desired. This consideration involved looking into using a magnetic field/force which will cause the Snap-Latch Ring to actuate. However, there are other important considerations for the successful functioning of the Snap-Latch Ring. From the previous section, we know that the Snap-Latch Ring needs to expand and contract within the confines of the Pin/Box connectors, meaning the Snap-Latch Ring must first be assembled onto either Pin or Box connection. This is completely impossible if the Snap-Latch Ring is made as one singular component, meaning there must be at least two segment that make one complete ring. Furthermore, each segment must be made of two components; one to handle the maximum tensile load and one flexible component to cause the actuation of the Snap-Latch Ring. This further leads to the understanding that such a device will be complex and heterogeneous in nature.

As per current design the Snap-Latch Ring is proposed to be assembled onto the Pin connector. As seen previously from Figure 3.3, the Snap-Latch Ring is initially in its natural state. A magnetic field is applied that causes the ring to compress into the allocated area of the Pin whist the Box connector is being joint and once successfully connected the magnetic field will be released and the Snap-Latch Ring should retract back to its natural shape. This mechanism for actuating and releasing the snap latch ring will be performed by either the use of mechanical switch magnets or by using an electrical source to generate the magnetic field. From theory and literature review it is found that traditionally magnetic forces on a magnetic material (not a magnet) attract not repulse them, meaning in the case of the Snap-Latch Ring, the component would have to retract outward into an allocated area of the box.

A number of Snap-Latch Ring prototypes were conceptualized as potential solutions for this project. The first concept Snap-Latch Ring has a central torsion ring which provides the flexibility to open outward (Figure 3.9a), however this means having to design a spring small enough and strong enough to keep the ring positioned in its original nature as well as cause it to retract back to this original position after the magnetic field is removed.

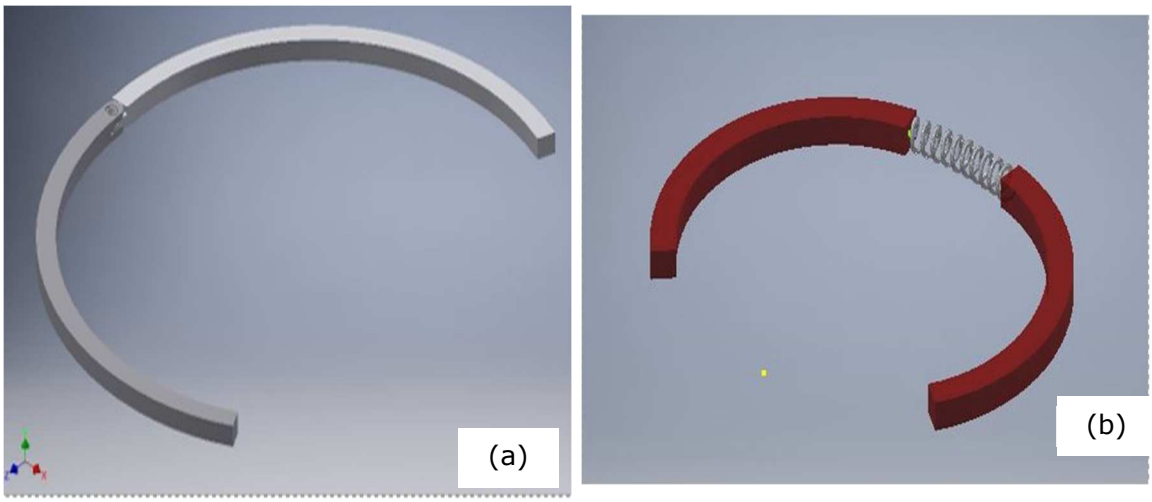

Figure 3.9: Snap-latch ring conceptual ideas: (a) snap-latch ring with two actuating arms pivoted by a torsional spring (b) snap-latch ring with actuating arms connected by compression spring.

Figure 3.9a shows Prototype I redesigned on simulation package (using ANSYS Workbench) with a few minor changes. There are several segmented sections, and these are for the purpose of Static-Structural Load Analysis which will be discussed in the following sections.

The second concept Snap-Latch Ring with a compression spring would be expected to do the same (Figure 3.9b), however due to the complex geometry of the spring between the two side arms, this would be very difficult to manufacture and due to being a significantly big compressions spring it would not be stable within the confines of the Pin/Box connections.

As shown in Figure 3.9a, the Snap-Latch Ring (Prototype I) was selected as the design for simulation test and physical production. The reason such a design was expected to work is because a thin strip can act as a flexible spring/leaf spring, keeping the arms in stiff position, and when a magnetic field is applied the arms would pull back and the thin strip would retract the arms back to its original position. This design keeps to the original constraints of 12 mm height and 12 mm width grooves in the Pin/Box connectors. The thickness of the thin strip is 4 mm, with a tapered height of 6 mm to 4 mm. A tapper feature which prevents the mid body from slipping out of the arms and keeps the entire ring system secured has been utilized and discussed in chapter 5.

3.4 Summary

This chapter has established the methods and process undertaken for the research. The primary design for pin and box connections as well a number of designs for the snap-latch ring have been explored with their potential applications whilst also stating their limitations. The ideal snap-latch ring design would require the strength to bear a very high tensile load axially however possess flexibility to retract outward and inward during magnetic actuation.

Furthermore, different actuation processes have been explored where it is apparent the best possible method for actuation would be through magnetic actuation, however even this possesses many challenges due to limited surface area available for magnetic attraction as well as physical properties of metals used in the oil and gas industry. The design complexities associated with the production of such a multifunctional product are addressed, mechanical strength, magnetic susceptibility and overall product usability.

The segmented snap-latch design would be the most desirable product as it would change diameters from natural to actuated state with magnetic actuation. However, such a product would require complex production which was beyond the scope of our research for development. Furthermore, multi-alloy metals where certain metals dominate certain regions is still a very new subject and requires further investigation being a research subject of its own.

It is also key to remember for a product design-oriented research, there must be consideration and justification of resources and long-term usability of product. The finished snap-latch assembly must be manufactured of minimal parts as possible as too many components present in downhole well intervention applications is not desired due to increased risk of failure and lost time during operations. Hence all efforts have been made to simply the design for our current analysis to assess feasibility of the research and its objectives.

Chapter 4

FINITE ELEMENT ANALYSIS AND DESIGN OPTIMISATION RESULTS

4.1 Introductions

This section presents CAD design and FE modelling methodology for tool joint of 8.3-inch (210 mm, see **Appendix A**) size, including snap latch (based on design of Pin and Box connections and snap latch design), i.e., models of snap latch Prototype I, see **Appendix C**). The chapter further shows the results based on the different parameters applied based on the boundaries available to optimise the tensile strength of the snap-latch ring.

4.2 Material Selection

For the design Grade S135 Stainless Steel (properties in **Table 2**) was finalized for tool joint (**Appendix A**) and part of the snap-latch ring due to its performance and current use in the deep well drilling industry, which has a low magnetic permeability. Mild Steel (for the thin strip part of the snap-latch ring, see **Appendix C**) for has been selected as the magnetic component due to its ease of availability, machinability and considerably modest strength properties.

Table 2. Mechanical properties S135 stainless steel and mild steel [44].

Properties	Grade S135 Stainless Steel Alloy	Mild Steel
Density	8000 kg/m^3	7870 kg/m^3
Youngs Modulus	200 GPa	205 GPa
Poison's Ratio	0.3	0.29
Tensile Yield Strength (max. allowable stress)	1,034 MPa / 149,969 psi	370 MPa / 53,664 psi
Tensile Ultimate Strength	1,137 MPa / 164,908 psi	440 MPa / 63,817 psi

4.3 Theoretical Modelling for Torsion Spring

The Snap-Latch requires freedom of motion so that It can snap inward and outward as required when actuated magnetically. If a solid piece of Stainless Steel were to be used, this would leave us with two problems. Can the Stainless-Steel ring be actuated magnetically? And if so, after deformation will it retract to its natural shape which is required to bear the tensile loads from the pin and the box during operation?

The Snap-Latch mechanism for our application has two key requirements: that it be flexible and can be magnetically actuated. A spring would be an ideal solution as is would allow for the degree of deflection we expect while at the same time it can be made from a Steel Alloy that displays strong magnetic properties. Since the spring will be encapsulated within the Snap-Latch securely it will not be affected heavily by the tensile and compressive tests and hence would be an ideal solution to the challenge faced. The Spring would only be affected by the radial force that it requires to open the snap latch ring.

A Torsional Spring is considered due to its simplicity, yet versatile feature. Theory will be mentioned as follows (Budynas and Shigleys.[45]):-

$$C = \frac{D}{d} \quad [7]$$

C is the Spring Index, preferred ranges from 4-12

D is the Mean diameter of the Coil

d is the diameter of the Coil Wire

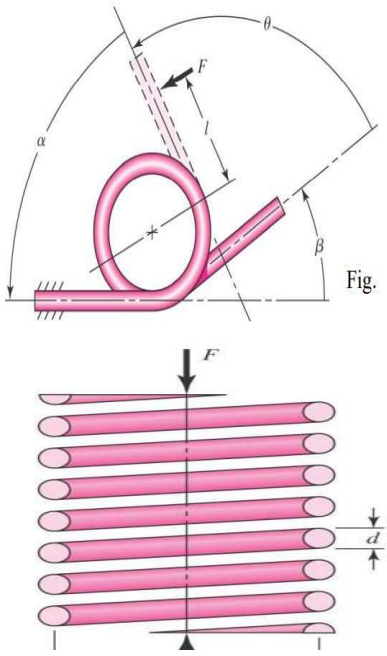

Figure 4.1: Torsional Spring Schematic Diagram [6]

C < 4, Spring is not practically applicable

4 < C < 12, Ideal Spring Range

12 < C <25, Manufacturing difficulty, expensive

C > 25, Hard to Manufacture, not commercially used

$$K_i = \frac{4C^2 - C - 1}{4C(C-1)} \qquad K_o = \frac{4C^2 + C - 1}{4C(C+1)} \quad [eq.8]$$

K_i Inner Stress Correction Factor

K_o Outer Stress Correction Factor

$$S_{ut} = \frac{A}{d^m} \qquad [MPa] \qquad [9]$$

$$\sigma = S_{ut} \times 0.78 \qquad [MPa] \qquad [10]$$

S_{ut} is the Ultimate Tensile Strength

A and m are constants obtained from the spring handbook as per choice of the spring material

σ is Ultimate Shear Strength

$$\mathrm{M} = \frac{\pi \mathrm{d}^3 \sigma}{32 \mathrm{K_i}} \qquad [\mathrm{N.m}] \qquad [11]$$

M is the Bending Moment

K_o is always less than 1 and hence is omitted and K_i is considered

$$\mathrm{N_b} = \mathrm{i} + \frac{\beta}{360^\circ} \qquad [12]$$

$$\mathrm{N_a} = \mathrm{N_b} + \frac{2\mathrm{l}}{3\pi \mathrm{D}} \qquad [13]$$

N_b is the initial turns and N_a is the complete turns of the Spring

i is the integer number of coil turns

β is the angle of one arm of the torsion spring with respect to the other

$$\theta_c = \frac{10.8 \mathrm{MDN_b}}{\mathrm{d^4 E}} \qquad [14]$$

$$\theta_s = \frac{\mathrm{M}}{\mathrm{K}} \qquad [\mathrm{rads}] \qquad [15]$$

θ_c is partial/minimum deflection

θ_s is the complete/maximum deflection

E is the elastic Modulus of the Spring material

$$K = \frac{d^4 E}{10.8 D N_a} \quad [N.m] \quad [16]$$

$$D' = \frac{N_b D}{N_b + \theta_c} \quad [m] \quad [17]$$

K is the Spring Rate

D' is the Helix Diameter

The Spring Rate and Spring Index are two important values that provide the overall performance of the ring. This Spring Index indicates the easy of manufacturability, furthermore, indicating the versatility of the spring. The Spring Rate indicates the torque required to turn the spring. These equations were used to select an ideal spring for configuration for the purpose of the design.

Spring Theory analysis will help in the selection of an ideal spring design for the SLR. The numeric equations can be used for a variety of parameters to give a range of possible design and their limitations for this project. Since the spring can be made of a steel with a relatively higher magnetic permeability and be capable of small deflection that is desired (6mm).

4.4 CAD Model and Mesh

Three-dimensional CAD models (using SOLIDWORKS) were developed for tool joint of 8.3-inch (210 mm) size (dimensions in **Appendix A**), based on the design of the pin and box and snap latch designs. As shown in Figure 4.2 and Figure 4.3, it consists of a non-threaded, double shouldered pin and box connection. The mating surface of shoulder (both in box and pin) prevent rotational motion of the two coupling members. In place of teeth, this design implements large splines which taper to a rounded point at the free end of the pipe. The splines prevent rotational relevant motion of the two coupling members while axial separation is prevented by an expanding snap latch seated on to the pin. The expanding snap latches (number of snap latches = 6) are fitted into a set of grooves on the pin so that any expansion occurs in the outward, radial direction. Each snap latch expands into a corresponding groove into the box, locking the pin and the box together.

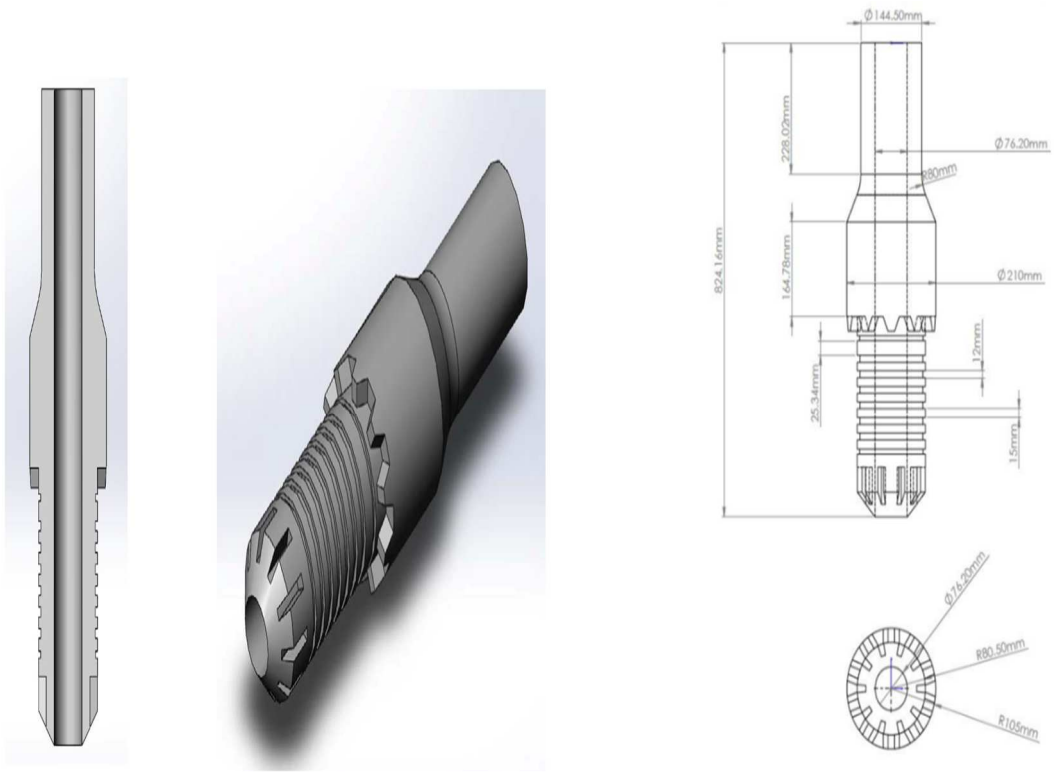

Figure 4.2: 3D view and schematic of the 6 ring Pin connector.

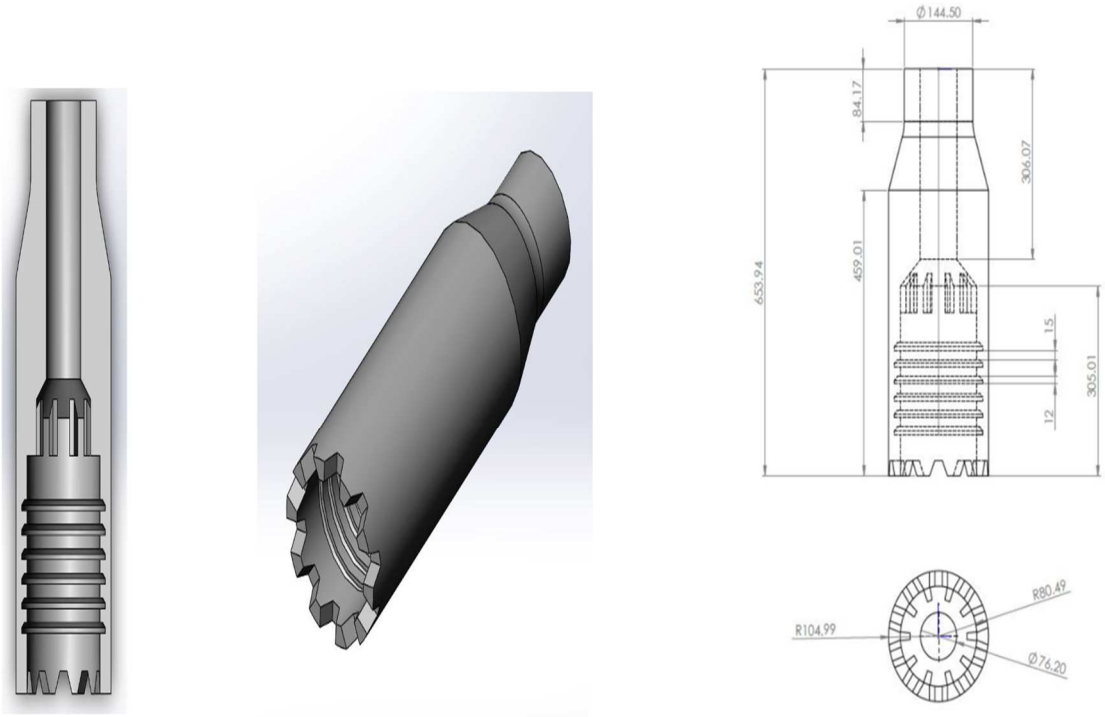

Figure 4.3: 3D view and schematic of the 6 ring Box connector.

Using material properties in Table 2 and CAD models defined in Section 4.2, finite element (FE) using ANSYS-Static Structural mesh models were created using tetrahedral sizing for snap latches and for pin/box sections. Finer mesh settings were applied at locations of contact between Pin and Snap-Latch Ring and Box and Snap-Latch Ring since the snap latch is the stress critical part in the proposed tool joint designs.

The boundary conditions (BC's) applied are shown in Figure 4.4 for elastic FE stress analysis in the tool joint design (e.g., Figure 4.4 a & b) with snap latch design (Figure 4.4 c & d). The overall maximum force under consideration is 8,565,233 N (1,925,541 lb.). Hence when the force is distributed to 6 Rings this force would be 1,427,539 N (320,924 lb.) and to 4 Rings would be 2,141,308 N (481,385 lb.). All visual results are set to 1:1 setup in terms of visible deformation. Full tool joint model and one snap latch were analysed. There are three components for each tool joint (i.e., box, pin and snap latch) and therefore, one fixed support is applied on each of them.

The simulation involved verifying the stress and deformation behavior under maximum tensile load of Pin and Box Connectors and Snap-Latch Ring to identify the ranges of forces the different components can safely function within. It should be noted that the strength of the entire system is dependent on the threshold of its weakest component (Snap-Latch Ring), therefore, ring size optimization was necessary, and there is a major part of the FE analysis in the following sections. This involved two simultaneous simulation considerations: (a) optimizing the dimensions of the Snap Latch Ring and assess their stress and deformation behavior under maximum tensile load 1,925,541 lb (8,565 kN), and the optimization included dimensions alteration (such as width and height (see Figure 4.5)) of the Snap-Latch Ring in different combinations, and (b) the current proposed number of Snap-Latch Rings is 6, and therefore, using 6 Snap-Latch Rings under the maximum tensile load of 320,924 lb. (1,427 kN) per Snap-Latch Ring, and also using 4 Snap-Latch Rings under the maximum tensile load of 481,385lb (2,141 kN) per Snap-Latch Ring. Hence simulations were carried to identify the optimum geometry of the Snap-Latch Ring as well as the ideal number of Snap-Latch Rings in the system. This involved 6 cases, and results and discussion are presented in the following section.

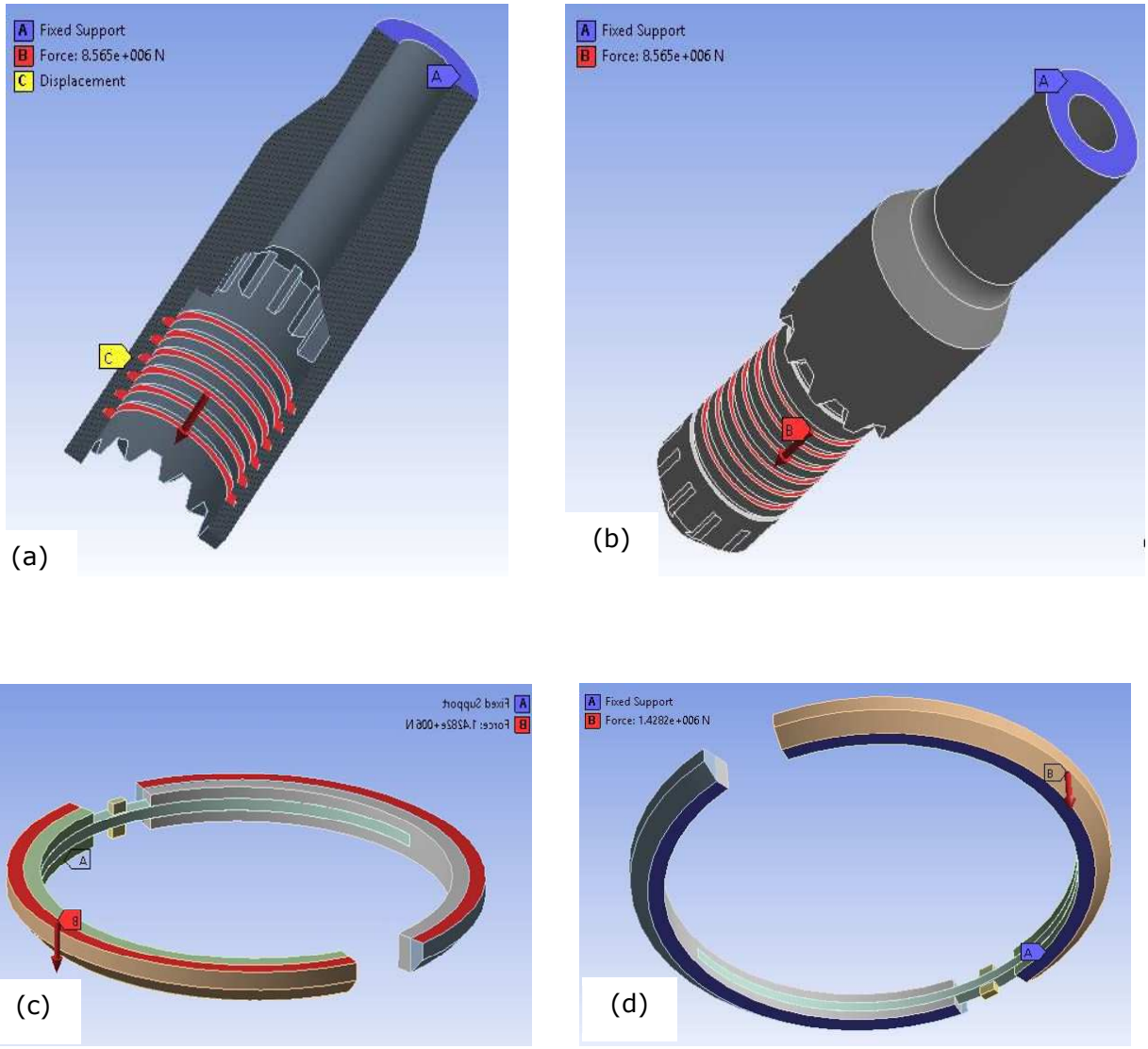

Figure 4.4: Boundary condition selection in tool joint showing fixed and frictionless support in various sections: (a) box, (b) pin, (c-d) two arm snap latch.

.

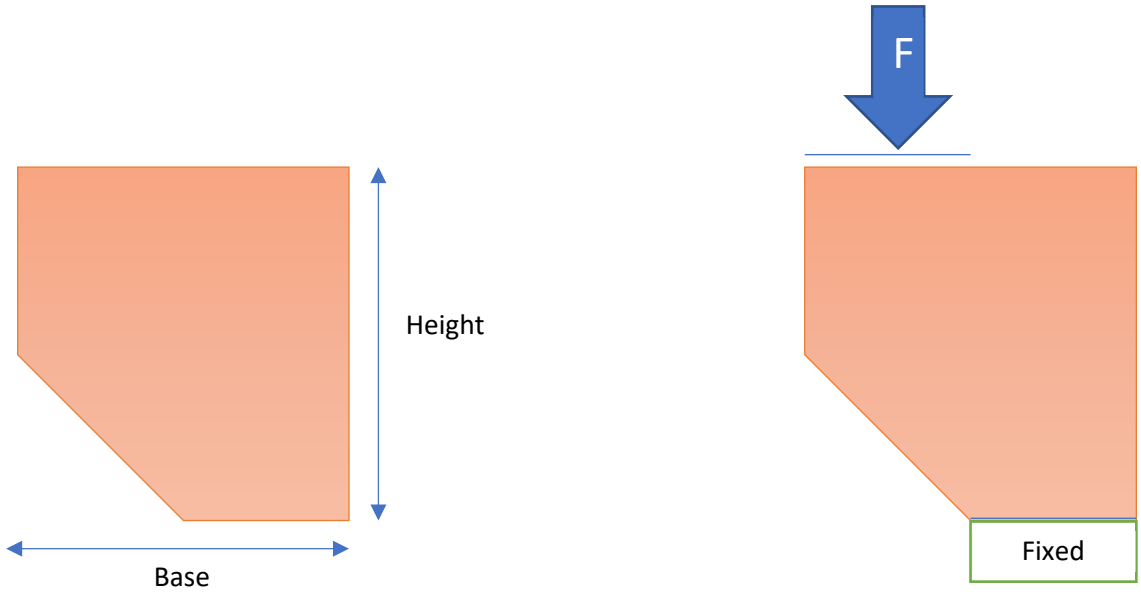

Figure 4.5: Snap Latch cross-section schematic and simulation parameters.

The Figure below shows the variation in the maximum deformation and stress for the mesh sizes in snap latch (i.e., identifying the mesh dependency). It shows clear convergence by increasing mesh number in snap latch designs; therefore, the mesh is fine enough and therefore the results produced through this criterion can be considered as reliable for snap latch analysis. A similar approach was used to identify Mesh convergence parameters to be applied for other simulation setups.

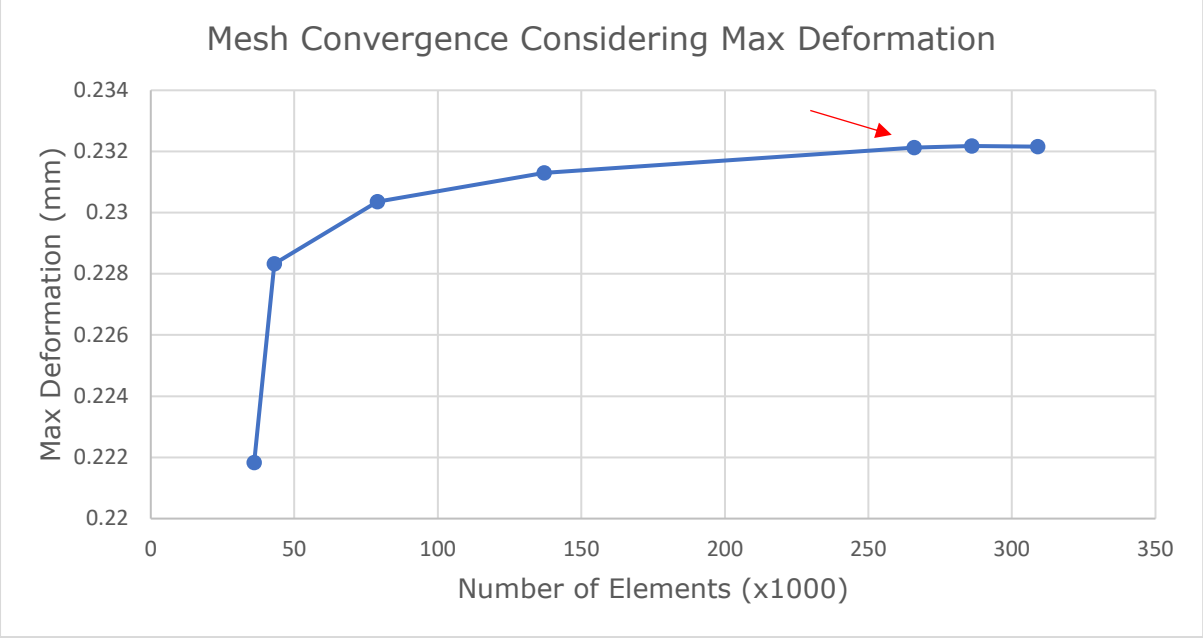

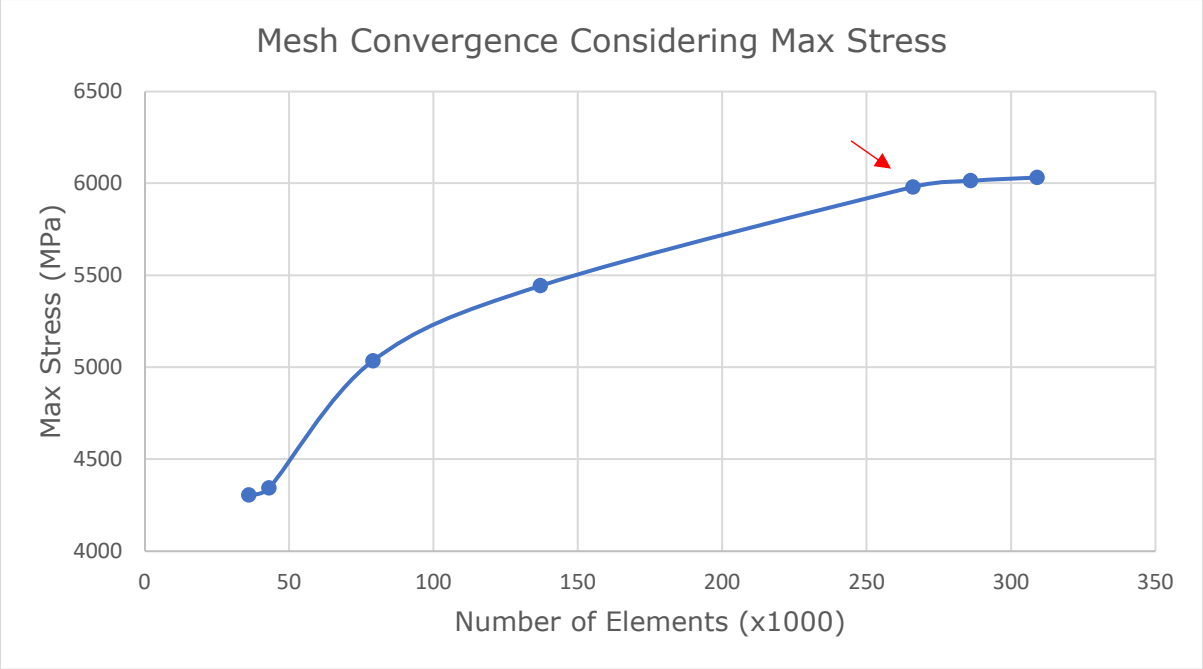

Figure 4.6: Mesh dependency for snap latch design using max stress and max deformation (selected mesh number shown here with red arrow).

4.5 Design Optimization of Snap Latch Ring and Pin and Box Connections

Solidworks CAD and ANSYS Static Structural analysis were used to set the parameters and simulate the results. The parameters of where the force is applied and what sides are constrained have been identified. The next steps were to see if altering the length or breath or both dimensions (cross-section, as shown in Figure 4.5) of the Snap-Latch Ring would affect its integrity. Furthermore, it would be beneficial to know if the number of snap latches can be reduced and if so, is there a significant change in deformation and stress on a single snap-latch. The total maximum force that would be theoretically exerted on the snap latch would be 8565 kN (1,925,541 lb). If there are 6 Snap-Latch Rings in a tool joint system, then a single Snap-Latch Ring would be exerted under 1427 kN (320,924 lb) and if this were reduced to 4 Snap-Latches then the force exerted on each span latch would increase to 2141 kN (486,385 lb) per Snap-Latch Ring. Table 3 shows different simulation setups in 6 cases.

Table 1. Finite Element simulation setups in 6 cases.

Case no.	Configurations	Tensile force (Newtons/ Pounds-Force)
1	Constant Base and Variable Height for a 6 Ring Configuration	1427 kN / 320,924 lb
2	Variable Base and Constant Height for a 6 Ring Configuration	1427 kN / 320,924 lb
3	Simultaneous Variable Base and Variable Height for a 6 Ring Configuration	1427 kN / 320,924 lb
4	Constant Base and Variable Height for a 4 Ring Configuration	2141 kN / 486,385 lb
5	Variable Base and Constant Height for a 4 Ring Configuration	2141 kN / 486,385 lb
6	Simultaneous Variable Base and Variable Height for a 4 Ring Configuration	2141 kN / 486,385 lb

Each case shows the stress and deformation behavior with an image of initial and extreme parameters. Additional images of the stress and deformation behavior at every parametric change will be in **Appendix H**.

4.5.1 Constant Base and Variable Height for a 6 Ring Configuration

As shown in Figure 4.6 and Table 4 (case 1), for constant base dimension at 12 mm and variable height dimensions (12 mm, 18 mm, 24 mm, 30 mm and 36 mm), the variation in deformation and stress can be observed. With increase in height, the overall maximum stress decreases. However, due to geometric change in the orientation of height there is larger deformation. An increase in deformation of any kind is highly undesirable as it would cause the Snap-Latch ring to lock the Pin and Box connectors in position permanently or break within the confines.

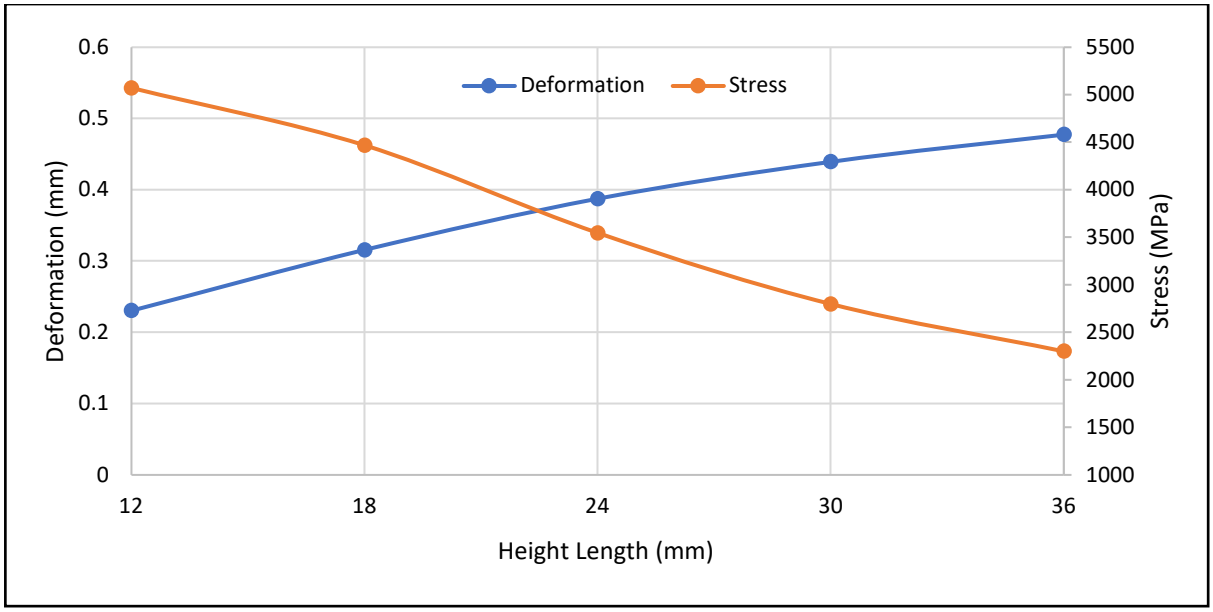

Figure 4.6: Stress and Deformation Chart for Case 1.

Table 2. Deformation and stress data based on Case 1.

Height	Base	Deformation (mm/inches)	% Deformation from original	Stress (MPa/psi)	% Stress from original
12	12	0.23053 / 0.0091	-	5,070.4 / 735,401	-
18		0.31551 / 0.0124	36.87	4,467.6 / 647,972	-12.43
24		0.3873 / 0.0152	68.01	3,546 / 514,305	-30.06
30		0.43931 / 0.0173	90.57	2,797.2 / 405,700	-44.83
36		0.47748 / 0.0091	107.13	2,301.6 / 333,819	-54.61

4.5.2 Variable Base and Constant Height for a 6 Ring Configuration

As shown in Figure 4.7 and Table 5 (case 2), for constant height dimension at 12 mm and variable base dimensions (12 mm, 18 mm, 24 mm, 30 mm and 36 mm), the variation in deformation and stress can be observed. An increase in base, reduces the stress exerted upon the top outer edge but an increase in the base further than 24 mm with a constant 12 mm height results in further deformation which is undesirable. An increase in base reduces the stress on the Snap-Latch Ring significantly but reaches a threshold when increasing the base further than 24 mm whilst keeping the height constant at 12 mm.

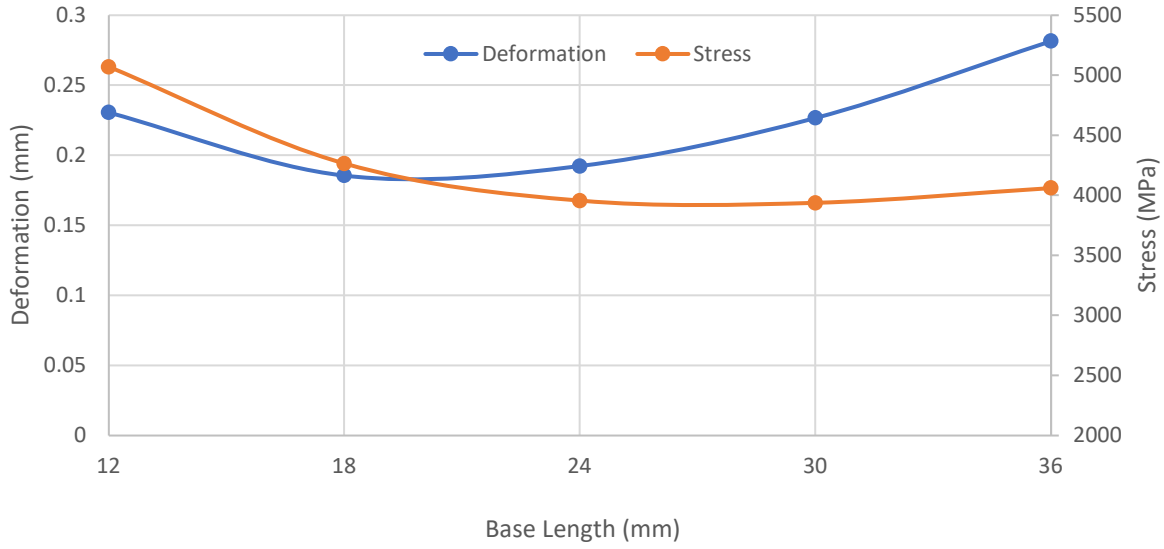

Figure 4.7: Stress and Deformation Chart for Case 2

Table 5. Deformation and stress data based on Case 2

Height	Base	Deformation (mm/inches)	% Deformation from original	Stress (MPa/psi)	% Stress from original
12	12	0.23053 / 0.0091	-	5,070.4 / 735,401	-
	18	0.18558 / 0.0073	-19.50	4,264.8 / 618,558	15.89
	24	0.19235 / 0.0076	-16.56	3,955.6 / 573,712	21.99
	30	0.22666 / 0.0089	-1.68	3,937.7 / 571,116	22.34
	36	0.28148 / 0.0111	22.10	4,060.5 / 588,927	19.92

4.5.3 Simultaneous Variable Base and Variable Height for a 6 Ring Configuration

As shown in Figure 4.8 and Table 6 (case 3), for changing both base and height dimensions (12 mm, 18 mm, 24 mm, 30 mm and 36 mm), the variation in deformation and stress can be observed. The deformation in both cases decreases linearly, whilst the stress decreases exponentially with increase in both height and base. This is a highly desirable feature as the stress reduces by a significant 58% and the deformation by 25%. Further increase in height and base simultaneously would result in the Snap-Latch ring being strong enough to take the maximum load, however, increasing the geometry would be exceeding the confines/constraints of the Pin/Box connectors.

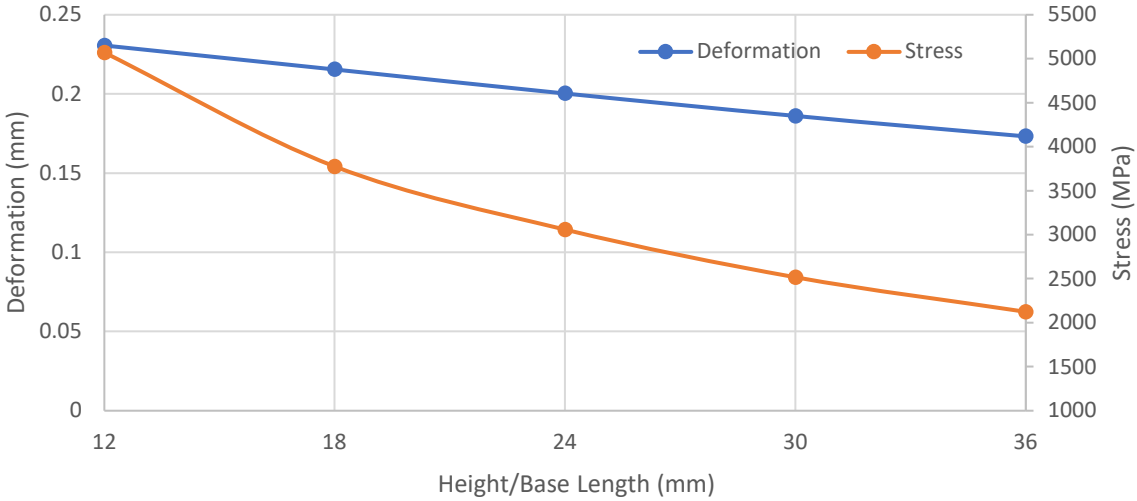

Figure 4.8: Stress and Deformation Chart for Case 3

Table 3. Deformation and stress data based on Case 3.

Height	Base	Deformation (mm/inches)	% Deformation from original	Stress (MPa/psi)	% Stress from original
12		0.23053 / 0.0091	-	5,070.4 / 735,401	-
18		0.21555 / 0.0085	-6.50	3,776.5 / 547,736	-25.52
24		0.20036 / 0.0079	-13.09	3,059.9 / 443,802	-39.65
30		0.18613 / 0.0073	-19.26	2,517.8 / 365,177	-50.34
36		0.17329 / 0.0068	-24.83	2,124.8 / 308,177	-58.09

Figure 4.9 (contour plots) shows stress and deformation concentration zones for Case 3 (simultaneous variable base and variable height; 6 ring configuration), with dimensions 12 mm height and 12 mm base, and with dimensions 36 mm height and 36 mm base. Stress and deformation concentration zones were extremely localised, but the stresses decreased rapidly to below the yield point (i.e. 1,034 MPa / 149,969 psi).

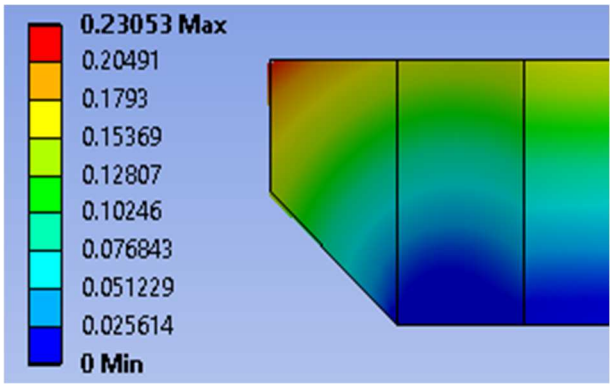

(a) Deformation (mm) for 12 mm height and 12 mm base

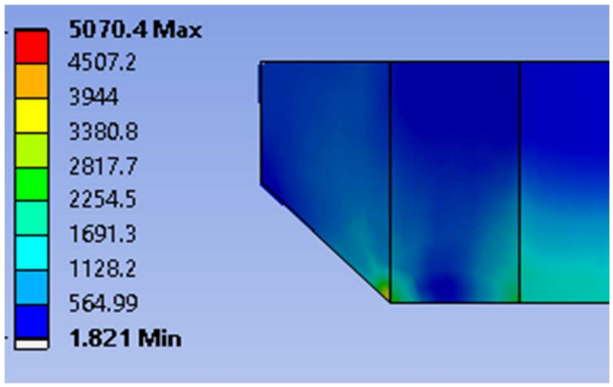

(b) Stress (MPa) for 12 mm height and 12 mm base

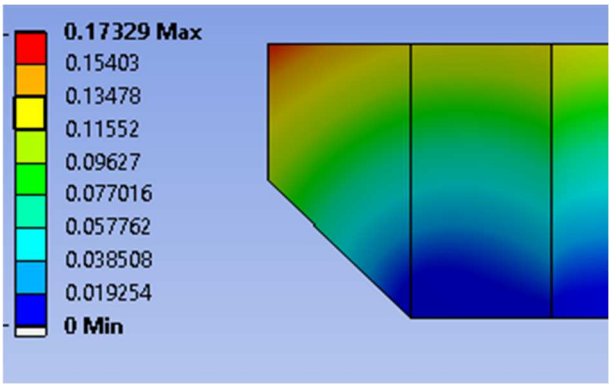

(c) Deformation (mm) for 36 mm height and 36 mm base

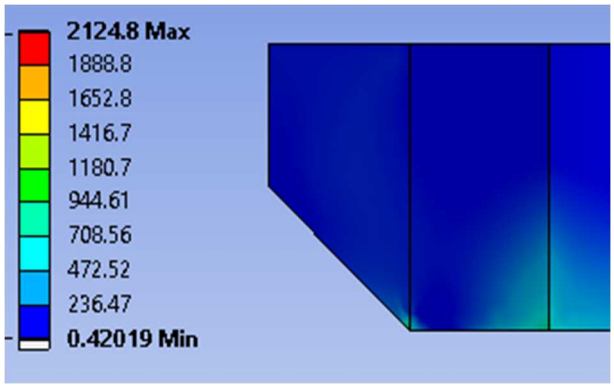

(d) Stress (MPa) for 36 mm height and 36 mm base

Figure 4.9: Case 3 stress and deformation of snap latch ring (simultaneous variable base and variable height; 6-ring configuration): (a) Deformation behavior at dimensions 12 mm height and 12 mm base, and (b) Stress behavior at dimensions 12 mm height and 12 mm base, (c) Deformation behavior at dimensions 36 mm height and 36 mm base, and (d) Stress behavior at dimensions 36 mm height and 36 mm base.

Figure 4.10 (contour plots) shows stress and deformation concentration zones for Case 1 (constant base and variable height; 6-ring configuration), with dimensions 36 mm height and 12 mm base, and for Case 2 (variable base and constant height; 6-ring configuration), with dimensions 12 mm height and 36 mm base. Stress and deformation concentration zones were extremely localised, but the stresses decreased rapidly to below the yield point (i.e., 1,034 MPa / 149,969 psi).

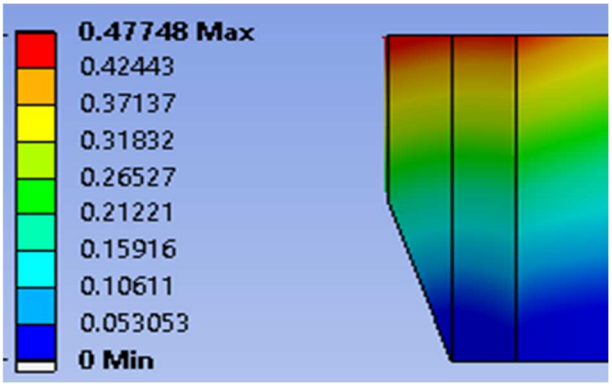

(a) Deformation (mm) for 36 mm height and 12 mm base

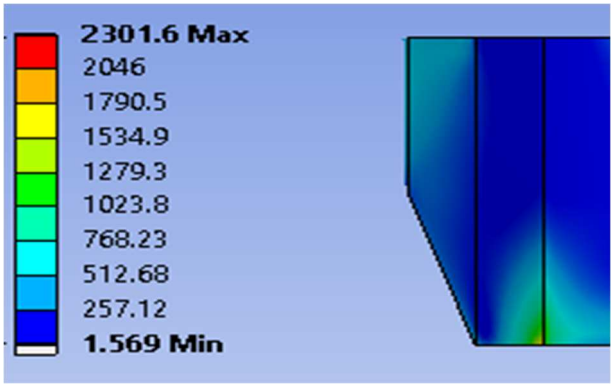

(b) Stress (MPa) for 36 mm height and 12 mm base

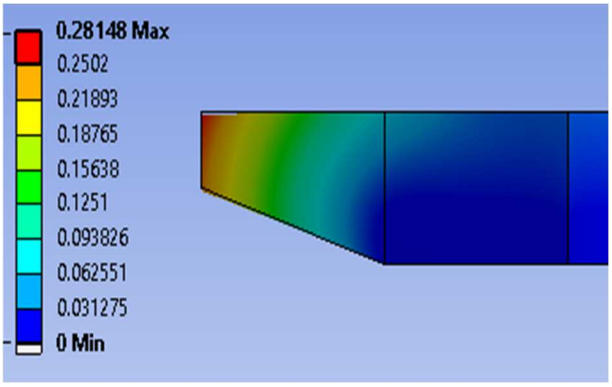

(c) Deformation (mm) for 12 mm height and 36 mm base

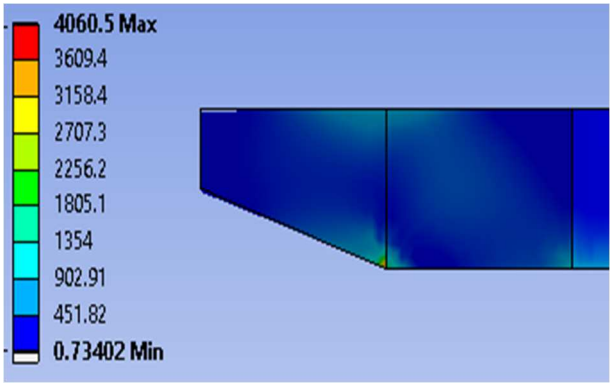

(d) Stress (MPa) for 12 mm height and 36 mm base

Figure 4.10: Stress and deformation of snap latch ring (6-ring configuration): (a) Case 1 (constant base and variable height), deformation behavior at dimensions 36 mm height and 12 mm base, and (b) Case 1 (constant base and variable height), stress behavior at dimensions 36 mm height and 12 mm base, (c) Case 2 (variable base and constant height), deformation behavior at dimensions 12 mm height and 36 mm base, and (d) Case 2 (variable base and constant height), stress behavior at dimensions 12 mm height and 36 mm base

4.5.4 Constant Base and Variable Height for a 4 Ring Configuration

As shown in Figure 4.11 and Table 7 (case 4), for constant base dimension at 12 mm and variable height dimensions (12 mm, 18 mm, 24 mm, 30 mm and 36 mm), the variation in deformation and stress can be observed. With increase in height, the overall maximum stress decreases. However, due to geometric change in the orientation of height there is larger deformation. An increase in deformation of any kind is highly undesirable as it would cause the Snap-Latch ring to lock the Pin and Box connectors in position permanently or break within the confines.

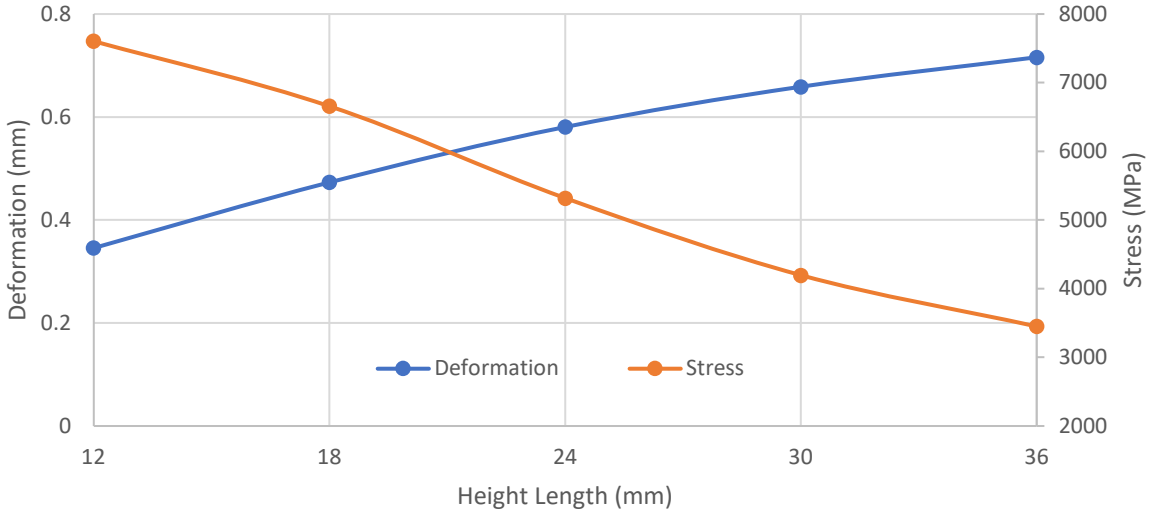

Figure 4.11: Stress and Deformation Chart for Case 4

Table 4. Deformation and stress data based on Case 4.

Height	Base	Deformation (mm/inches)	% Deformation from original	Stress (MPa/psi)	% Stress from original
12	12	0.34579 / 0.0136	-	7,605.5 / 1,103,087	-
18		0.47329 / 0.0186	36.87	6,660.3 / 965,997	-12.43
24		0.58095 / 0.0229	68.01	5,319.1 / 771,472	-30.06
30		0.65896 / 0.0259	90.57	4,195.7 / 608,536	-44.83
36		0.71622 / 0.0282	107.13	3,452.3 / 500,715	-54.61

4.5.5 Variable Base and Constant Height for a 4 Ring Configuration

As shown in Figure 4.12 and Table 8 (case 5), for constant height dimension at 12 mm and variable base dimensions (12 mm, 18 mm, 24 mm, 30 mm and 36 mm), the variation in deformation and stress can be observed. An increase in base, reduces the stress exerted upon the top outer edge but an increase in the base further than 24 mm with a constant 12 mm height results in further deformation which is undesirable. An increase in base reduces the stress on the Snap-Latch Ring significantly but reaches a threshold when increasing the base further than 24 mm whilst keeping the height constant at 12 mm.

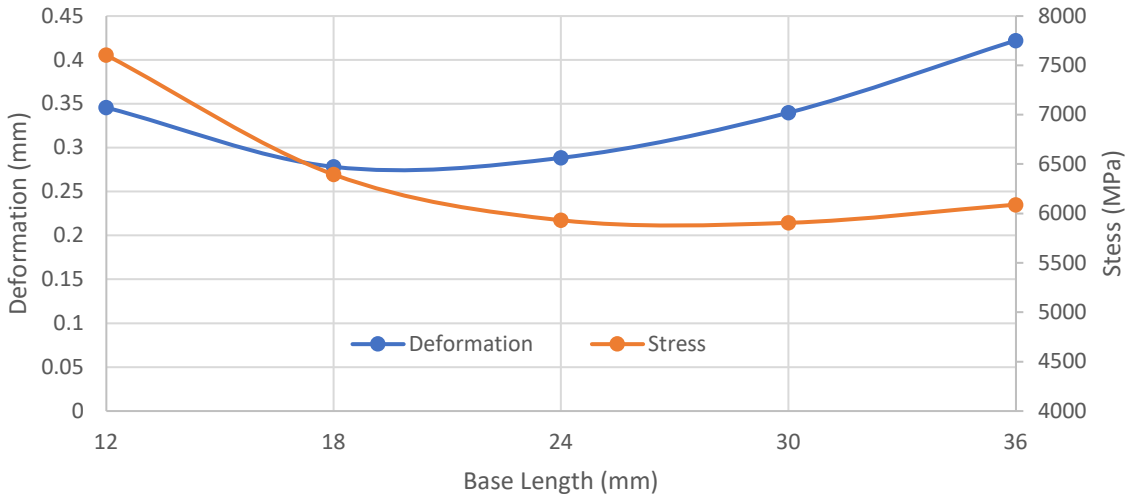

Figure 4.12: Stress and Deformation Chart for Case 5

Table 5. Deformation and stress data based on Case 5.

Height	Base	Deformation (mm/inches)	% Deformation from original	Stress (MPa/psi)	% Stress from original
12	12	0.34579 / 0.0136	-	7,605.5 / 1,103,087	-
	18	0.27836 / 0.0110	-19.50	6,397.2 / 927,837	-15.89
	24	0.28853 / 0.0114	-16.56	5,933.4 / 860,569	-21.99
	30	0.33999 / 0.0134	-1.68	5,906.5 / 856,667	-22.34
	36	0.42222 / 0.0166	22.10	6,090.8 / 883,397	-19.92

4.5.6 Simultaneous Variable Base and Variable Height for a 4 Ring Configuration

As shown in Figure 4.13 and Table 9 (case 6), for simultaneous variable base and variable height dimensions (12 mm, 18 mm, 24 mm, 30 mm and 36 mm), the variation in deformation and stress can be observed. The deformation in both cases decreases linearly, whilst the stress decreases exponentially with increase in both height and base. This is a highly desirable feature as the stress reduces by a significant 58% and the deformation by 25%. Further increase in height and base simultaneously would result in the Snap-Latch ring being strong enough to take the maximum load, however, increasing the geometry would be exceeding the confines/constraints of the Pin/Box connectors.

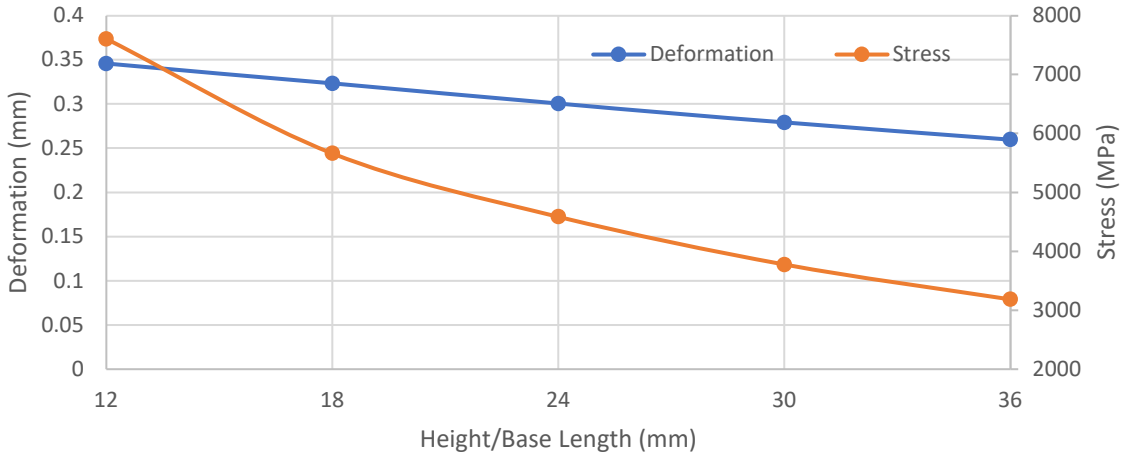

Figure 4.13: Stress and Deformation Chart for Case 5

Table 6. Deformation and stress data based on Case 6.

Height	Base	Deformation (mm/inches)	% Deformation from original	Stress (MPa/psi)	% Stress from original
12		0.34579 / 0.0136	-	7,605.5 / 1,103,087	-
18		0.32333 / 0.0127	-6.50	5,664.7 / 8215,967	-25.52
24		0.30054 / 0.0118	-13.09	4,589.8 / 665,695	-39.65
30		0.27919 / 0.0110	-19.26	3,776.7 / 547,765	-50.34
36		0.25993 / 0.0102	-24.83	3,187.3 / 462,280	-58.09

Figure 4.14 (contour plots) shows stress and deformation concentration zones for Case 6 (simultaneous variable base and variable height; 4-ring configuration), with dimensions 12 mm height and 12 mm base, and with dimensions 36 mm height and 36 mm base. Stress and deformation concentration zones were extremely localised, but the stresses decreased rapidly to below the yield point (i.e., 1,034 MPa / 149,969 psi).

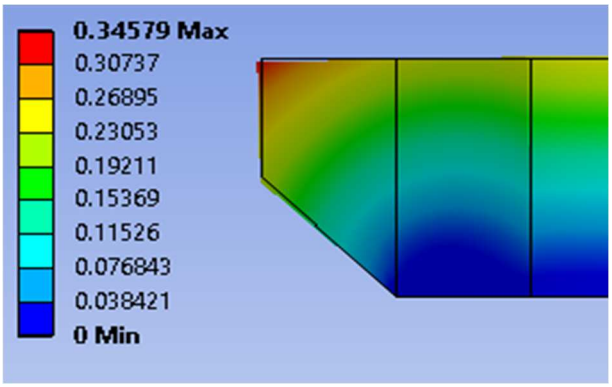

(a) Deformation (mm) for 12 mm height and 12 mm base

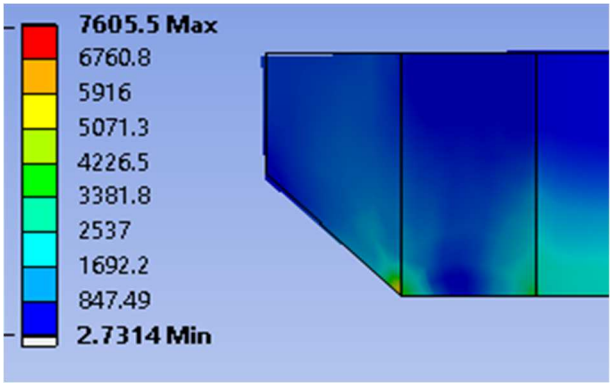

(b) Stress (MPa) for 12 mm height and 12 mm base

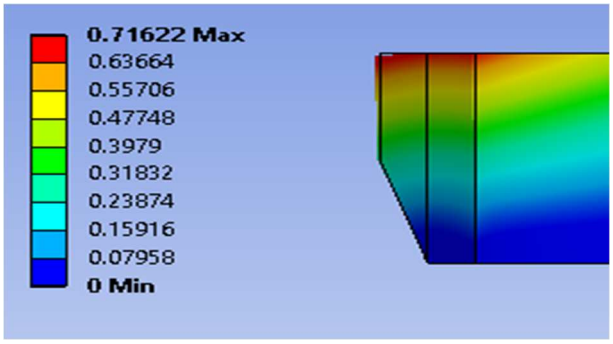

(c) Deformation (mm) for 36 mm height and 36 mm base

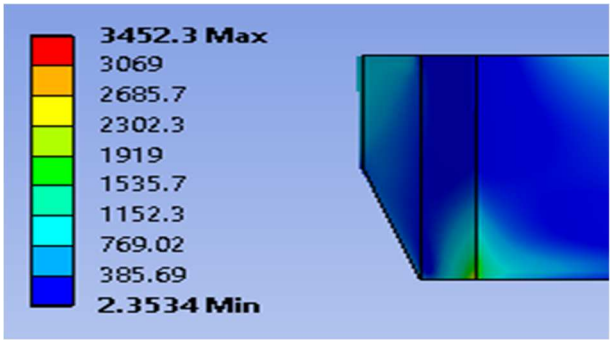

(d) Stress (MPa) for 36 mm height and 36 mm base

Figure 4.14: Case 6 stress and deformation of snap latch ring (simultaneous variable base and variable height; 4-ring configuration): (a) Deformation behavior at dimensions 12 mm height and 12 mm base, and (b) Stress behavior at dimensions 12 mm height and 12 mm base, (c) Deformation behavior at dimensions 36 mm height and 36 mm base, and (d) Stress behavior at dimensions 36 mm height and 36 mm base.

Figure 4.15 (contour plots) shows stress and deformation concentration zones for Case 4 (constant base and variable height; 4-ring configuration), with dimensions 36 mm height and 12 mm base, and for Case 5 (variable base and constant height; 4-ring configuration), with dimensions 12 mm height and 36 mm base. Stress and deformation concentration zones were extremely localised, but the stresses decreased rapidly to below the yield point (i.e. 1,034 MPa / 149,969 psi).

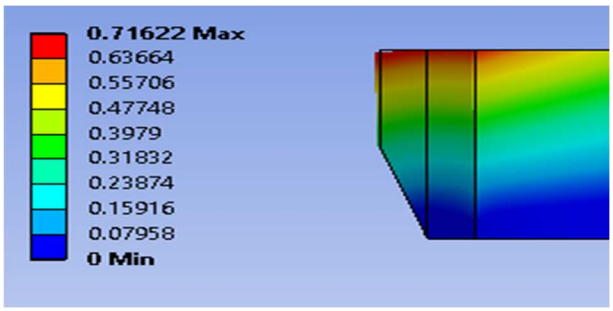

(a) Deformation (mm) for 36 mm height and 12 mm base

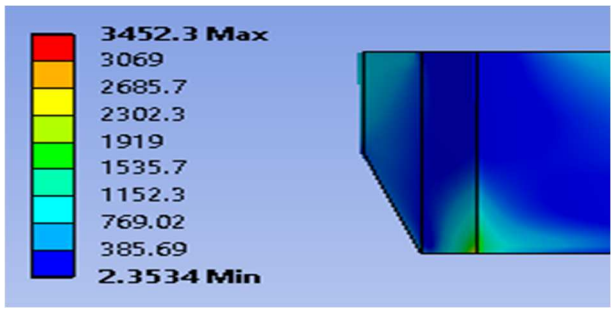

(b) Stress (MPa) for 36 mm height and 12 mm base

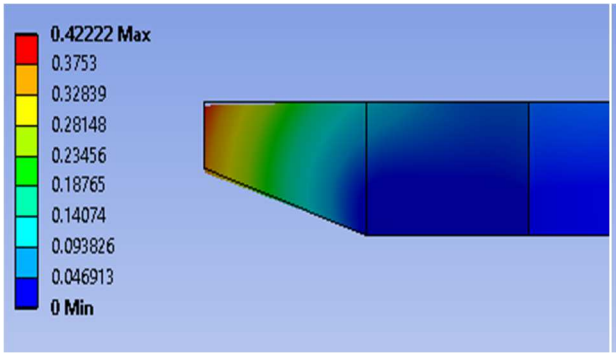

(c) Deformation (mm) for 12 mm height and 36 mm base

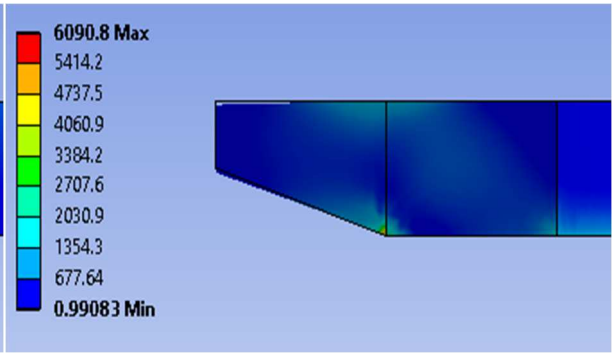

(d) Stress (MPa) for 12 mm height and 36 mm base

Figure 4.15: Stress and deformation of snap latch ring(4-ring configuration): (a) Case 4 (constant base and variable height), deformation behavior at dimensions 36 mm height and 12 mm base, and (b) Case 5 (constant base and variable height), stress behavior at dimensions 36 mm height and 12 mm base, (c) Case 4 (variable base and constant height), deformation behavior at dimensions 12 mm height and 36 mm base, and (d) Case 5 (variable base and constant height), stress behavior at dimensions 12 mm height and 36 mm base.

4.5.7 Snap Latch Ring Optimization Discussion

It is noticed that Cases 1 and 4, 2 and 5, 3 and 6 have similar trends for the same geometric parameters. The change in force applied only increases the trend patterns with increase in force, implying that decreasing the number of Snap-Latch Rings (Which increases the force exerted per ring) is not a viable solution given the geometric constraints.

Furthermore, all prototypes fail under the maximum load conditions showing stress values in the range of over 5,000 MPa (725,189 psi) which is 5 times the Yield Tensile Load of S135 Stainless Steel (see Table 2), i.e., 1,034 MPa / 149,969 psi. Hence it would be necessary to identify the optimal working ranges of the Snap-Latch Ring. These results seem realistic considering the size of the rings as seen by the prototypes. Hence currently it would be ideal to consider using 6 snap-latch rings per pin and box connection. Having any more reduces the strength of each snap latch ring creating potential locking of tool joints due to broken rings. The option to have lesser but bigger snap latch rings is also limited to the thickness available from the pin and box connections.

4.6 Pin and Box Geometry Optimization

Based on the results discussed above related to ring optimization as seen in the previous section, further simulations were performed on the Pin and Box Connectors with a design for the 12 mm height/base Snap-Latch Ring and 18 mm height/base Snap-Latch Ring (e.g., contour plots shown in **Figure 4.16** and **Figure 4.17**). The results obtained are shown in **Table 10**.

It can be seen that for the Pin Connector, a change in design from 4- ring to 6-ring has little effect on the deformation and maximum stress when a tensile or compressive load is applied. However, the box connector has more deformation in the direction of the load and has higher stresses at the Snap-Latch Ring slots in a 4-ring configuration as opposed to a 6-ring configuration. Between the 4-ring Pin/Box Connector and the 6-ring Pin/Box Connector it can be said that the 6-ring Pin/Box Connector has much better stress/deformation performance. However, since both models show high values of tensile stress leading to plastic deformation a new range of limiting forces need to be applied to identify a range of forces with

a reasonable safety factor (ideal safety factor of 2) for both Pin and Box Connectors.

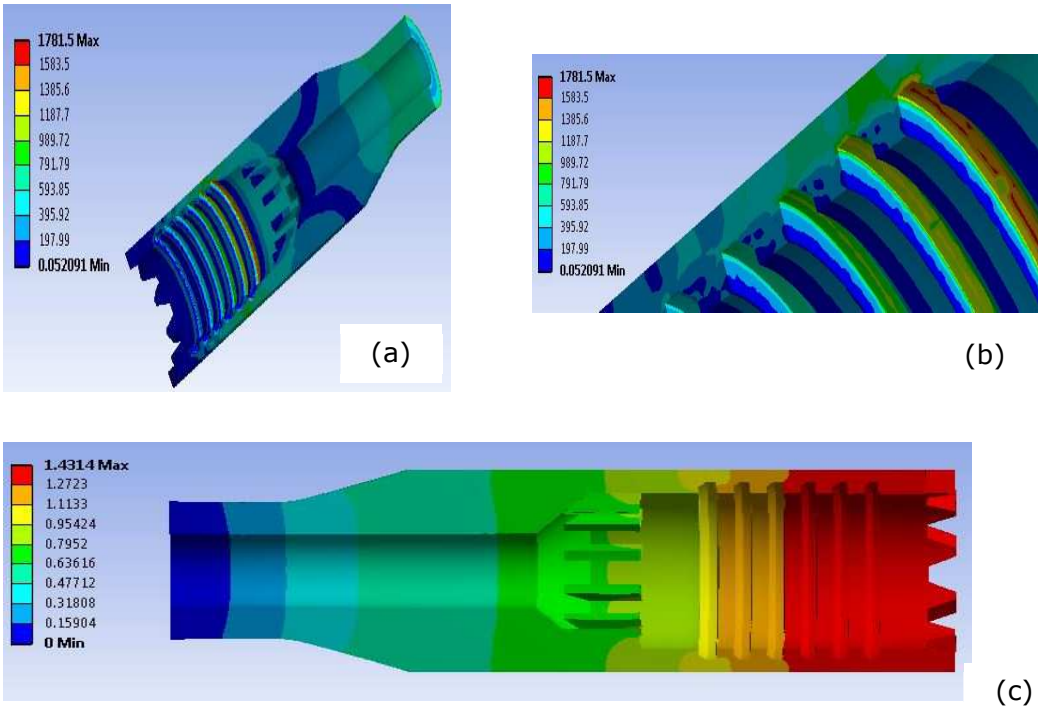

Figure 4.16: Stress analysis on 6-ring Box Connector: (a,b) Stress (MPa) behavior, (c) deformation (mm) behavior.

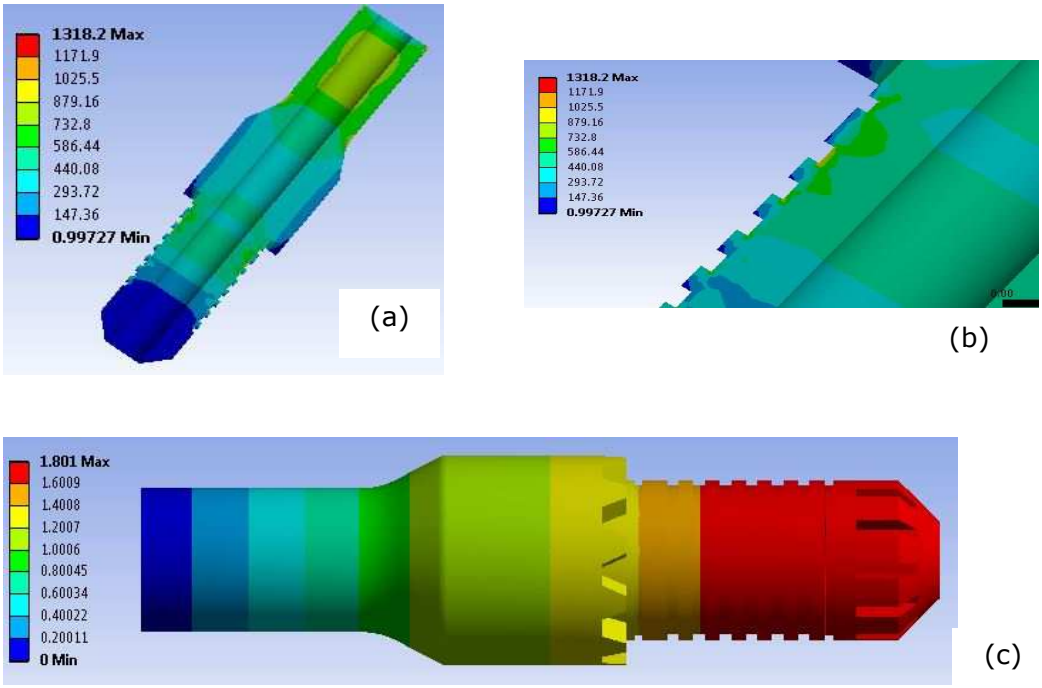

Figure 4.17: Stress analysis on 6-ring Pin connector: (a,b) Stress (MPa) behavior, (c) deformation (mm) behavior.

Table 7: Pin/Box connector stress/deformation data for 4- and 6-ring configurations.

Pin Connector Data		Max Deformation (mm / inches)	Max Stress (MPa / psi)
Tensile Force	6 Ring Model	1.8011 / 0.0709	1,318.2 / 191,189
	4 Ring Model	1.8772 / 0.0739	1,361.3 / 197,440
Box Connector Data			
Tensile Force	6 Ring Model	1.4314 / 0.0564	1,781.5 / 258,385
	4 Ring Model	1.7276 / 0.0680	2,712.9 / 393,473

An attempt was made to add fillets at the edge of maximum stress however this only resulted in larger concentrated stresses and would only decrease with increase in fillet radius. However, increase in fillet radius would significantly affect the ring design and make it geometrically impractical for the application required. Designing a connector that would need more than 6-rings would not be efficient as this would require the design of the ring to be smaller than 10 mm which would in effect reduce the strength of the ring which keeps the whole system together.

From the data presented so far it seems that the 6-ring Pin and Box Connectors remain the best option and further analysis must be done to identify the range of forces the drill pipe connectors can sustain before plastic deformation. Analysis in the following section will be performed to find the limits of stress the Box and Pin can withstand with appropriate safety factors.

4.7 Tool Joint System Tensile Load and Stress Analysis

The aim of this section is to present and discuss a suitable range of tensile forces that can be applied to the Pin Connector and Box Connector and identify the common range of practically applicable tensile loading force. For this analysis, the Pin Connector, Box Connector and Ring for the configuration of 6-ring module were selected and analyzed with a range of tensile forces to identify the forces where each component would fail and regions of safe operation. The data

presented has similar simulation assumptions as those made in the previous sections.

As shown in Figure 4.18, the relationship between exerted tensile force and resulting stress on the Pin are linear in nature as obtained by applying a range of forces to find the safe range of stresses where the component would fail, with the maximum force on the Pin being on the inner corner of the first ring groove. From the linear line, an equation can be derived which can be then used to identify the respective values of stress for respective values of force applied and vice versa.

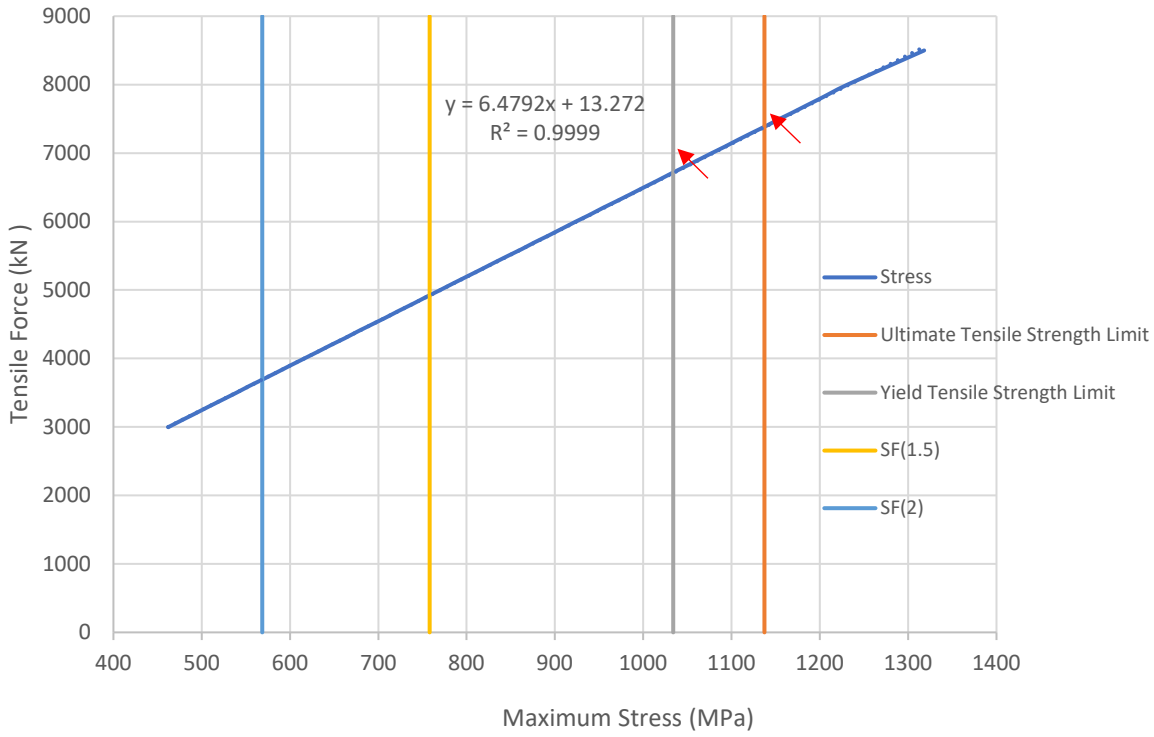

Figure 4.18. Pin Connector Analysis (6 ring module): Stress values for a range of tensile force applied on the Pin connector (arrow shows locus of working range of force).

Hence, the acceptable working range of force is between 6712 kN to 7380 kN (1,508,917 lbs to 1,659,090 lbs), see Figure 4.18 and Table 11. Applying a safety factor of 2 and 1.5, safe range of forces between 3696.7 kN to 4924.5 kN (831,119 lbs to 1,107,072 lbs) can be applied, as shown in Table 11. For the Pin Connector it can be said that by considering a safety factor of 2, the working force that should be applied is 3,696.7 kN (831,119 lbs)

Table 8: Pin connector stress/deformation data for 6-ring configurations.

	Maximum Tensile Load	Yield Tensile Load	Safety Factor 1.5	Safety Factor 2
Force Exerted	7,380.12 kN (1,659,090lbs)	6,712.76 kN (1,508,917lbs)	4,924.5 kN (1,107,072lbs)	3,696.7 kN (831,119lbs)
Maximum Stress	1,137 MPa (164,908 psi)	1,034 MPa (149,969 psi)	758 MPa (109,939 psi)	568.5 MPa (82,454 psi)

Again, as shown in Figure 4.19, the relationship between exerted tensile force and resulting stress on the Box are linear in nature, with the maximum force on the box being on the inner corner edge of the first ring groove. Similarly, a linear line equation can be used to identify other limits. From the linear line, an equation can be derived which can be then used to identify the respective values of stress for respective values of force applied and vice versa.

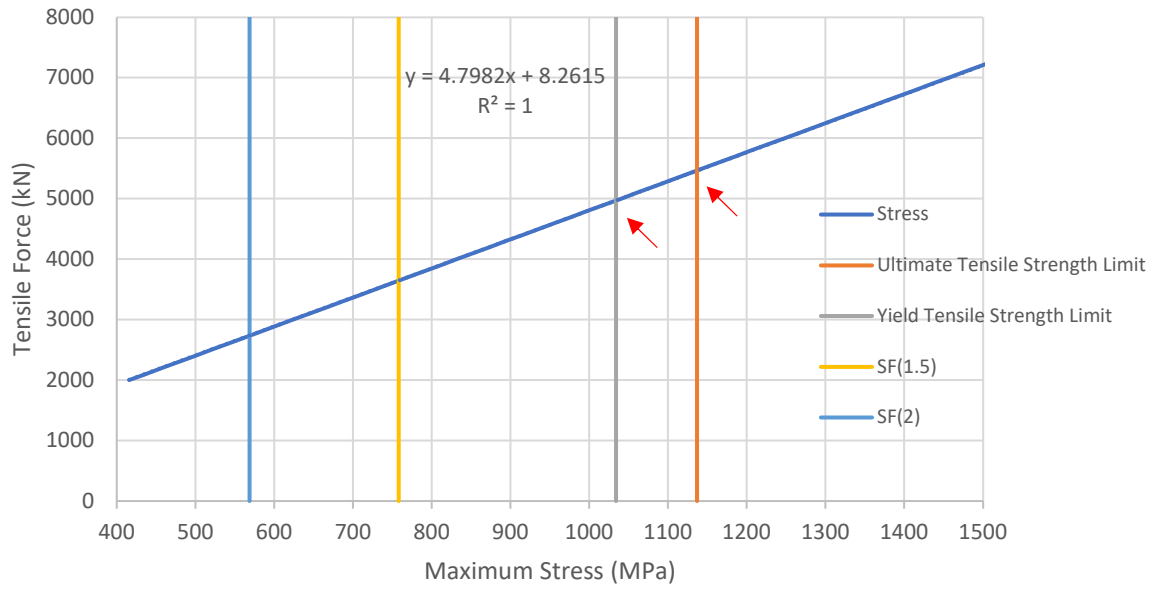

Figure 4.19**.** Box Connector Analysis (6 ring module): Stress values for a range of tensile force applied on the Box connector (arrow shows locus of working range of force).

Hence, the acceptable working range of force is between 4,970.74 kN to 5,464.54 kN (1,117,525 lbs to 1,228,581 lbs), see Figure 4.19. Applying a safety factor of 2 and 1.5 a safe range of forces between 2,739.04 kN to 3,647.5 kN (615,752 lbs to 820,103 lbs) can be applied, as shown in Table 12. For the Box Connector it can be said that by considering a safety factor of 2 the working force that should be applied is 2,739.04 kN (615,752 lbs). It is not noticed that the maximum threshold for the Box Connector is lower than the Pin Connector and since the whole system is taken into consideration the max force applied will be with respect to the capacity of the lowest force applicable.

Table 9: Box connector stress/deformation data for 6-ring configurations.

	Maximum Tensile Load	Yield Tensile Load	Safety Factor 1.5	Safety Factor 2
Force Exerted	5,464.54 kN (1,228,581lbs)	4,970.74 kN (1,117,525lbs)	3,647.5 kN (820,103lbs)	2,739.04 kN (615,752lbs)
Maximum Stress	1,137 MPa (164,908 psi)	1,034 MPa (149,969 psi)	758 MPa (109,939 psi)	568.5 MPa (82,454 psi)

Again, as shown in Figure 4.20, the relationship between exerted tensile force and resulting stress on the ring are linear in nature, with the maximum force on the ring being on the middle area where the force is applied as seen in previous result sets. Similarly, a linear line equation can be used to identify another requirement. Since only one ring was used for the simulation with the distributed force applied the results have been multiplied by a factor of 6 to provide with appropriate data with respect to the actual model.

Hence the acceptable working range of force is between 2,260.2 kN to 2,055.48 kN (461,982 lbs to 508,068 lbs), see Figure 4.20. However, in reality safety factors must be applied to ensure better performance over a period of time. Applying a safety factor of 2 and 1.5 a safe range of forces between 1,130.22 kN to 1,506.6 kN (254,034 lbs to 338,787 lbs) can be applied, as shown in Table 13. For each Ring it can be said that by considering a safety factor of 2 the working force that should be applied is 1,130.22 kN (254,034 lbs). Since the Rings are a crucial

component of the entire system, the maximum applicable force will be limited by the stress limitation of the Ring. Hence the safe operational force that can be applied is 1,130.22 kN (254,034 lbs) which is 13.2% of the original suggested maximum tensile force 8,565 kN (1,925,541lbs). Hence the application of the current design may need reconsideration.

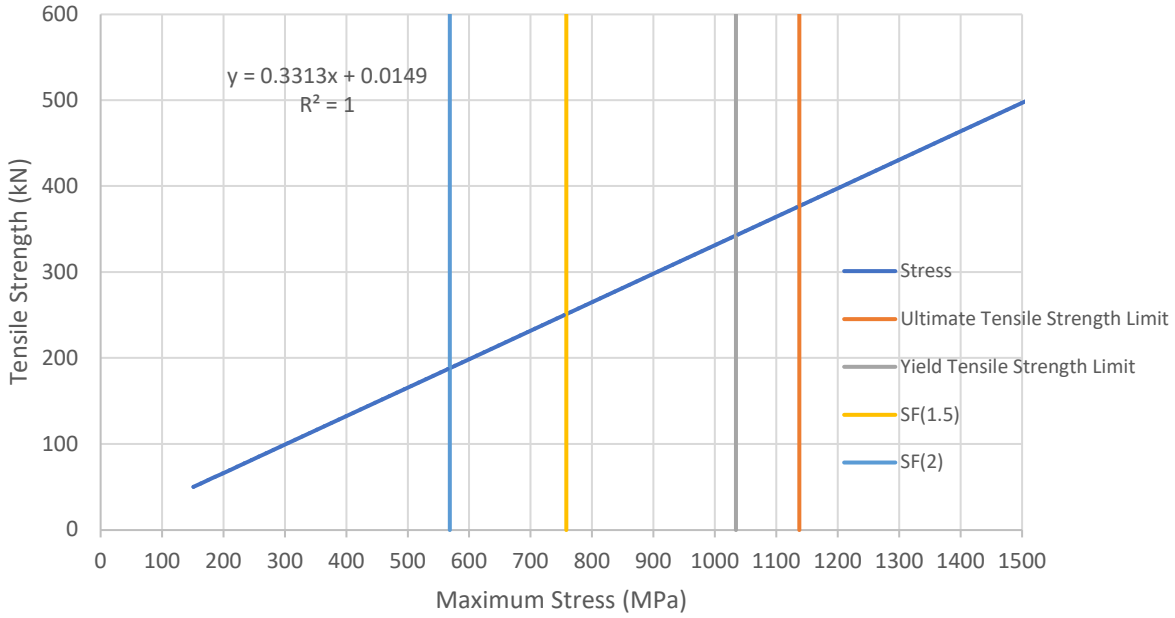

Figure 4.20**.** Snap-Latch Ring Analysis (6 ring module): Stress values for a range of tensile force applied on the Box connector (arrow shows locus of working range of force).

Table 10. Snap-Latch Ring stress/deformation data for 6-ring configurations.

	Maximum Tensile Load	Yield Tensile Load	Safety Factor 1.5	Safety Factor 2
Force Exerted	2,260.2 kN (508,068lbs)	2,055.48 kN (461,982lbs)	1,506.6 kN (338,787lbs)	1,130.22 kN (254,034lbs)
Maximum Stress	1,137 MPa (164,908 psi)	1,034 MPa (149,969 psi)	758 MPa (109,939 psi)	568.5 MPa (82,454 psi)

4.8 Summary

Through the approach of Finite Element Analysis, using SOLIDWORKS and ANSYS Static Structural, several findings were made. The first part of this chapter shows the material parameters applied for the design as well the boundary conditions that would most realistically represent the forces exerted on the snap-latch ring. Mesh convergence was performed to acquire optimal results within boundary conditions.

The snap-latch ring with a 12mm width and height was found to have 5,070MPa of maximum stress exerted on the external edge of the ring with a 0.23 mm deformation. The result of stress is around 5 times the yield stress of the material and the 0.23mm deformation around the edge is highly undesirable as any deformation protruding outwards will result in the snap latch ring getting damaged during actuation. Hence the option of changing the width and height of the snap-latch were looked into to see if these changes would improve the design and how these differences would vary. Furthermore, another option was considered where 4 snap-latch rings of larger sizes could be used instead of 6. This was also considered in the dimension of 18mm height and width with similar simulations performed varying height and width.

The Pin and Box were also simulated to identify their limits of tensile load comparing two models where one model pair had 6 grooves and one model pair had 4 grooves. From the results obtained it was clear that the pin and box connectors were more appropriate due to more deformation seen in the 4-groove pin and box connector. This can be attributed to the fact that if we increase the dimension of the snap-latch ring, we reduce the thickness of the pin and box connections respectively and hence reduce their tensile load strength.

From the results of the snap-latch ring, varying height significantly reduces the maximum tensile load exerted on the snap-latch ring compared to varying the width. However, there is an inverse relation with respect to the deformation, where the more height in the design there is a higher deformation present in the outer edge which is a highly undesirable feature. The optimal parameters is where the snap-latch ring is 36mm height and width with 58% reduction in exerted stress compared to the model with 12mm height and width. This is highly desirable however, not practically applicable as this would require a huge alteration to the

Pin and Box connections which would highly deviate from standard tool joint design, not making it an optimal design. Hence the choice to have a 12mm width and height snap-latch is concluded to be idea.

Since the maximum limits of each component has been identified, it is important to ascertain safe working limits for operational use. Hence, taking the existing data and projecting safety factors of 1.5 and 2, which would provide an operational safe working range for the system of Pin, Box and Snap-latch rings. The operational limits for the Pin Connector with a safety factor of 2 is 3,696.7 kN, the Box Connector with a safety factor of 2 is 2,739.04 kN and the Snap-latch ring with a safety factor of 2 is 1,130.22 kN. Now since the maximum safe load rating of an entire system is limited to its lowest maximum safe load, our entire system is limited to work safely under a maximum tensile load of 1,120.22kN, which is $1/8^{th}$ the required tensile load as initially proposed for our application. These FEA results have provided substantial evidence that application under current requirements of high tensile load is not suitable, however a range of operable loads have been provided.

Chapter 5

PROTOTYPE MANUFACTURING PROCESSES AND RESULTS

5.1 Introduction

This chapter will present all the manufacturing and production methods applied to produce the different prototypes and design assessed during the project. These steps and processes have helped identify the challenges associated with the production of the components and how the overall assembly fit together to give a final product. The chapter further provides the alternative design made and shows the application of a mag-switch magnet on the snap-latch ring prototype. A conclusion is provided summarizing the results and observations gathered from the process and methods applied in this chapter.

5.2 3D Printing Manufacturing using Acrylonitrile-Butadiene-Styrene (ABS)

Based on tool joint design with six snap latch design [1], the Pin and Box connectors (at a scale of 1:3) made of Acrylonitrile-Butadiene-Styrene (ABS) polymer were manufactured using the INTAMSYS FUNMAT PRO HT 3D printer at School of Engineering in Robert Gordon University (Figure 5.1). The process involved converting 3D CAD models developed in Chapter 5 in to an STL format to be read by the 3D printing software. The STL files for each component were then configured for the best final product results. Some of the key settings involved were wall thickness, number of layers per millimeter, body density and construction pattern. These settings were chosen based on the required structural integrity and time to build each model with ease for post analysis. Since the products were of cylindrical nature with many complex features, support structures were designed carefully to ensure the final product is easy to finish post-production [3]. All these parameters were carefully considered. 3D CAD model of Pin and Box Connector is in **Appendix A**.

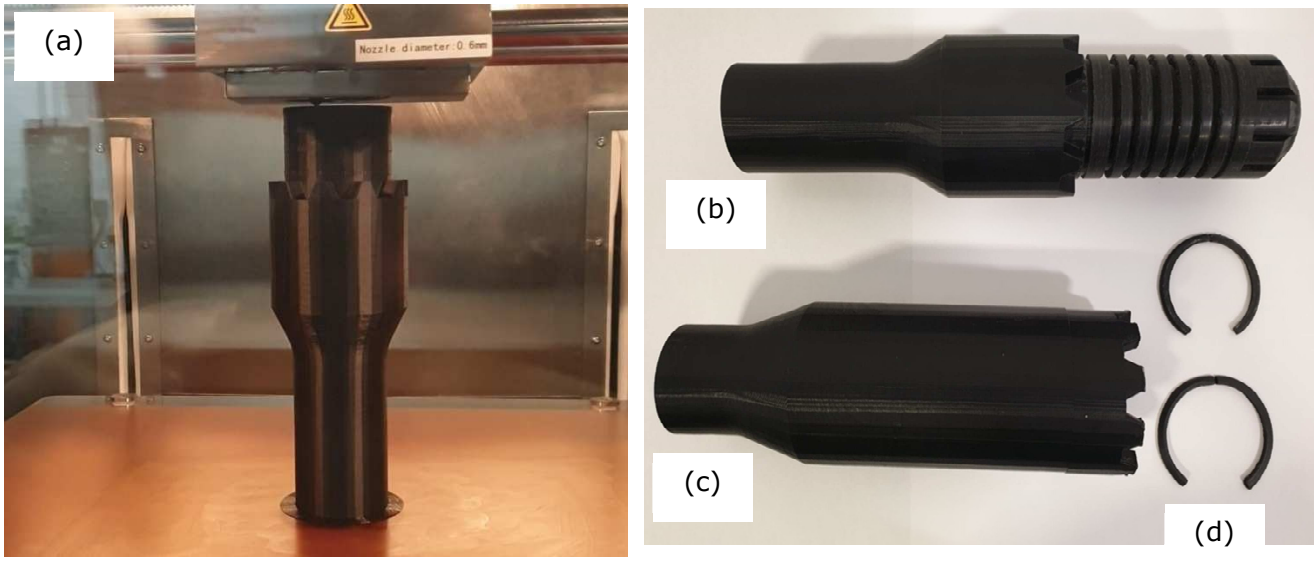

Figure 5.1: 3D printed models of non-threaded tool joint (Acrylonitrile-Butadiene-Styrene): (a) 3D printing of Pin Connector under progress, (b) Pin Connector, (c) Box Connector, and (d) Snap-Latch Rings design.

The manufactured parts (pin, box, snap latch) revealed a specific foreseeable challenge with the two connections in the possibility of limited interference clearance that would generate constant friction during connections. However, such a case would result in undesirable consequences during functional application, that is, pipes slipping off or fluids leakage. This issue needs to be addressed in future work by considering dimensional error and tolerances in design for manufacturing stage.

5.3 CNC Machine Manufacturing using Aluminum Alloy

The designed prototype of the Pin and Box connectors (**Appendix B**) made of aluminum were manufactured (at a scale of 1:2) by Combined Pumps Ltd using both Computerized Numeric Control machining (CNC) and Electrical Discharge machining (ED). The male/female test pieces were run to prove the wave form at the shoulder (48° areas) to see if the parts would fit together before programming, following which the female piece (Box) was manufactured first and shoulder & taper beyond fin area was machined then sent away for electrical discharge machining to remove material to create the fins. The male piece (Pin) was next machined omitting the outer diameters grooves until it was ensured that orientation of the fins and the wave form on front face matched the male design and all fitted together smoothly. The finished product (Figure 5.2) had a high-

quality finish and possessed no manufacturing challenges, and the connection was an exact fit with no contact friction issues.

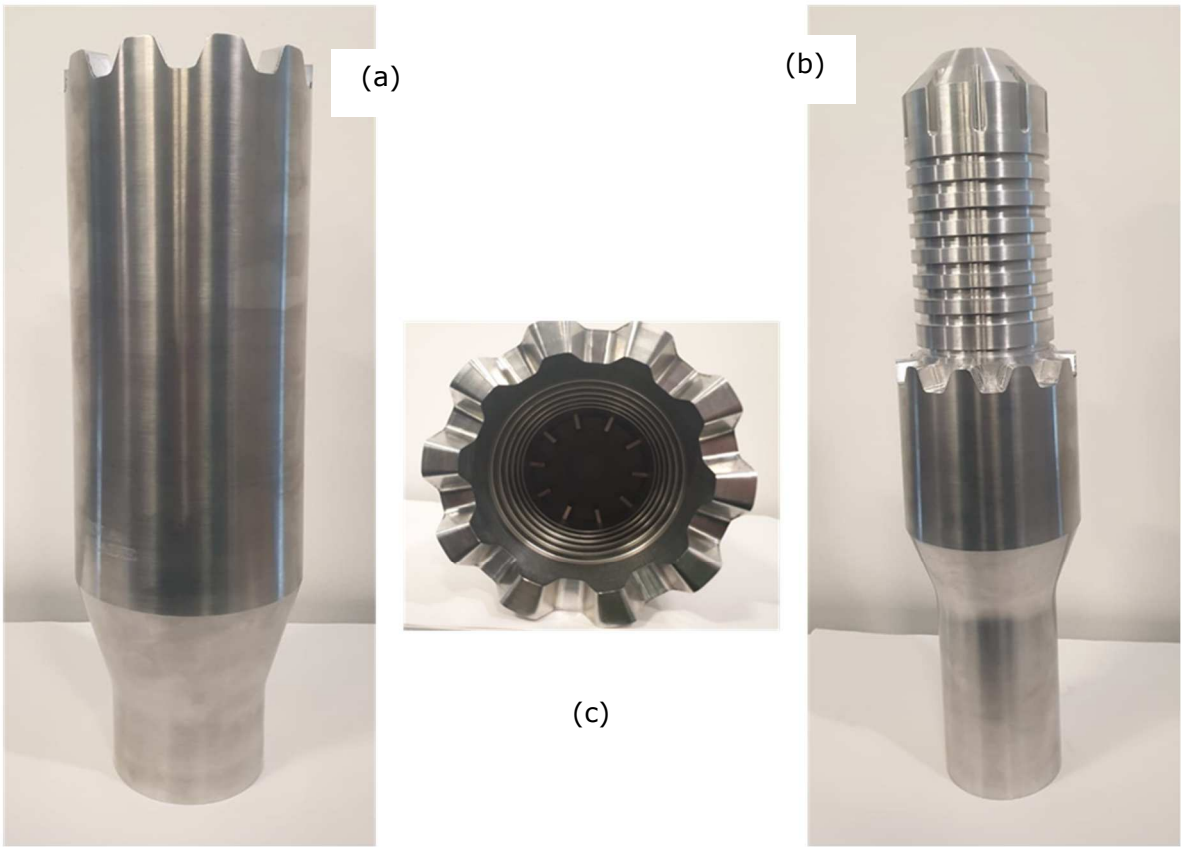

Figure 5.2: Completed CNC machined models of non-threaded tool joint (aluminium): (a) Box Connector, (b) Pin Connector, and (c) top view of Box Connector based on Snap-Latch Rings design (3D CAD model of Pin and Box Connector in Appendix B).

5.3.1 CNC Manufacturing of Snap Latch Design (Prototype I) using Aluminum and Steel

The designed snap latch Prototype I was manufactured by 3D Hubs (Netherlands) by CNC machining (Figure 3.11). The arms of the ring were made of a non-magnetic steel alloy and the mid body thin strip was made of Mild Steel 1018. The process involved creating the CAD model (**Appendix C**) and requesting quotations from several machining and 3D metal printing companies. 3D Hubs provided the best solution within a suitable time frame, cost and correct design and material specifications.

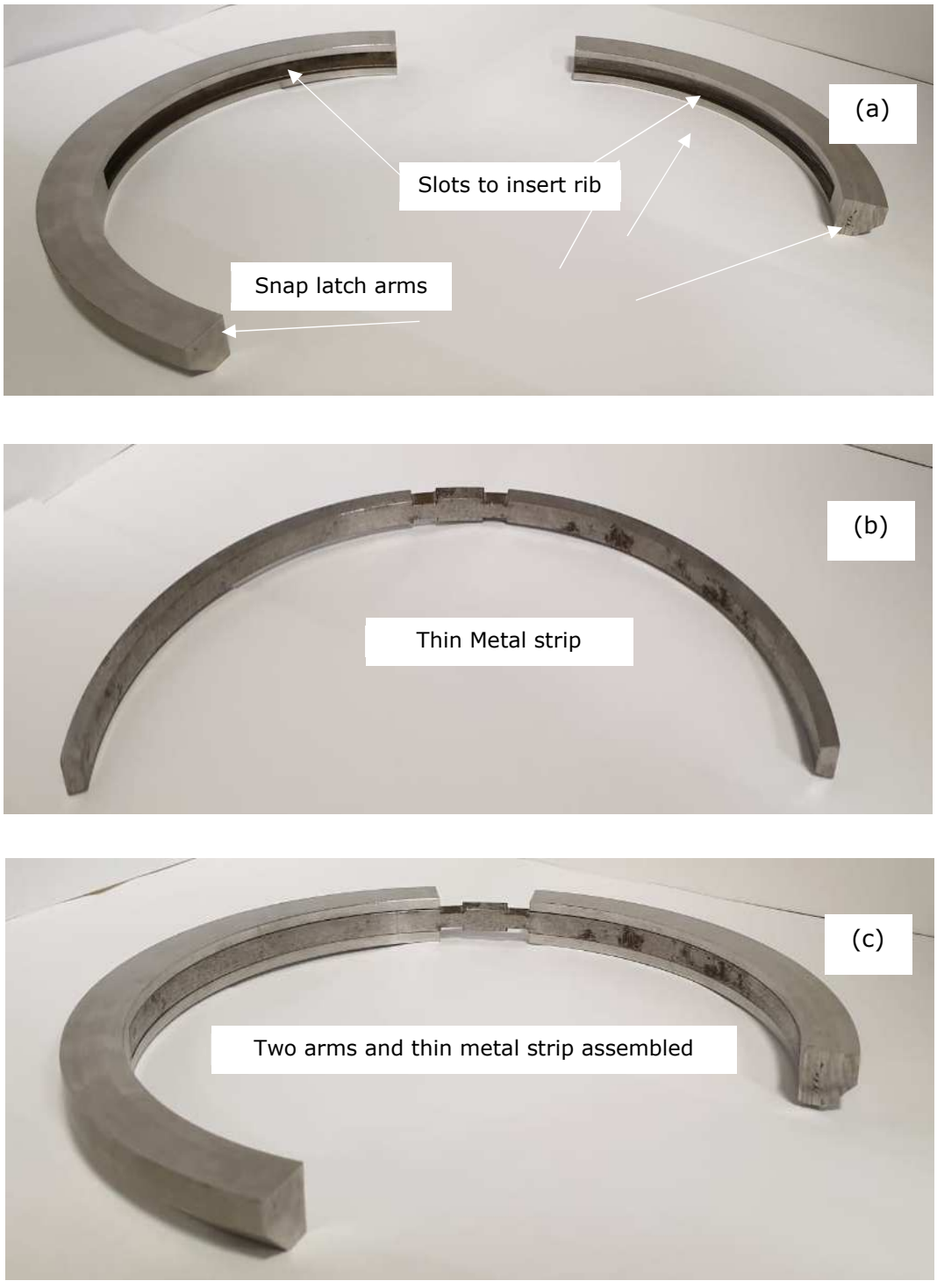

Figure 5.3: Completed CNC machined models of snap latch Prototype I: Manufacturing using CNC machining of aluminium & mild steel: (a) two arms, (b) rib, and (c) two arms and rib assembled (based on modified Snap-Latch Rings design (3D CAD model in Appendix).

The final snap-latch ring product (Prototype I) showed one unforeseen design challenge related to the arm lengths and the angle gap between the arms. The angle gap between the arms was too small (90 degrees) to assemble both arms onto the mid body and hence one of the arms had to be cut by 20 degrees for both arms to be attached. This implies that the surface area of the Ring would have to be smaller in such a prototype for successful manufacturing and assembly, which would imply it would handle a lower load than expected.

To check the actuations process Switch Magnets of 40 kg strength were used to actuate the Ring at extreme ends. Electro-Magnets of 400 kg strength were used as well. Prototype I would sense the magnetic force lightly, yet not strong enough to have the significant pull required. Furthermore, the mid body strip was still too thick and mechanically stiff to possess any significant bending like a spring. A reason the magnetic pull felt by the Snap-Latch is low could be attributed to the low surface area of the mid body of the Snap-Latch Ring or the overall design of the magnetic actuating system (which is a huge development consideration of its own).

As Prototype I did not possess the flexibility to expand and contract as expected due to the high stiffness of the midbody, the introduction of a spring seemed necessary. Hence a torsion spring was integrated to create a new Prototype (II) as seen in Figure 3.3. The torsion spring would allow for opening and closing of the Snap-Latch Ring. One challenge is the limited space available which is 8 mm diameter to manufacture a spring strong enough to bring the arms back to initial position. This is a challenge only observable with a physical model.

The Prototype II was made of seven individual components (see **Appendix D**), which includes: (a) two external side arms made of S135-Stainless Steel, to handle the tensile load during operation, (b) two internal arms made from magnetic mild steel, to retract upon magnetic field, (c) one central torsion spring which would allow the arms to retract backward and then pull them back into position, and (d) a pair of male and female pins to secure and protect the torsion spring and secure the assembly as a whole.

Figure 5.4: Exploded view of Prototype II (showing all the seven components).

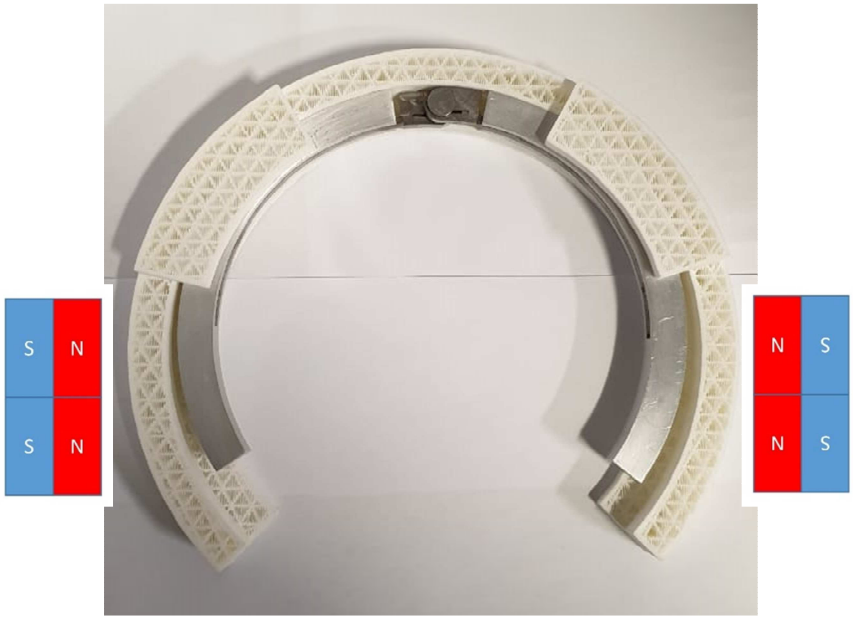

Figure 5.5: Magnets to actuate snap latch: (a) switch magnet, (b) electromagnet, and (c) assembly scheme of magnets to test actuation.

5.3.2 Manufacturing of Modified Snap Latch Design (Prototype II) using Aluminum Alloy and Steel

The designed snap latch Prototype II was manufactured by 3D Hubs (Netherlands) by CNC machining (Figure 5.6). This involved a similar process as that undertaken to design Prototype I. The spring part of the snap latch was difficult to manufacture due to complexity and hence the spring was designed and manufactured as per spring design parameters by FlexoSpring.

Figure 5.6: Completed CNC machined models of Phase 2 snap latch Prototype II: Manufacturing using CNC machining of aluminium & mild steel: two arms with two ribs, a pin and spring assembled (based on modified Snap-Latch Rings design B (3D CAD model in Appendix D).

As shown in Figure 5.7, molds were also made to physically simulate what the Pin and Box grooves would look like and how the Snap-Latch Ring would behave inside them. This was a good tool designed to observe what would happen internally, as shown in Figure 5.8. In order to physically simulate the modified Snap-Latch Ring, the Pin and Box grooves (full scale model, 1:1) made of Acrylonitrile-Butadiene-Styrene (ABS) were manufactured using the INTAMSYS FUNMAT PRO HT 3D printer at School of Engineering in Robert Gordon University. The aim of this assembly was to provide a visual of how the snap latch ring (Prototype I and Prototype II) would behave inside the Pin and Box connectors. The sections made as per scale of the real pin and box grooves; however, sections were carefully cut as seen in the images. Theses section windows allow to see clearly how the rings

actuate within the confines of the system during natural and actuated states. This further allows to better understand the challenges associated with the system mechanics.

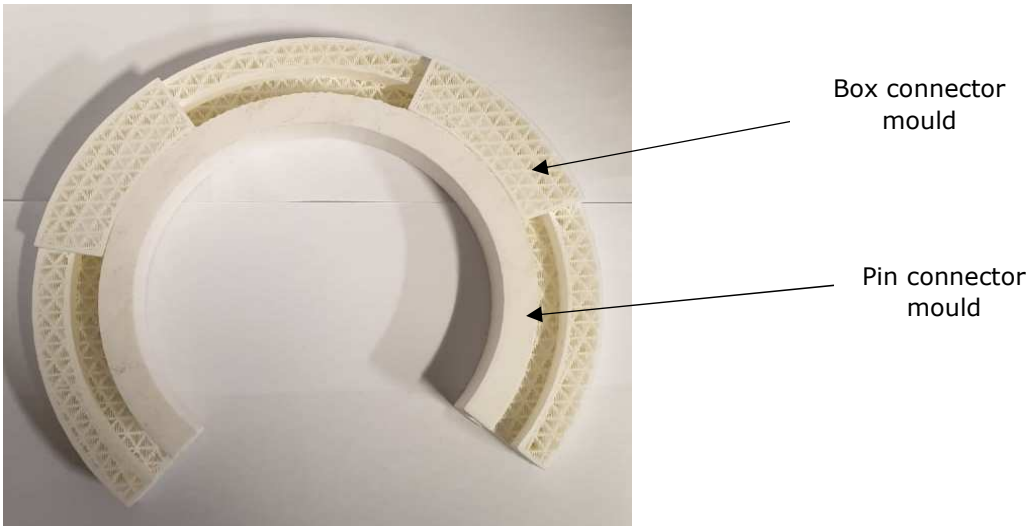

Figure 5.7: Completed 3D printed models of moulds (Acrylonitrile-Butadiene-Styrene) for non-threaded tool joint to physically simulate what the Pin and Box grooves would look like and how the Snap-Latch Ring would behave inside them, for Prototype II.

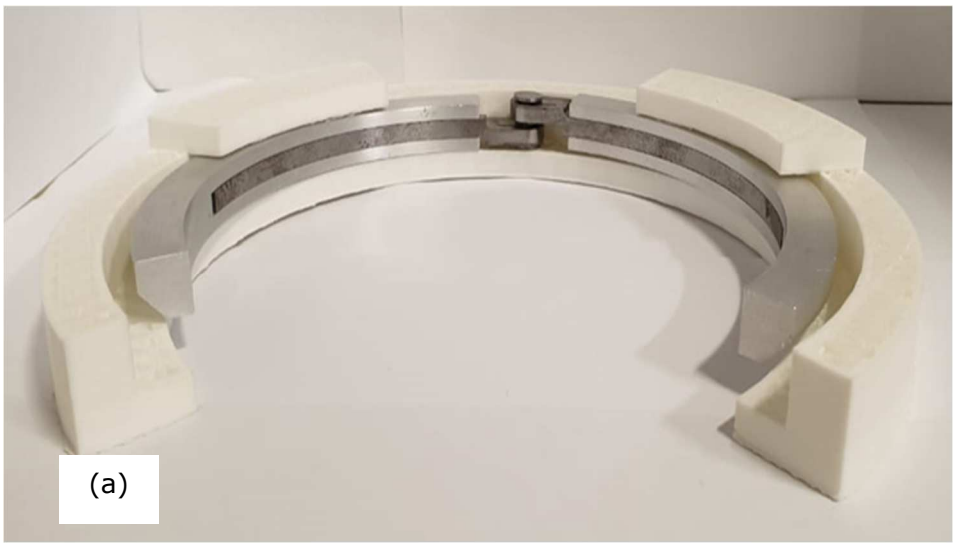

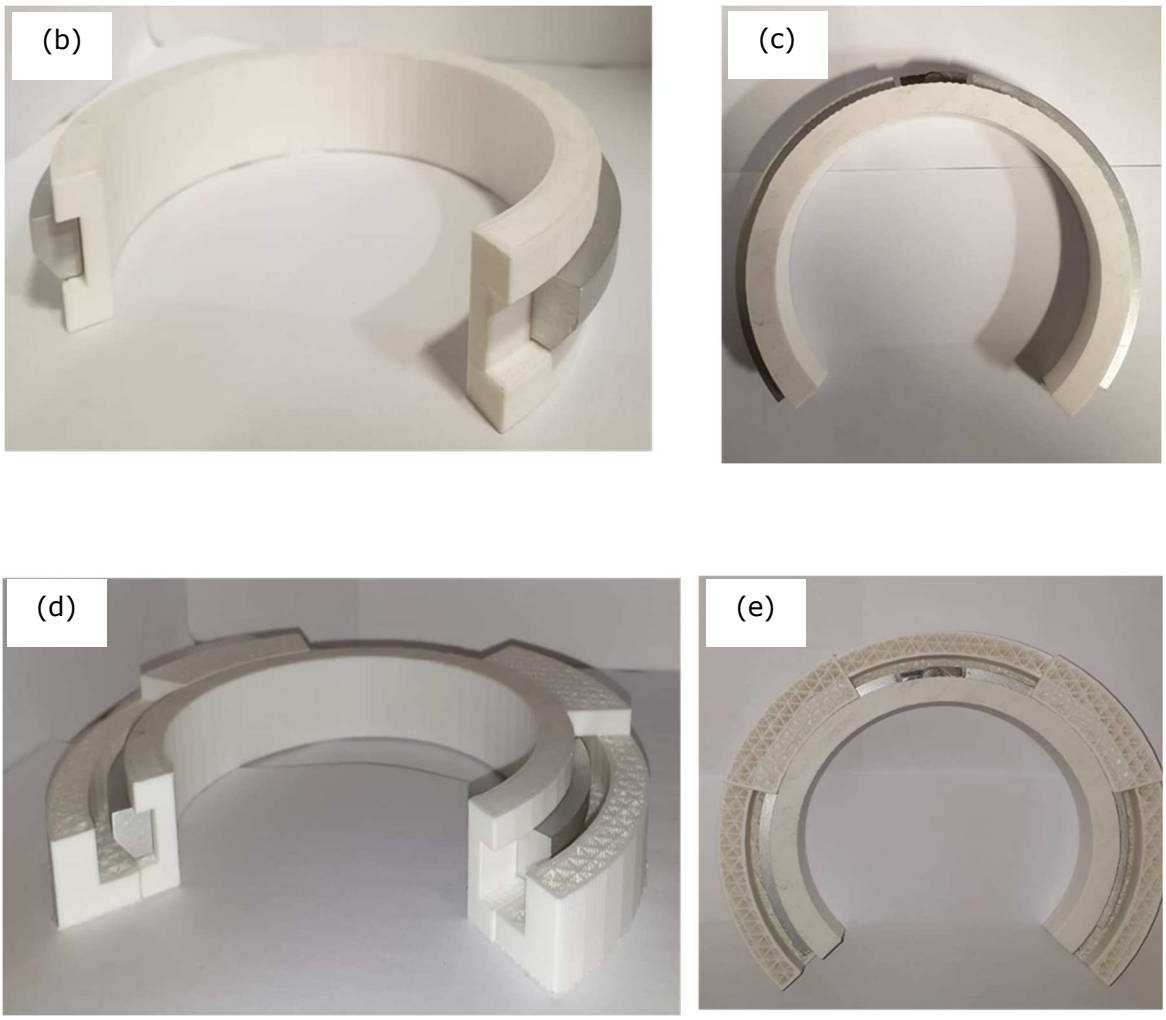

Figure 5.8: Completed 3D printed models of moulds (Acrylonitrile-Butadiene-Styrene) for non-threaded tool joint to physically simulate what the Pin and Box grooves would look like and how the Snap-Latch Ring would behave inside them, for prototype II (based on modified Snap-Latch Rings design B): (a) to (e) showing different views of the assembly.

As shown in Figure 5.8, the manufactured components for Prototype II were assembled successfully. A detailed examination revealed that, the torsion spring (from FlexoSpring) fitted in the allocated space, but over time due to high friction contact the spring started to unwind and expand. This is undesirable feature is due to the manufacturing limitations of a spring in the minimal space available and would require further improvements. The spring had stiffness that allowed it to actuate but not enough mechanical stiffness force to retract it back to its natural state. Furthermore, over repeated mechanical actuations of Prototype II, the spring began to lose its natural stiffness.

5.4 Snap Latch Actuation Setup

Snap latch actuation tests were conducted to understand the properties and limitations of the design, Figure 5.9. The instrumentation of the actuation test included magnets, electromagnets, power supply unit. In the first instance, a magnet based on the pole switch method was used. This included a Magswitch MAGSQUARE 165 On/Off Magnetic Work-holding Square with 150 lb/68 kg holding capacity [4]. These electromagnets are used for lifting and holding applications. The magnets were used with the produced models. The magnets were able to attract the arms at a distance of 25mm however at further distance did not possess the magnetic permeability to attract the arms.

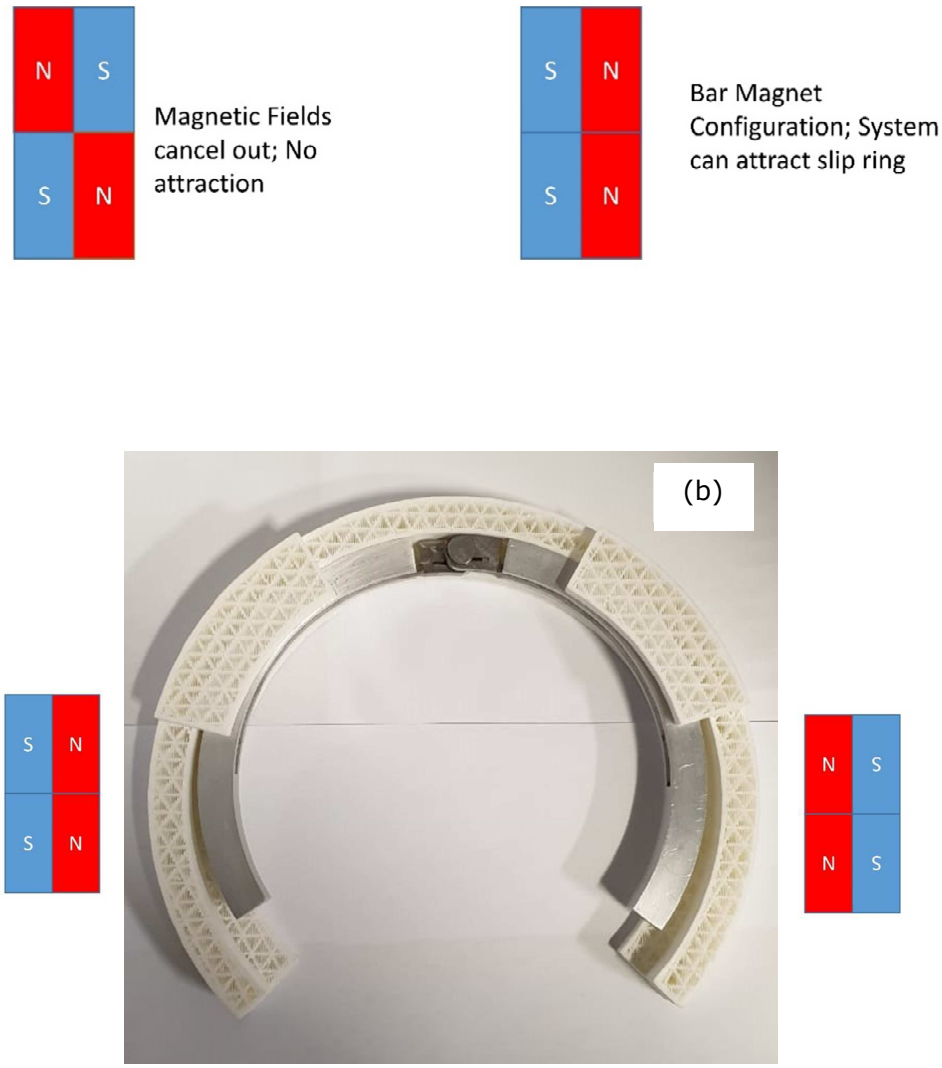

Figure 5.9: Magnets to actuate snap latch: (a) switch magnet, (b) assembly scheme of magnets to test actuation.

5.5 Summary

The 3D production of the Pin and Box connections provided a suitable idea of how the two connections would fit and the feasibility of a snap latch ring and the challenges associated with such a design. This process showed the requirement of some non-contact force that would be able to actuate the snap-latch ring and provided an insight to the installation process of the snap-latch ring within the pin or box connections. The CNC manufactured prototypes of the Pin and Box provided a similar set of results, but the machined prototypes provided a more realistic representation taking into account the metal-to-metal contact and dimensional tolerance.

The production of the Prototype I snap-latch ring was a 3-piece product made of two load bearing arms and the central magnetic strip. This model needed a redesign, where the gap between the arms had to be increased from 90 to 110 degrees for the purpose of successful assembly of the snap-latch ring. Furthermore, the internal magnetic strip would feel the exertion of a magnetic force but not strong enough to cause the strip to radial bend outward. This can be due to the strength of the strip and low surface area of the strip to cause any significant magnetic attraction or force. Prototype II was made of two load bearing arms but a more intricate internal magnetic strip system comprising of a torsional spring which allowed for radial deflection. A summary of the two prototypes, their components and function are provided in Table 14.

Two ABS components were made to represent the grooves of the Pin and Box connections respectively. These were ideal as they provided a real representation of what the snap-latch ring would do within the Pin and Box connections and how the actuation would realistically occur, and the challenges associated with such a process. It was found that both Prototype I and Prototype II did not possess the radial flexibility to fit within both the changing diameters of the Pin and Box connector. This is a design challenge that currently could only be overcome by the snap-latch ring design proposed in Section 3.3.3 (Segment Snap Latch) which requires further investigation and development in the 3D metal production subject. This is because the diameter of the snap-latch ring has to change from its original diameter within the Pin connector and then completely fit within the

diameter of the Box connector upon actuation, which is physically not possible to that extent from a high tensile strength metal.

The snap-latch ring within the confines of the ABS Pin and Box connections were further analyzed with the use of the use of the Mag-switch magnets but the strength of the magnets at a distance of 50mm away, showed a very weak pull force not causing any significant actuation. This is due to low surface area and low magnetic susceptibility of the metal. An alternate solution would be to produce a highly susceptible magnetic metal however this would be a trade-off as the metal would have a much lower tensile load. Further developments and the gap of knowledge bridge from these methods and process will be discussed in the following chapters.

Table 14**:** Snap latch designs Prototype I and Prototype II final description and function.

Product	**Components and function**	**Product Description**
Prototype I	• Left and Right Arm made of S135-Stainless Steel, to handle the tensile load during operation. • Mid Body made of Mild Steel, to retract and reposition upon activation and de-activation of magnetic field	A Snap-Latch Ring with a central bending strip which will actuate (Open arms) into the groove of the Box connector and retract back into its natural state upon deactivation of magnetic field.
Prototype II	• Two external side arms (Left and Right) made of S135-Stainless Steel, to handle the tensile load during operation. • Two internal arms made from magnetic mild steel, to retract upon magnetic field. • One central torsion spring which would allow the arms to retract backward and then pull them back into position. • A Pair of male and female pins to secure and protect the torsion spring and secure the assembly as a whole.	A Snap-Latch Ring with a central torsion spring and mild steel arms which will actuate (Open arms) into the groove of the Box connector and retract back into its natural state upon deactivation of magnetic field. The spring allows for better flexibility.

Chapter 6

DISCUSSION

The project involved a series of processes ranging from literature review, CAD modelling, ANSYS static stress structural simulations to understand product behavior, conceptualization of new ideas and mechanism, material selection, product design and manufacturing, additive and subtractive manufacturing methods and critical analysis. Following discussion can be made regarding the following:

Pin and Box Connectors: It is noticed that maximum stress occurs at the 1st groove in both Pin and Box connector and this behavior is seen in threaded drill pipes where maximum stress is exerted on the 1st thread [8-9]. A reason for poor stress performance can be attributed to the lack of surface area contact between the Pin and Snap-Latch Ring, and Box and Snap-Latch Ring. Threaded drill pipes have a large direct contact area between the two connections. However, the pipe connections can perform at lower ranges of load force. However, the stress limit of the entire system is limited to that of the Snap-Latch ring. Which means the Snap-Latch ring needs to be critically analyzed for strength behavior before analyzing the Pin and Box connectors. The Pin and Box connections due to their teeth like geometry features handle torsional stress as required. Physical prototype models look as expected with quality detail and smoothly connect. For future work it would be important to conduct internal pressure tests to verify the integrity of the design in terms of internal leakages. This would help further identify appropriate choice of sealants and placement of chosen sealants.

Snap Latch Ring: The Snap-Latch Ring was optimized, by changing dimensions of the base and height. It was found that increasing both dimensions would significantly improve its strength and deformation behavior, and this is expected based on mechanical principles. However, increasing the cross-sectional area of the Snap-Latch ring implies the grooves in the Pin and Box connector would have to be proportionally big and hence make the overall pipe connectors big, which is not a desirable outcome. Increasing Pipe connector diameters would indirectly increase pipe weight and underground hole size which would require change in the entire drilling process and subsequent tooling.

Since the Rings are a crucial component of the entire tool joint system, the maximum applicable force will be limited by the stress limitation of the Ring. Hence the safe operational force that can be applied is 1,130.22 kN (254,034 lbs) which is 13.2% of the original suggested maximum tensile force 8,565 kN (1,925,541 lbs). Hence the application of the current design needs reconsideration.

Magneto-strictive materials are not suitable due to their low expansion (9-10%). However, they could be used as sealants at different locations of the Pin and Box. As the Snap-Latch Ring is located (sandwiched) between the Pin and Box connectors, the only means of actuation is by non-contact forces. This is only possible through magnetic actuation. However, the surface area of the ring is too small to be attracted with the required pull force.

One key challenge is the fixed radius of the Snap-Latch Ring for a given sector length which does not accommodate within both the grooves of the Pin and Box during natural and actuation state. This is expected as the Snap-Latch Ring is made of a high stiffness metal. The material must be very strong to handle the tensile forces during operation and hence this challenge can only be overcome by designing several segments (i.e., segmented snap-latch design). The Snap-Latch Ring needs to stay firm in its natural position and once actuated must possess a flexible mechanism that causes it to retract back into position. Prototype I incorporated a bending strip; however, it was still too stiff and further reducing the thickness of the bending strip would not be desirable in a high load, high temperature and high corrosion environment. A torsion spring was critically chosen for Prototype II and the components successfully fit, however, over a period of time the spring began to lose its elasticity and strength and deform under repeated loads. Future work could investigate advanced spring design however this is a challenge due to limitations in spring manufacturing and the limitations of space available to position a spring within the Snap-Latch Ring.

Manufactured Snap Latch Ring: One major problem with design in both case of Prototype I and Prototype II which was only noticeable after manufacturing, was that the radius to remain its natural state would extend the arms during actuation. This means that upon actuation, the Pin and Box connectors would not be able to successfully be connected due to the Ring arms not being flush along the groove

of the box connector (Figure 6.1). This is a huge geometric challenge that implies the Snap-Latch Ring model would have to be made of multiple segments whose arc radius would fit both radii required in natural state and actuated state. Multiple segments are not ideally a desired feature to lack of mechanical stability as a single system and too many components in a system result in multiple dependents and causes of failure in the entire system.

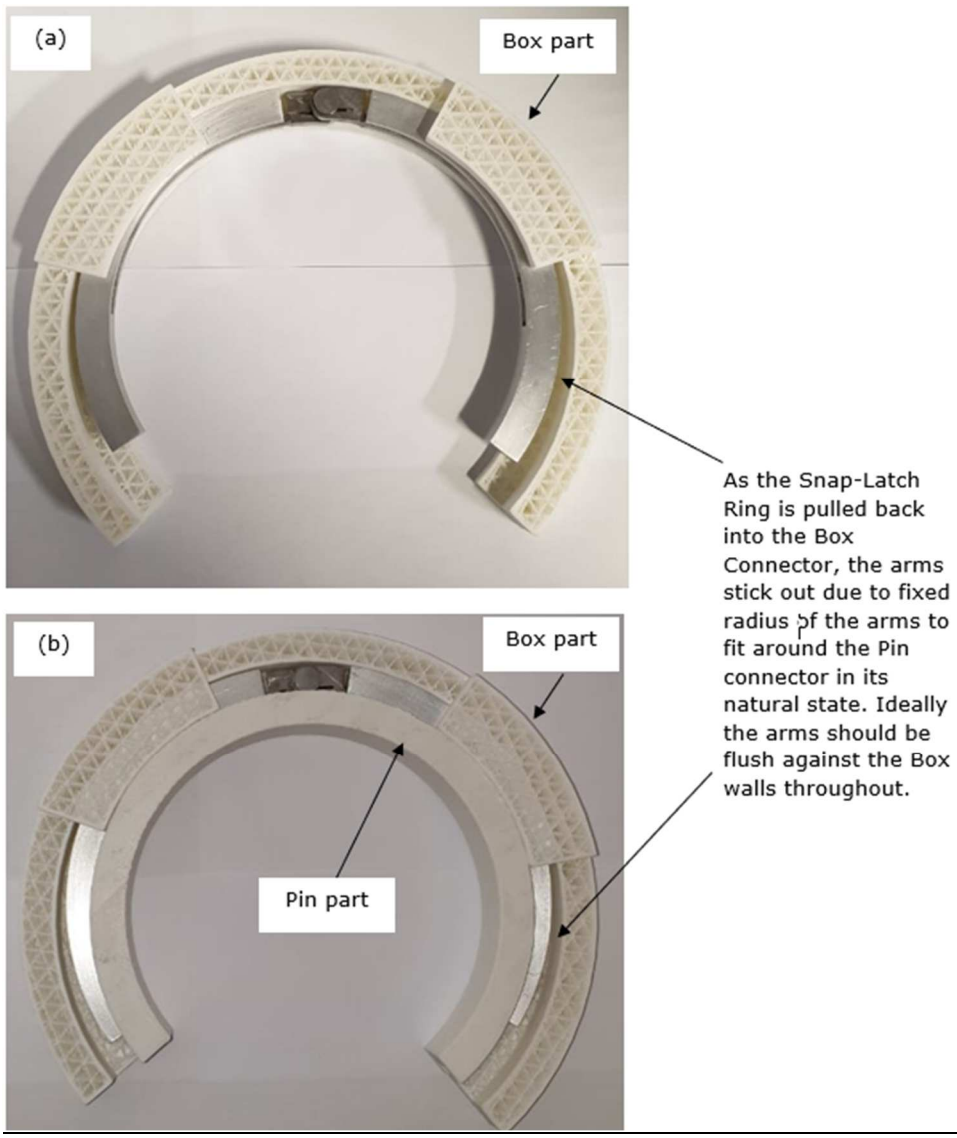

Figure 6.1**:** Prototype II in its actuated state inside the Pin and Box Connector showing arms sticking out: (a) without pin and (b) with pin.

Magnetic Actuation: Since magnetism can work over a distance and magnets can exert a force (push or pull) on objects without contacting them, the test included putting snap latch close to magnet to attract and induce actuation while holding the snap latch in a fixed position. Like Prototype I snap latch, Prototype II snap latch showed tendency to be attracted to magnetic force exerted by the switch magnet but not significant to cause the required actuation.

For both Prototype I and Prototype II, qualitative tests were conducted to assess the Snap-Latch Rings actuation. In a typical process, two switch magnets of 40 kg strength were set at various positions of the Snap-Latch ring symmetrically and turned on. They were then adjusted at different distances to gauge the magnet strength force. Similar setup was done using two electromagnets of 400 kg. It is understood that the magnetic force was felt by the Snap-Latch ring but was not strong enough to cause bending or actuation as desired. This is a challenge which could be solved by doping the material composition with high magnetic elements however this intern affects other properties such as temperature and corrosivity resistance. Hence further research would be recommended in high curie temperature, high strength magnetic alloys.

Summary

The stress patterns seen in the Pin and Box connections are like those seen in traditional threaded joint connections however the placement of a snap-latch ring is not suitable due to the high tensile loads subjugated on the snap-latch ring itself. Furthermore, having too many components within downhole assemblies increase the risk of downhole failures which can stall operations costing time and money which are highly undesirable to the industry. The Snap latch ring has a tensile limit under which it can safely operate with the entire system however the fact that the snap-latch ring has low magnetic susceptibility and cannot actuate radially while changing radius make the current snap-latch designs proposed not suitable with current technological resource. Both physical models produced were checked to ascertain the challenges associated with such a design.

Chapter 7

CONCLUSION

The process of identifying the feasibility of a Non-Threaded drill pipe connector has been reviewed extensively with multiple approaches; both through the process of simulation analysis and by production and testing. Both approaches have indicated that with the current technology a non-threaded tool joint connector is not a sustainable development due to the high tensile load, high load cycling, high temperatures and highly corrosive environment. The main conclusions are given below.

- The drill pipe connectors by design could be designed to handle high levels or torque however due to the lack of surface area for contact for all three components the high tensile load causes significant amounts of deformation which would damage the tool string assembly and lead to undesirable conditions during operation. Furthermore, there is a challenge in the Snap Latch design that demands high tensile yielding in the direction of the load but at the same time must be elastic radially to actuate within the Pin and Box connectors. Current technology in the oil and gas sector has advanced to automated threaded tool joint connection which appears to tackle the safety aspect of tool joint connection on a platform. This would lead to the conclusion that the development of a non-threaded tool joint may not necessarily be financially beneficial for the oil and gas industry given the challenges associated with the design considerations.
- During the course of the research, demonstrations were produced through FEA simulations and prototype productions to empirically and practically display the feasibility of a non-threaded drill pipe connection system and the challenges associated with such a novel design and that the findings from such a novel concept may not be applicable to the use of downhole tool joint connections, but aspects of the research may be applicable to a multitude of different applications.

Chapter 8

FURTHER RECOMMENDATIONS

Based on the results and conclusion the following recommendations have been provided if future work is to be considered in this subject.

- The Pin and Box design could be altered to look at creating maximum shear contact between the components. More shear contact area means more stress distribution and better stress and deformation performance.
- The materials chosen to have must crucially consider 3 significant factors: high repetitions of high ranges of loads, high temperature and high corrosion environment. If principles of magnetism were to be involved all three factors must be considered even more carefully.
- Furthermore, keeping in mind, the Snap-Latch Ring needs to be strong to handle the operational load under repetition, be flexible radially to contract and retract, high thermal, high corrosion and highly magnetic. These are an array of material properties which do not coexist currently due to physical and chemical limitations associated with physical principles. This is, however, subject to possible change with advances in technology and material sciences.
- The segment rings alternative is a heterogeneous design of multiple small segments and hence requires research in development of a single heterogeneous composite made in such a way, where desired properties can be allocated at desired positions of the component. This is a new field of study. Ideally, the Snap-Latch Ring should be made of minimal components as minimal components means less dependents for failure. The traditional threaded connections only involve two components for each connection and hence any mechanism involving more components for such a process would need strong justification.

REFERENCES

[1] Schlumberger, 2020. Bottomhole Assembly. Available from: https://www.glossary.oilfield.slb.com/en/Terms/b/bottomhole_assembly.aspx.

[2] FlowtechEnergy, 2018. Drill Pipe. Available from: https://www.flowtechenergy.com/oil-gas-questions/drill-pipe/

[3] Texas International Oilfield Tools, 2019. All about drill pipes. Available from: http://www.texasinternational.com/all-about-drill-pipes/

[4] IADC, 2020. Meet the Bottom Hole Assembly. Available from: https://drillingmatters.iadc.org/meet-the-bottomhole-assembly/

[4] PetroWiki, 2015. Drillpipe Failures. Available from: https://petrowiki.org/Drillpipe_failures

[5] AAPG, 2019. Drilling Problems. Available from: https://wiki.aapg.org/Drilling_problems

[6] Hare. J and Johnson. M, 2009. Underlying Causes of Offshore Incidents, Available at: http://www.hse.gov.uk/offshore/offshore-incidents.pdf.

[10] Bjorheim. F, 2015. Drillpipe Thread Types. Available from: https://blog.odfjellwellservices.com/drilling-thread-types-for-dummies

[11] IADC Drilling Manual, 2000. Chapter B – Drill String

[12] GlobalSpec, 2020. Drill Pipe Information. Available from : https://www.globalspec.com/learnmore/specialized_industrial_products/mining_equipment/drill_pipe]

[13] DrillingManual, 2017. API Drill Pipes Description and Specifications. Available from: https://www.drillingmanual.com/2017/11/drill-pipes-description.html

[14] Schlumberger, 2020. Tool Joint. Available from: https://www.glossary.oilfield.slb.com/en/Terms/t/tool_joint.aspx

[15] Drilling Manual, 2017. Drill String Design. Available from: https://www.drillingmanual.com/2017/11/drilling-string-design.html

[16] Yan. H et al, 2014. Failure Analysis on Fracture of a S135 Drill Pipe. Procedia Materials Science 3, 447-453, Elsevier.

[17] Zhang. Z and Zhu. X, 2019. Failure Analysis and improvement measure steps transition zone of drill pipe joint. Engineering Failure Analysis 109.

[18] Ming. L et al, 2019. Corrosion fatigue crack propagation behaviour of S135 high strength drill pipe steel in H2S environment. Engineering Failure Analysis 97, 493-505.

[19] Luo. S. and Wu. S, 2013. Effect of stress distribution on the tool joint failure of internal and external upset drill pipes. Materials and Design 52, 308-314

[20] Shahani. A.R and Sharifi. S.M.H, 2009. Contact stress analysis and calculation of stress concentration factors at the tool joint of a drill pipe. Materials and Design 30, 3615-3621.

[21] Dong. L, 2018. Study on mechanical behaviours of double shoulder drill pipe joint thread. Petroleum 5, 102-112

[22] Nielsen. A.E, 1938, Threadless interlocking rotary drill pipe coupling, US Patent USPTO 2121710.

[23] Ohls. R.L, 1941, Tool Joint, US Patent USPTO 2238706.

[24] Winberg. D.F. and Mccurdy. D.K., 1966, Drilling shaft coupling having pin securing means, US Patent USPTO 3258283.

[25] Vincent. R.P. et al, 1969, Joint for coupling two tubular members together, US Patent USPTO 3472538.

[26] Mefferd. F.R. 1993, Apparatus and method for coupling elongated members, US Patent USPTO 5269572.

[27] Lurie. P.G. and Head. P, 2004, Non-threaded expandable pipe connection system, European Patent EP1704299B1

[28] Buytaert. J.P, 2010, Threadless drill pipe connector, US Patent USPTO 2010/0213707 A1.

[29] Herrera. D, 2013, Non-threaded drill pipe connection, US Patents 8474879 B2

[30] Institute of Rock Magnetism, 2019. Magnetic Anisotropy. Available at: http://www.irm.umn.edu/hg2m/hg2m_c/hg2m_c.html

[31] Olabi. A.G. and Grunwald, A. 2008. Design of a magnetostrictive (MS) actuator. Sensors and Actuators A, 161-175.

[32] Olabi. A.G. and Grunwald, A. ,2007. Design and application of magnetostrictive materials. Materials and Design 29, 469-483.

[33] Elhajar. R, Law. C.T, Pegoretti. A,2018. Magnetostrictive polymer composites: Recent advances in materials, structures and properties. Progress in Material Sciences 97, 204-229.

[34] Zuberek. R. et al. ,2018 Magnetocaloric effect and magnetoelastic properties of NiMnGa and NiMnSn Heuler alloy thin films. Journal of Alloys and Compounds 748, 1-5.

[35] Zhao, Y and Kang, M. ,2018. Strain-magnetization effect in superelastic NiMnGa microfiber. Scripta Materialia 162, 397-401.

[36] Ulaby, T.F. 2005. Electromagnetisc for Engineers: Pearson Education Publications.

[37] Spaldin, N. 2003. Magnetic Materials: Fundamentals and Device Applications. Press Syndicate, Cambridge Publications.

[38] Madhu. R, 2018. Difference Between Magnetic Permeability and Susceptibility. Available at: https://www.differencebetween.com/difference-between-magneticpermeability-and-vs-susceptibility/

[39] Institute of Rock Magnetism, 2019. Classes of Magnetic Materials. Available at: http://www.irm.umn.edu/hg2m/hg2m_b/hg2m_b.html.

[40] Birmingham University, (2019) Classification of Magnetic Materials. Available at: https://www.birmingham.ac.uk/Documents/college-eps/metallurgy/research/Magnetic-Materials-Background/Magnetic-Materials-Background-4-Classification-of-Magnetic-Materials.pdf

[41] Clarke, R. (2008) Magnetic Properties of Materials. Available at: http://info.ee.surrey.ac.uk/Workshop/advice/coils/mu/

[42] Britannica (2019) Curie Point. Available from: https://www.britannica.com/science/Curie-point

[43] K&J Magnetics (2019), Magnets with an OFF Switch. Available at: https://www.kjmagnetics.com/blog.asp?p=magswitch

[44] Underwood, P (2014). Switchable Permanent Magnetic Device. Available at: https://patents.google.com/patent/US6707360B2/en

[45]Budynas, R.G. (2011), Mechanical Engineering Design: 9th Edition. McGraw-Hill Publications

Appendices

Appendix A – Tool Joint Drawings of Box and Pin Connection ends

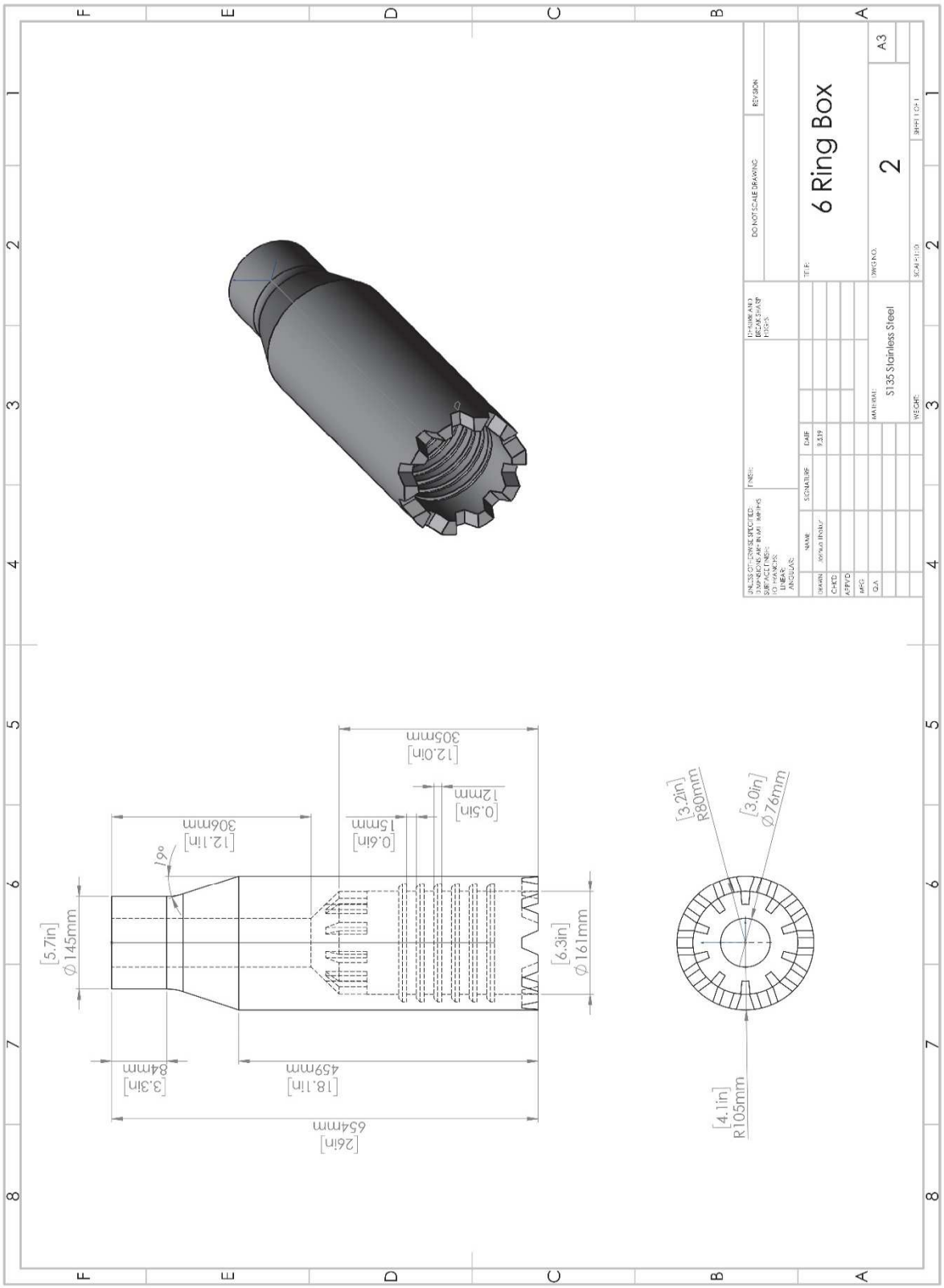

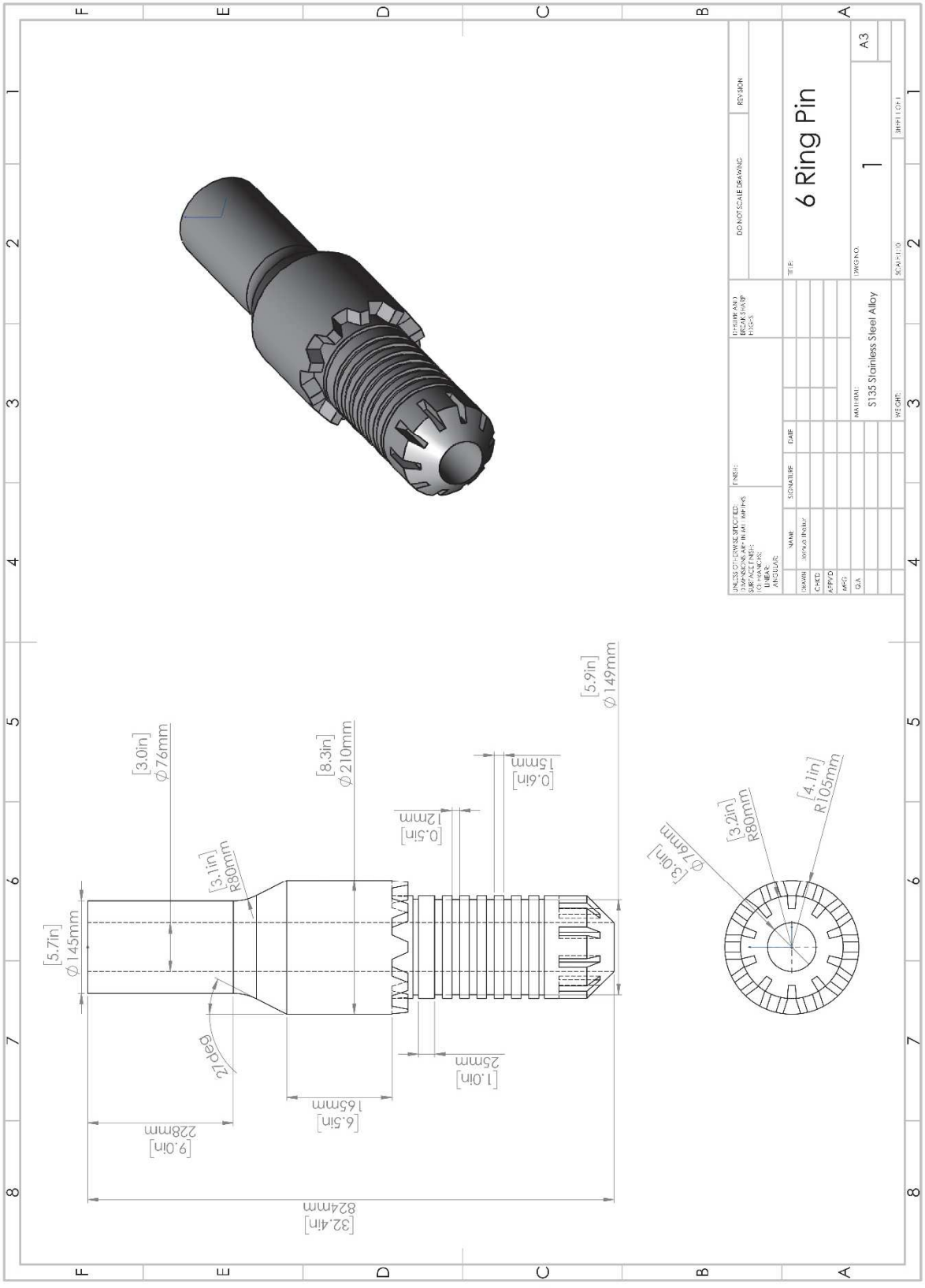
6 Ring Pin
S135 Stainless Steel Alloy
A3
DO NOT SCALE DRAWING
[32.4in]
824mm
[9.0in]
228mm
[6.5in]
165mm
[1.0in]
25mm
[0.5in]
12mm
[0.6in]
15mm
[5.9in]
Ø149mm
[8.3in]
Ø210mm
[3.0in]
Ø76mm
[3.1in]
R80mm
[5.7in]
Ø145mm
21deg
[3.0in]
Ø76mm
[3.2in]
R80mm
[4.1in]
R105mm

Appendix B – Tool Joint Drawings of Pin and Box for CNC Production

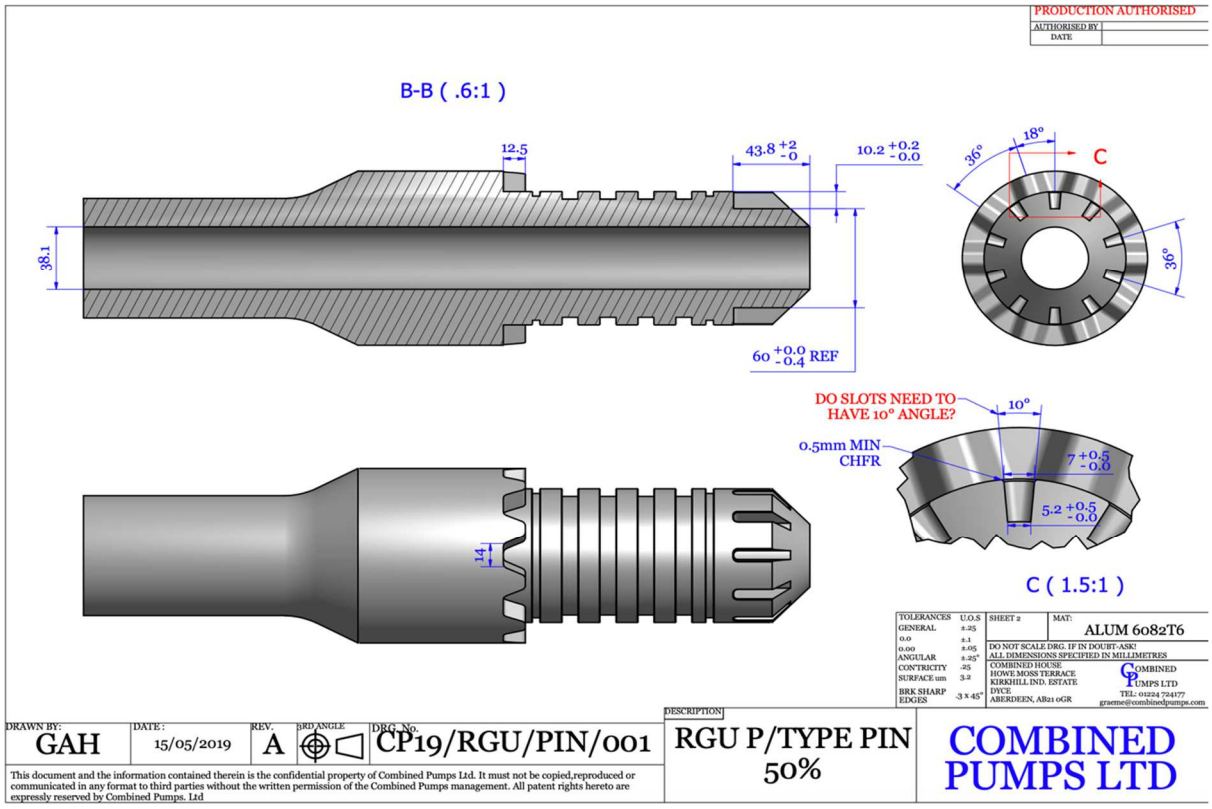

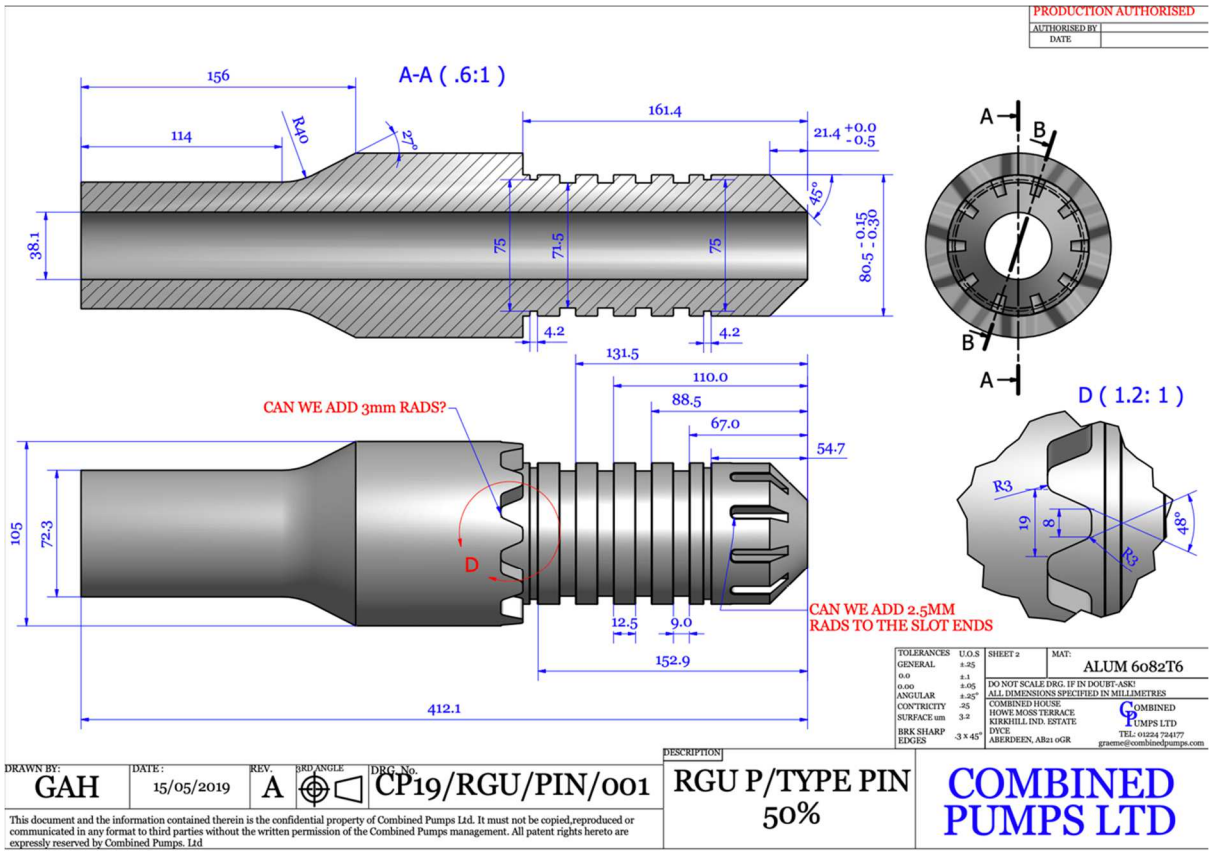

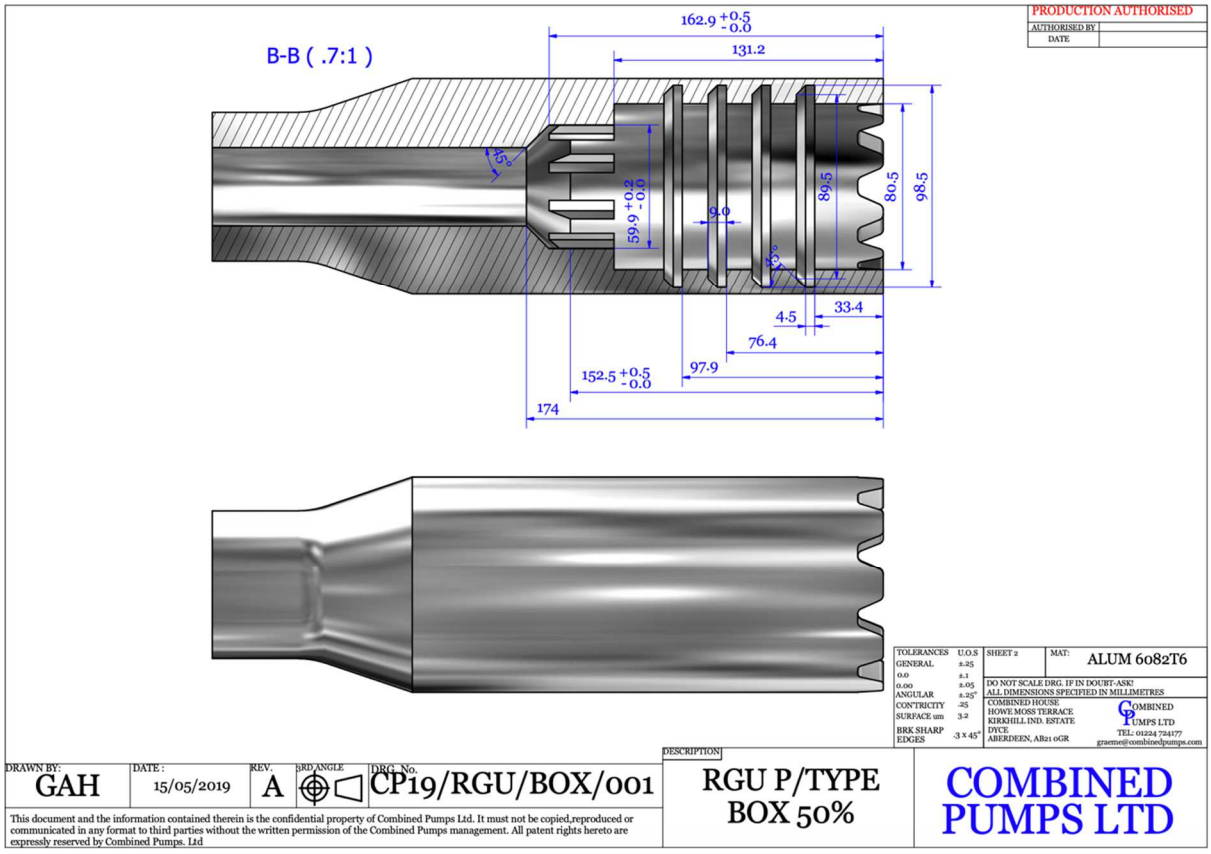
PRODUCTION AUTHORISED
AUTHORISED BY
DATE
B-B (.7:1)
162.9 +0.5 -0.0
131.2
45°
59.9 +0.2 -0.0
9.0
89.5
80.5
98.5
30°
4.5
33.4
76.4
97.9
152.5 +0.5 -0.0
174
TOLERANCES U.O.S
GENERAL ±.25
0.0 ±.1
0.00 ±.05
ANGULAR ±.25°
CON'TRICITY .25
SURFACE um 3.2
BRK SHARP EDGES .3 X 45°
SHEET 2
MAT: ALUM 6082T6
DO NOT SCALE DRG. IF IN DOUBT-ASK!
ALL DIMENSIONS SPECIFIED IN MILLIMETRES
COMBINED HOUSE
HOWE MOSS TERRACE
KIRKHILL IND. ESTATE
DYCE
ABERDEEN, AB21 0GR
COMBINED PUMPS LTD
TEL: 01224 724177
graeme@combinedpumps.com
DRAWN BY: GAH
DATE : 15/05/2019
REV. A
3RD ANGLE
DRG. No. CP19/RGU/BOX/001
DESCRIPTION
RGU P/TYPE BOX 50%
COMBINED PUMPS LTD
This document and the information contained therein is the confidential property of Combined Pumps Ltd. It must not be copied,reproduced or communicated in any format to third parties without the written permission of the Combined Pumps management. All patent rights hereto are expressly reserved by Combined Pumps. Ltd

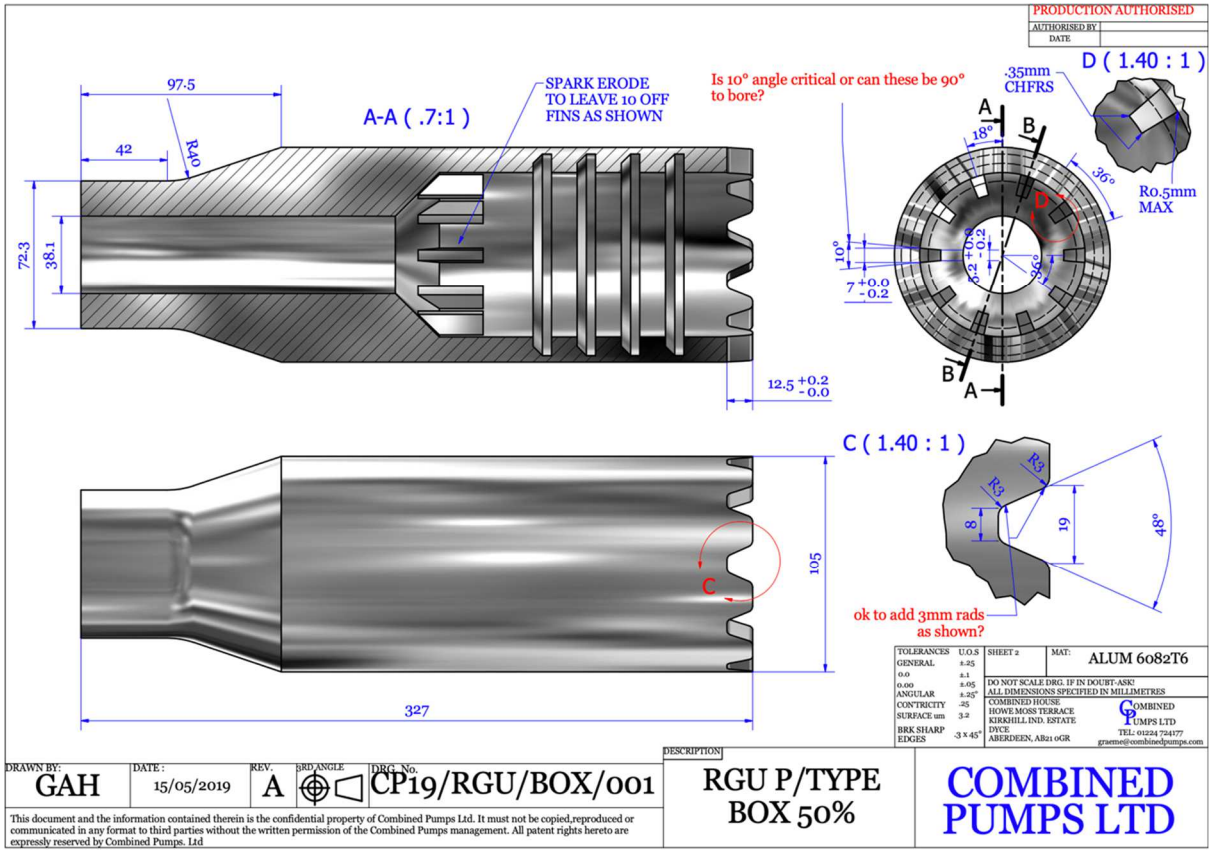
PRODUCTION AUTHORISED
AUTHORISED BY
DATE
A-A (.7:1)
97.5
42
R40
72.3
38.1
SPARK ERODE TO LEAVE 10 OFF FINS AS SHOWN
12.5 +0.2 -0.0
Is 10° angle critical or can these be 90° to bore?
D (1.40 : 1)
.35mm CHFRS
Ro.5mm MAX
A
B
18°
36°
10°
7 +0.0 -0.2
5.2 +0.3 -0.2
36°
C (1.40 : 1)
R3
R3
8
19
48°
ok to add 3mm rads as shown?
105
327
TOLERANCES U.O.S
GENERAL ±.25
0.0 ±.1
0.00 ±.05
ANGULAR ±.25°
CON'TRICITY .25
SURFACE um 3.2
BRK SHARP EDGES .3 X 45°
SHEET 2
MAT: ALUM 6082T6
DO NOT SCALE DRG. IF IN DOUBT-ASK!
ALL DIMENSIONS SPECIFIED IN MILLIMETRES
COMBINED HOUSE
HOWE MOSS TERRACE
KIRKHILL IND. ESTATE
DYCE
ABERDEEN, AB21 0GR
COMBINED PUMPS LTD
TEL: 01224 724177
graeme@combinedpumps.com
DRAWN BY: GAH
DATE : 15/05/2019
REV. A
3RD ANGLE
DRG. No. CP19/RGU/BOX/001
DESCRIPTION
RGU P/TYPE BOX 50%
COMBINED PUMPS LTD
This document and the information contained therein is the confidential property of Combined Pumps Ltd. It must not be copied,reproduced or communicated in any format to third parties without the written permission of the Combined Pumps management. All patent rights hereto are expressly reserved by Combined Pumps. Ltd

Appendix C – Snap Latch Ring Prototype I

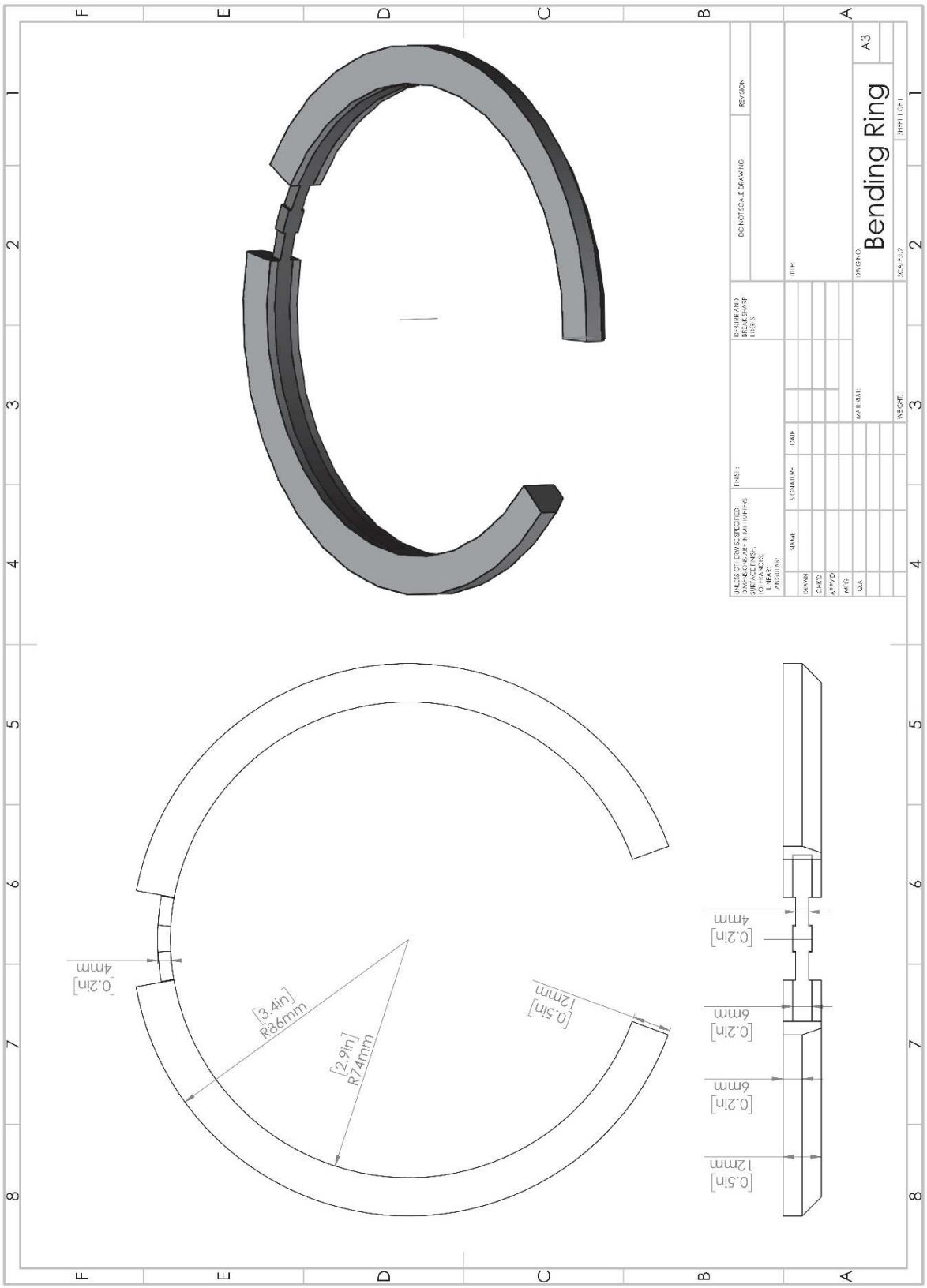

Appendix D – Snap Latch Ring Prototype II

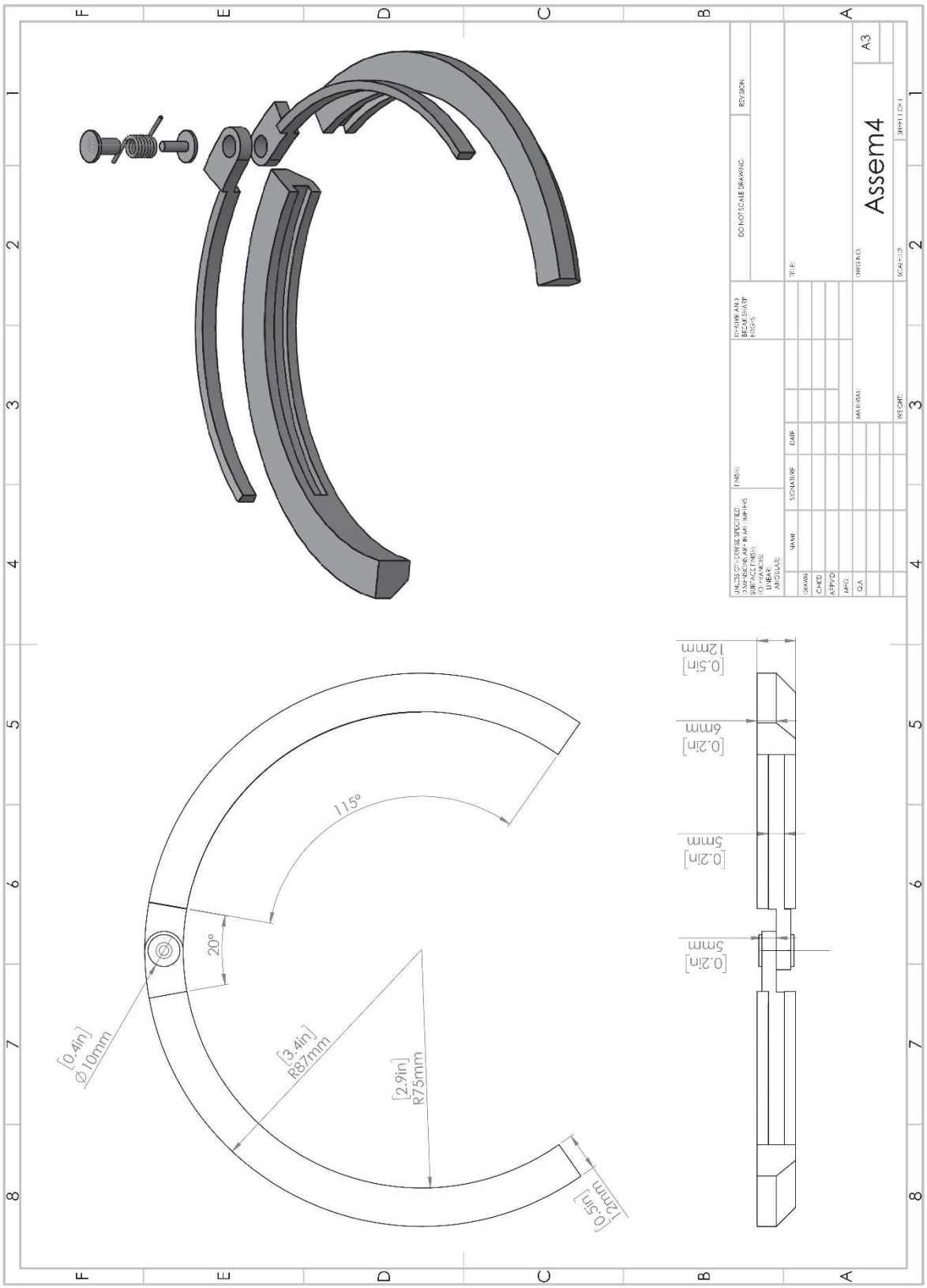

Appendix E – Thin Strip Analysis

Aim: Simulation of the Thin Strip of the Snap-Latch Ring to find optimal thickness for flexibility to engage and disengage.

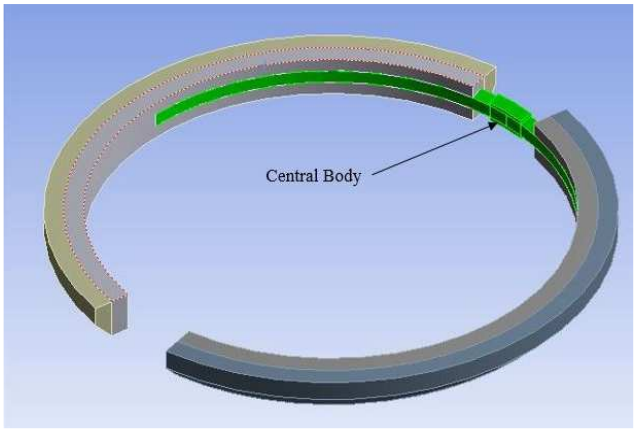

Figure: Thin Strip (Central Body) of Snap-Latch Ring Assembly

Assumptions

- Thin Strip being used is made of mild steel (AISI 1080) which displays magnetic behaviour.
- The Tensile Yield Strength is 370MPa and the Tensile Ultimate Strength is 440MPa
- Modulus of elasticity is 205GPa and Poisson Rations is 0.3
- The strip is being simulated as an independent component and is independent of the effects of the arms.
- The strip deformation and stress behaviour will be investigated at thickness of 4mm, 3mm, 2mm and 1mm.
- The forces will be applied on each body side horizontally at a range of forces and the central pivot point of the strip will be allowed to move vertically by 6mm as it would in actual operation.

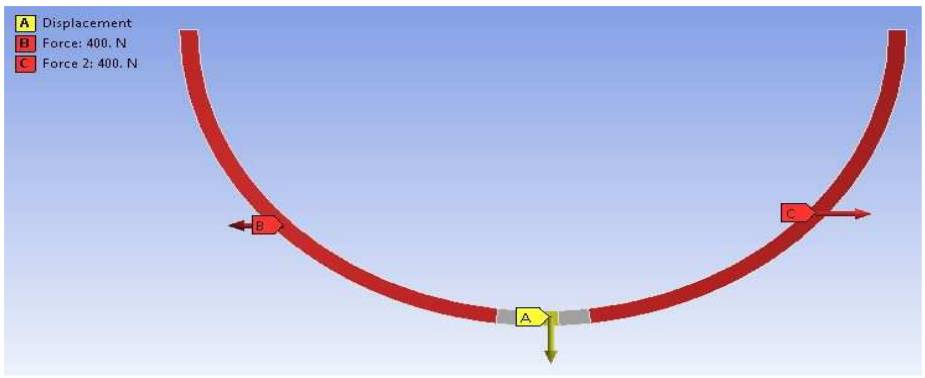

Figure: Simulation Parameters on Snap-Latch Thin Strip

4mm Thickness of Thin Strip

Figure: Stress and Deformation Results

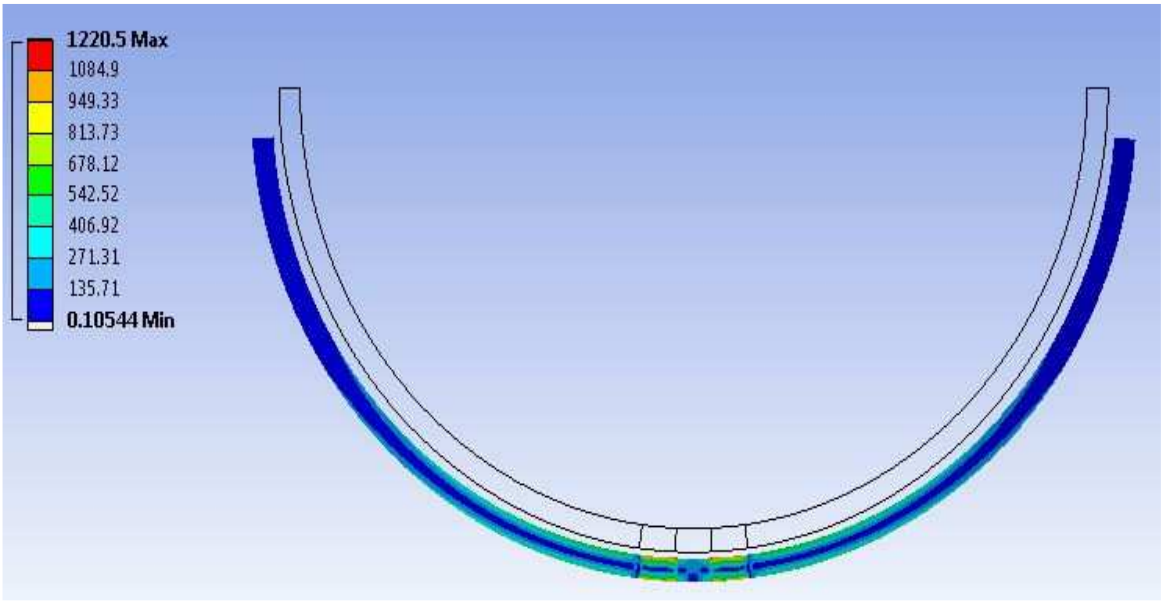

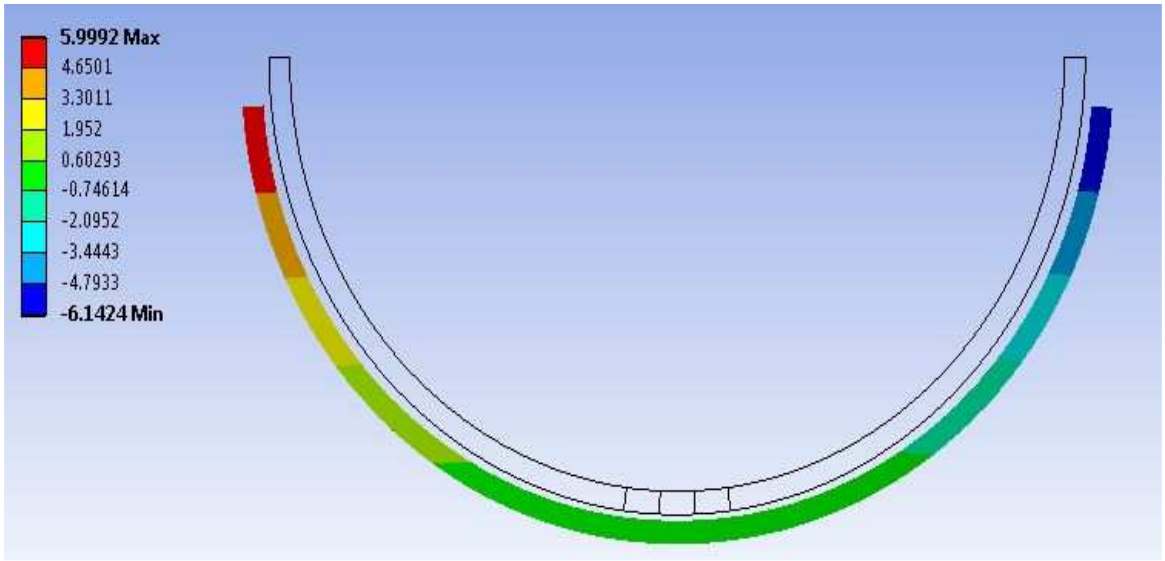

Tabular Results

Table 1: 4 mm Strip Thickness

Force (N)	Max Stress (MPa)	Max Horizontal Deformation (mm)
400	1251.19	6.30
380	1188.63	5.99
360	1126.07	5.67
340	1063.51	5.36
320	1000.95	5.04
300	938.39	4.73
280	875.83	4.41
260	813.27	4.10
240	750.71	3.78
220	688.15	3.47
200	625.59	3.15
180	563.03	2.84
160	500.47	2.52
140	437.91	2.21
120	375.35	1.89
100	312.80	1.58
80	250.24	1.26
60	187.68	0.95
40	125.12	0.63
20	62.56	0.32

Table 2: 3 mm Strip Thickness

Force (N)	Max Stress (MPa)	Max Horizontal Deformation (mm)
200	1076.24	7.28
190	1022.42	6.91
180	968.61	6.55
170	914.80	6.18
160	860.99	5.82
150	807.17	5.46
140	753.36	5.09
130	699.55	4.73
120	645.74	4.37
110	591.93	4.00
100	538.12	3.64
90	484.30	3.27
80	430.49	2.91
70	376.68	2.55
60	322.87	2.18
50	269.06	1.82
40	215.25	1.46
30	161.44	1.09
20	107.63	0.73
10	53.81	0.36

Table 3: 2 mm Strip Thickness

Force (N)	Max Stress (MPa)	Max Horizontal Deformation (mm)
100	1622.62	11.96
90	1460.36	10.76
80	1298.10	9.57
70	1135.84	8.37
60	973.58	7.17
50	811.32	5.98
40	649.06	4.78
30	486.80	3.59
20	324.54	2.39
10	162.28	1.20

Table 4: 1 mm Strip Thickness

Force (N)	Max Stress (MPa)	Max Horizontal Deformation (mm)
50	3426.73	46.13
45	3084.05	41.52
40	2741.38	36.91
35	2398.71	32.29
30	2056.03	27.68
25	1713.35	23.07
20	1370.69	18.45
15	1028.03	13.84
10	685.37	9.23
5	342.70	4.61

Appendix F – Ring Optimisation All Cases

Stress and Deformation images for each condition for every case have been provided

Figure Set1: Deformation Changes with increase in Height at Force for Case 1 (Left) and Stress Changes with increase in Height at Force for Case 1 (Right)

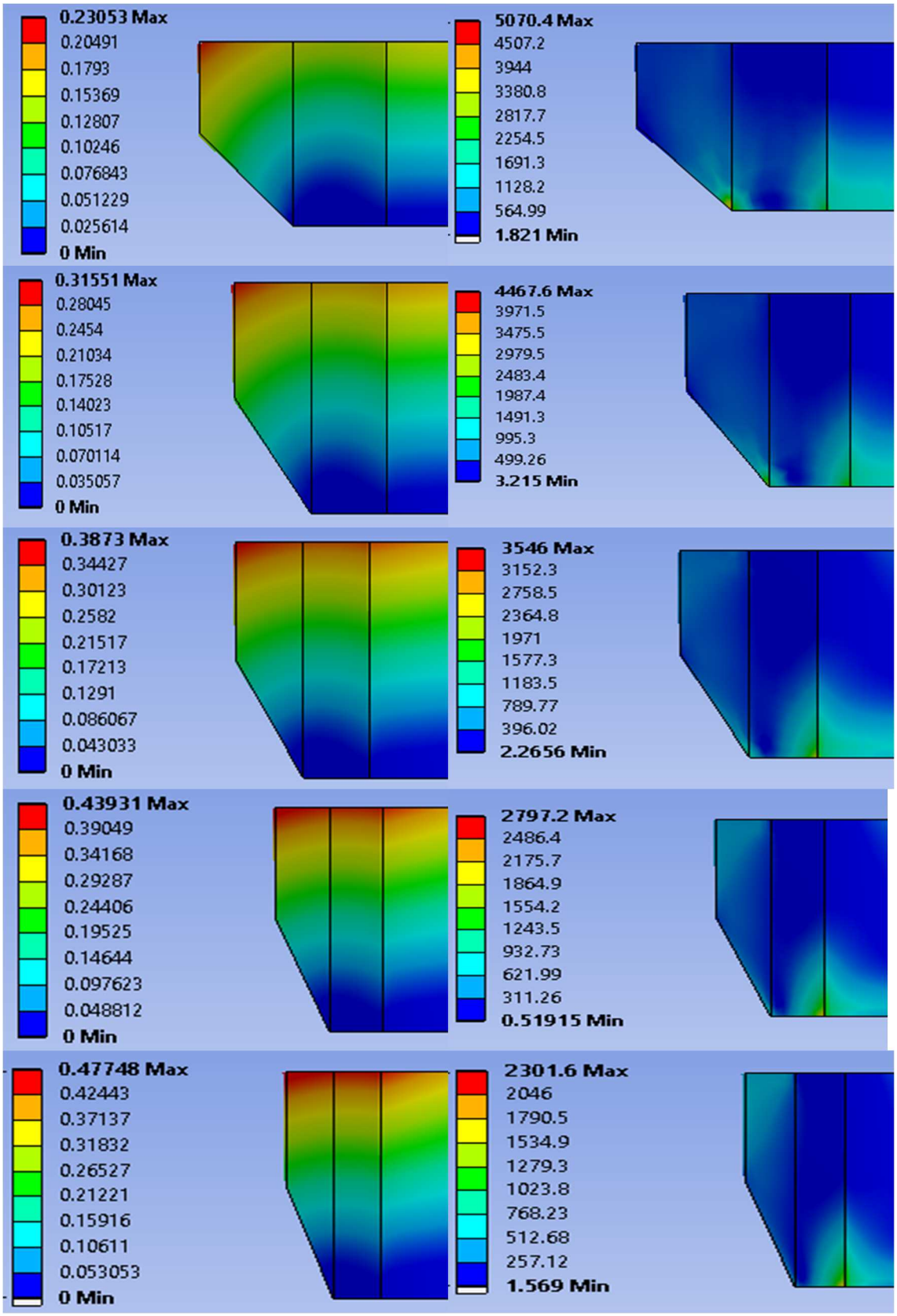

Figure Set2: Deformation Changes with increase in Base at Force for Case 2 (Left) and Stress Changes with increase in Base at Force for Case 2 (Right)

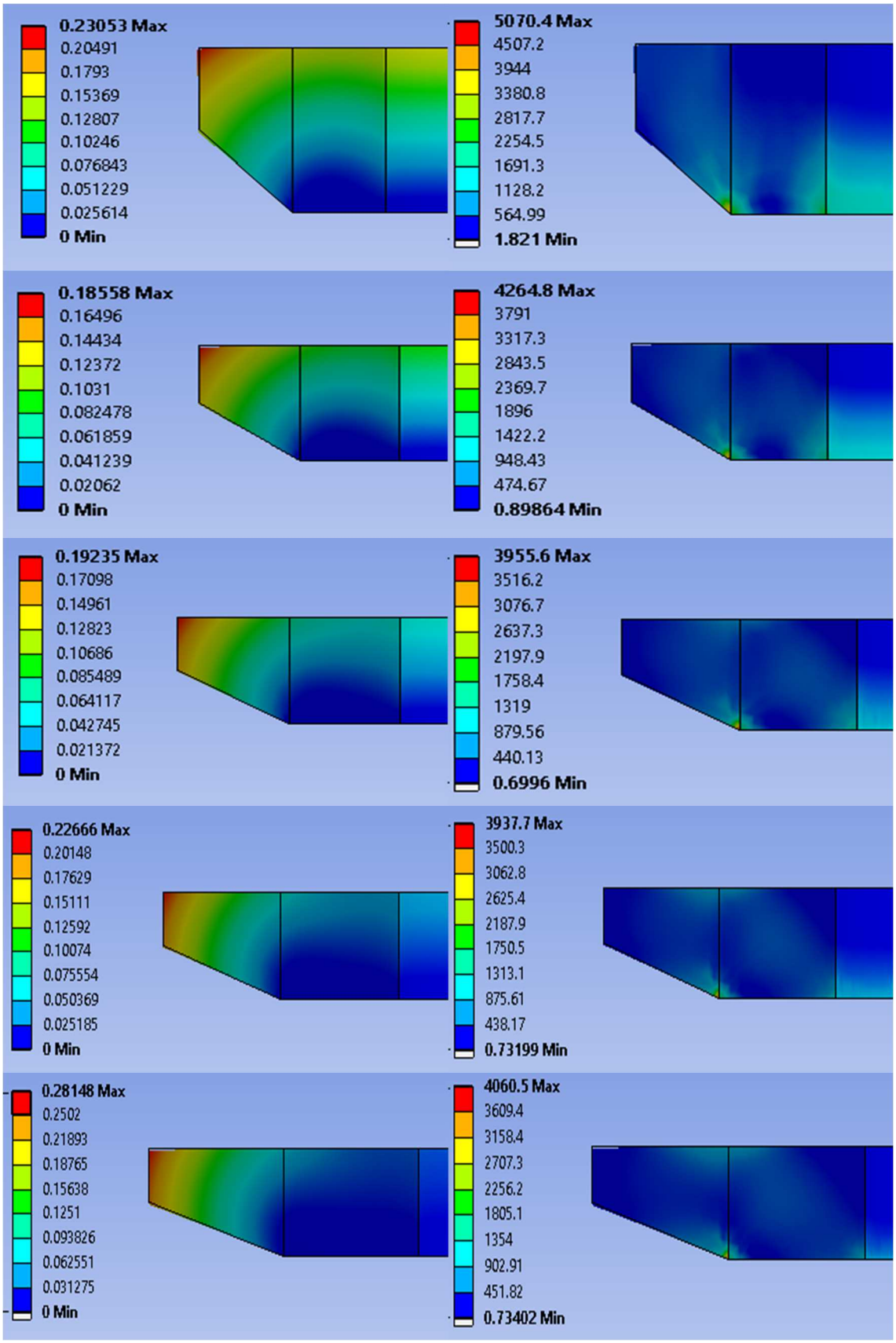

Figure Set3: Deformation Changes with increase in Base and Height at Force for Case 3 (Left) and Stress Changes with increase in Base and Height at Force for Case 3 (Right)

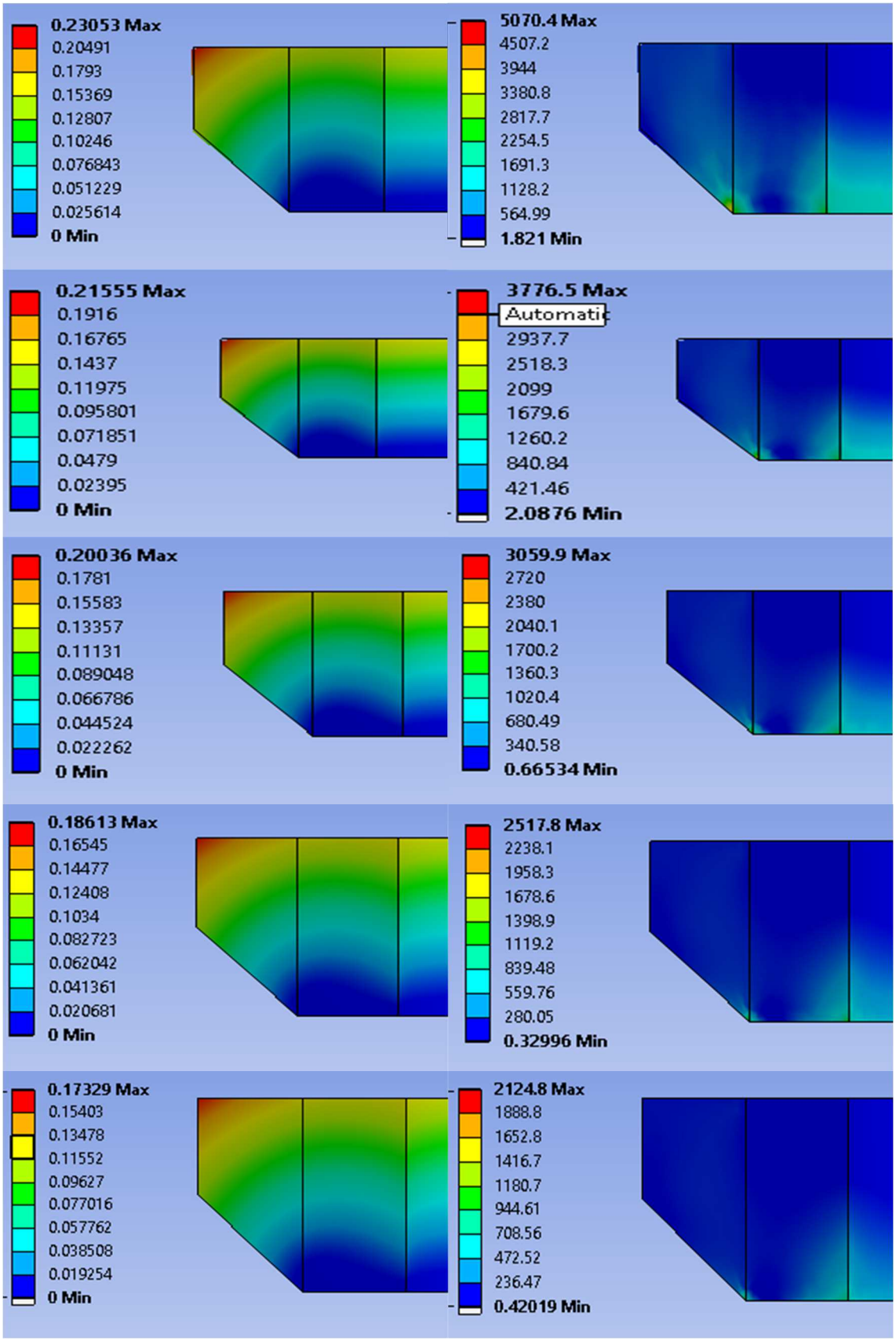

Figure Set4: Deformation Changes with increase in Height at Force for Case 4 (Left) and Stress Changes with increase in Height at Force for Case 4 (Right)

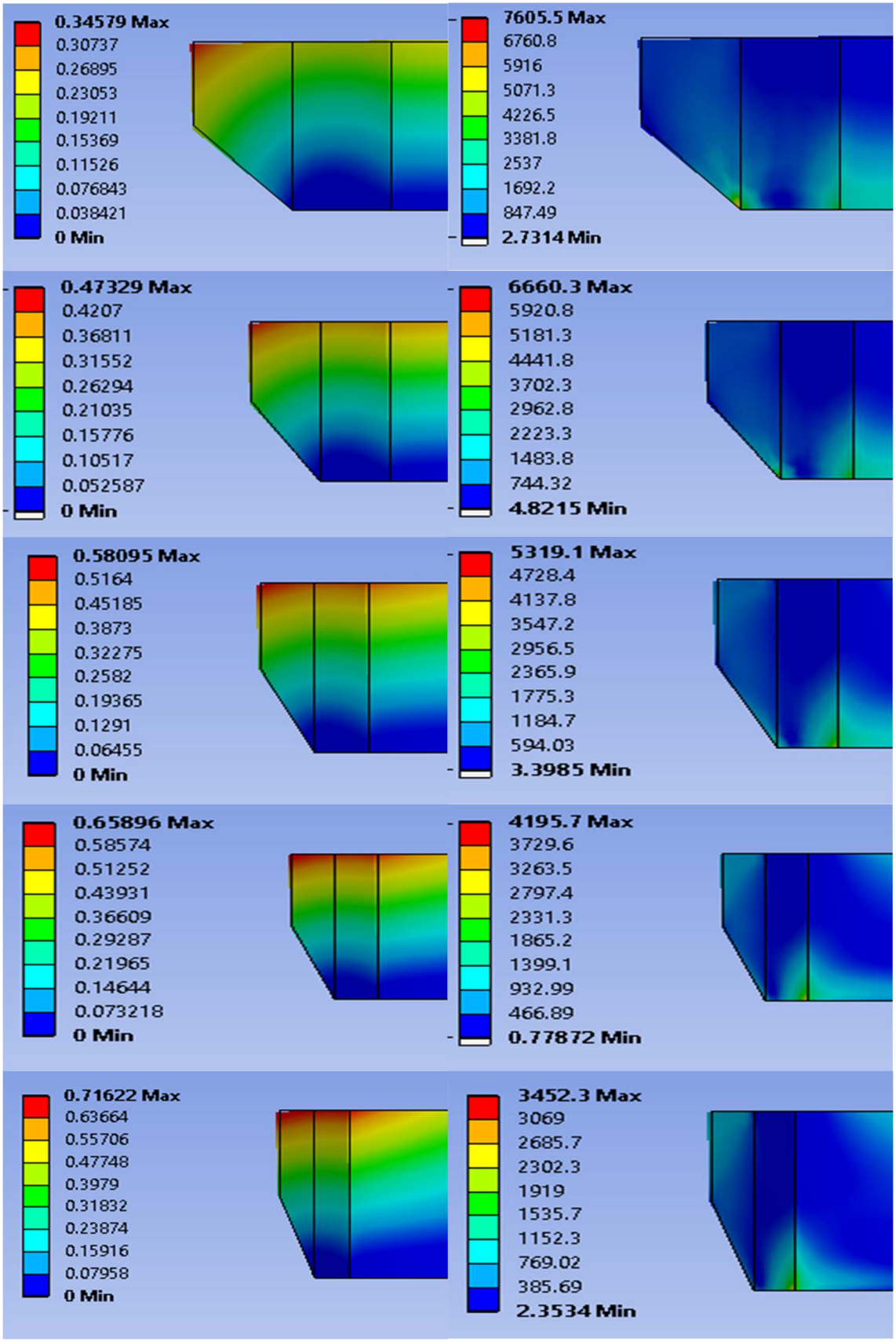

Figure Set5: Deformation Changes with increase in Base at Force for Case 5 (Left) and Stress Changes with increase in Base at Force for Case 5 (Right)

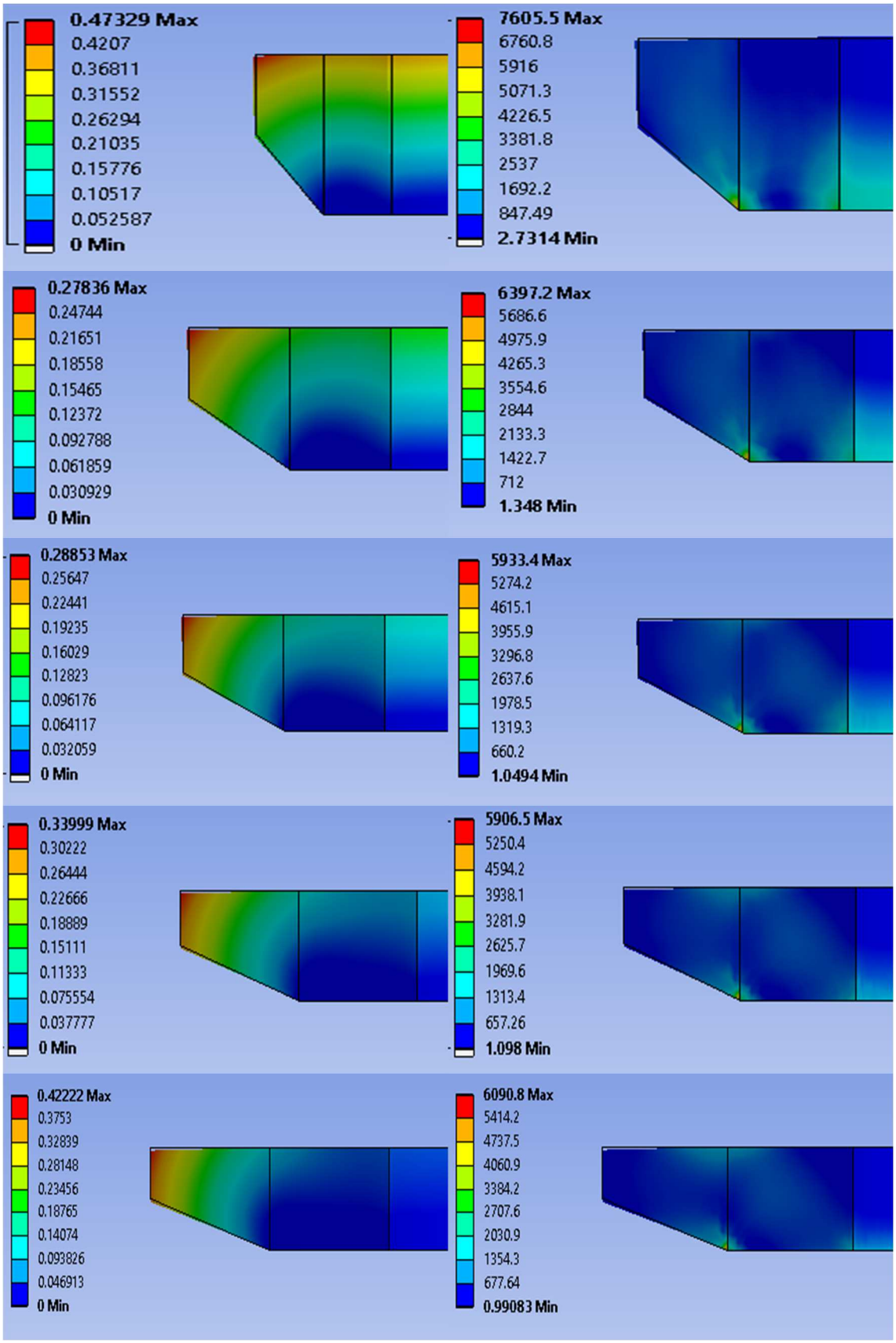

Figure Set6: Deformation Changes with increase in Base and Height at Force for Case 6 (Left) and Stress Changes with increase in Base and Height at Force for Case 6 (Right)

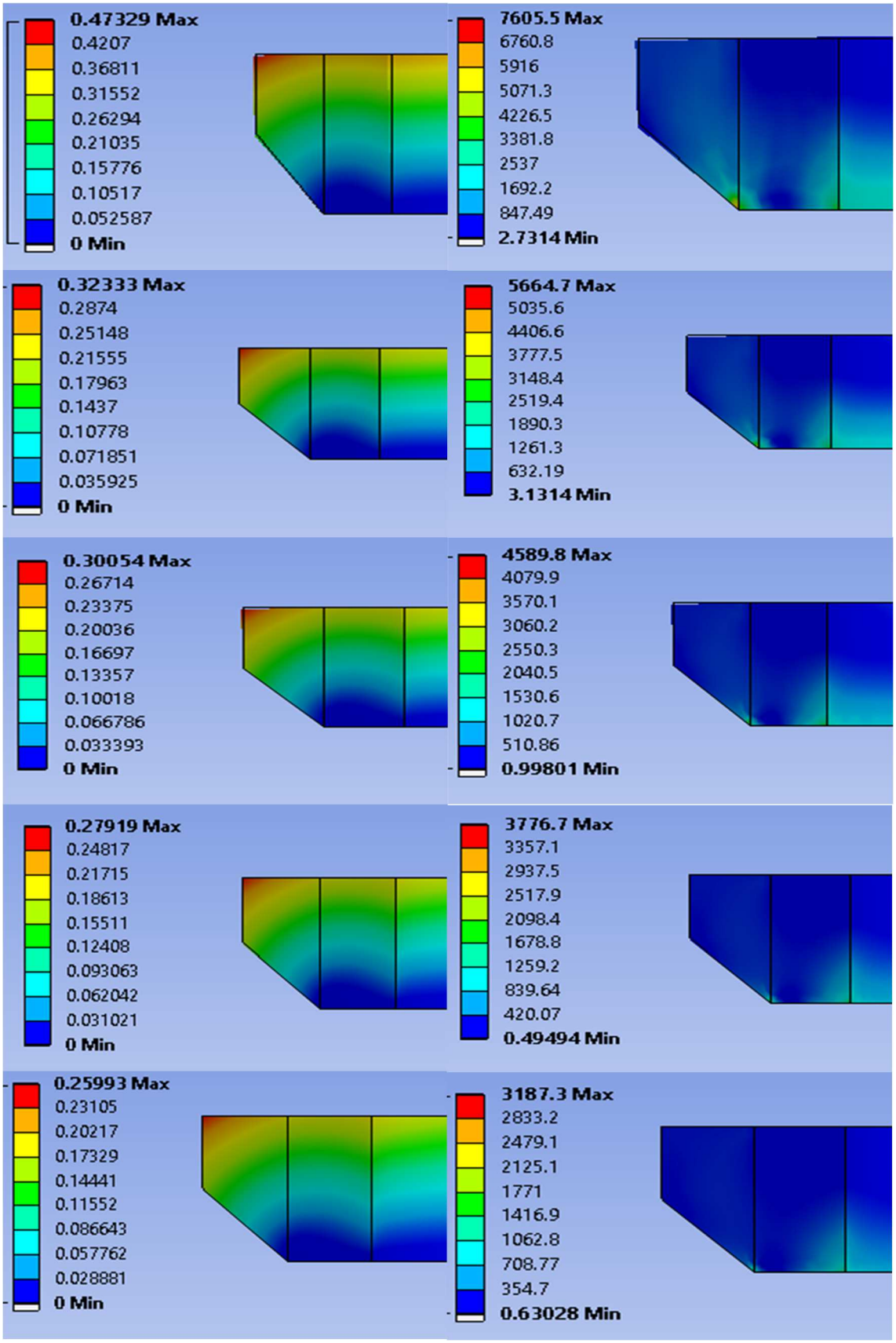

Appendix G – Torsion Snap Latch Ring